

Contents

Articles

The Reduction of Uncertainties for Absolute Piston Gage Pressure Measurements in the Atmospheric Pressure Range	B. E. Welch, R. E. Edsinger, V. E. Bean, and C. D. Ehrlich	343
Absolute Isotopic Abundance Ratios and Atomic Weight of a Reference Sample of Nickel	J. W. Gramlich, L. A. Machlan, I. L. Barnes, and P. J. Paulsen	347
The Absolute Isotopic Composition and Atomic Weight of Terrestrial Nickel	J. W. Gramlich, E. S. Beary, L. A. Machlan, and I. L. Barnes	357
<i>Special Report on Standards for Radioactivity</i> Report on the 1989 Meeting of the Radionuclide Measurements Section of the Consultative Committee on Standards for the Measurement of Ionizing Radiations	Dale D. Hoppes	363
On Measuring the Root-Mean-Square Value of a Finite Record Length Periodic Waveform	E. Clayton Teague	367
A Search for Optical Molasses in a Vapor Cell: General Analysis and Experimental Attempt	A. L. Migdall	373
SUBJECT INDEX TO VOLUME 94		397
AUTHOR INDEX TO VOLUME 94		401

News Briefs

GENERAL DEVELOPMENTS

379

Gravimeters Used Successfully
Ductile-to-Brittle Fracture Behavior of Steel Studied
Certification of Aluminum in Serum Albumin for FDA
CAC QA Program Improves the Quality of Measurements Made in Cancer Chemoprevention Studies
Atomic Liquid and Solid Behavior Observed in Plasmas
NIST Service for Setting Computer Clocks
Proposed Revision of Standard for POSIX: Portable Operating System Interface for Computer Environments
Presence of Toxic S_2F_{10} Confirmed for First Time in SF_6 Exposed to Discharge
NCWM Training Module Published
High-Speed Metallizing of Fibers
Electrochemical Deposition of Al-Mn Quasicrystals and Intermetallics
Structural Ceramics Database Developed
Magnetic Order Observed in Artificial Superlattices
Collaborative Research Effort on Materials Research Renewed
NY Firm Joins With NIST to Investigate CID Sensors
Cold Neutron Workshop on Analytical Measurements With Cold Neutron Beams
High Efficiencies of Soft X-Ray Mirrors Measured at Surf II
Laser Ablation Source for Structural Studies
Frequency Tables for Carbon Monoxide Lasers
New Record Beam Current, 300 mA, Accelerated to Full Energy in SURF-II, the NIST Electron Storage Ring
Agreements of Open Systems Interconnection (OSI) Protocols Published
NCSL Releases Revised Structured Query Language (SQL) Test Suite
Optional Module for Information Resource Dictionary System (IRDS) Standard to be Developed
NSF Grant for NIST Senior Research Fellowship
First Demonstration of Soliton-Like Compression of Pulses from Optical Fiber Laser
EIA Committee Asks NIST to Develop Standards for Fiber Geometry
GMAP System Architecture Installed at the National PDES Testbed
NIST Quality-in-Automation Project Draws Machine Tool Company Collaborators
CBT Develops New Design Procedure for Heat Losses from Underground Piping Systems
CBT Monitors the Source Strengths of Volatile Organic Compounds in a Major New Federal Office Building
X-Ray Method Removes Aids Virus from Evidence
Baldrige Quality Award Program Seeks Examiners
International Directory of Standards Groups Updated
Equation Developed for Predicting Steel Behavior in Fire
High-Quality Amorphous Silicon Films Produced
Non-Toxic Acids are Basis for New Class of Cements

Quick Way to Measure Heat Conduction
 Is There a Robot in Your Future?
 Properties of Methane Developed
 Fiber Laser Research Progressing
 HAZARD I Released to Help Reduce Fire Deaths, Cost
 NIST Launches Consortium to Develop Futuristic Lab
 Industry to Study Wear of Ceramics at NIST
 Evaluation of High-Frequency Power Meters
 Portland Cement Clinker Materials Available
 Oh, Say Can You See?
 New NIST Standard Reference Database
 Ceramic Powders Synthesis—Magnetic Media
 Expert System for Material Selection Advice for the Petroleum Industry
 Sandia to Participate in Cold Neutron Facility Instrument Development
 Industry Supports Research on the Development of Optical Waveguide Sensors
 Federal Information Processing Standard (FIPS) Proposed for the User Interface
 Component of the Applications Portability Profile (APP)
 Open Systems Interconnection/Integrated Services Digital Network (OSI/ISDN) Trial Held
 NIST Break-Junction Measurement Provides First Determination of SIS Tunneling
 Gap of a Thallium-Based High-Temperature Superconductor
 NIST to Participate in Consortium Organized to Study S₂F₁₀
 NIST Miniature Broadband Electric-Field Probe Design Commercialized
 National PDES Testbed in CME Applies Hypertext to Support PDES/STEP Effort

CALIBRATION SERVICES

393

New Automated Gage Block Calibration System at NIST

Calendar

395

The Reduction of Uncertainties for Absolute Piston Gage Pressure Measurements in the Atmospheric Pressure Range

Volume 94

Number 6

November–December 1989

**B. E. Welch, R. E. Edsinger,
V. E. Bean, and C. D. Ehrlich**

National Institute of Standards
and Technology,
Gaithersburg, MD 20899

NIST pressure calibration services with nitrogen are now based on two transfer standard piston gages for which the effective areas have been determined by calibration with the manometer developed at NIST for gas thermometry. Root-sum-squared three sigma uncertainties for the areas for the two gages are 3.05 ppm and 4.18 ppm.

Key words: manometer; piston gage; pressure; pressure measurement; pressure metrology; pressure standards.

Accepted: September 5, 1989

1. Introduction

There are presently only two technologies that can be developed into practical primary pressure standards in the atmospheric pressure range. They are the piston gage (pressure balance, dead weight tester) and the manometer.

The essential features of the piston gage include a vertical hollow cylinder which is closed at the top by a close-fitting piston and closed at the bottom with appropriate plumbing to admit the pressurizing fluid. The piston is loaded with known weights to counter-balance the effect of the pressure so that it floats at a specified reference level and is rotated to relieve friction. The pressure is calculated as the ratio of the force due to the weights to the effective cross-sectional area of the piston. The piston gage measures the difference between the pressure at the bottom and the top of the piston. When the top of the piston is at ambient atmospheric pressure, we speak of using the device in the gage mode. The absolute mode requires that the top of the piston be in a vacuum. The accuracy

of a piston gage is limited by our ability to determine the effective area. For a primary standard piston gage, the area must be determined from dimensional metrology. The highest accuracy reported in the literature is on the order of 15 parts per million (ppm) [1] while repeatability of 1 ppm is common. The limitation is in the accuracy of the dimensional measurements and in the manufacture of truly straight and round cylinder bores and pistons.

The essential feature of a manometer is a vertical column of fluid, suitably contained and supported at the bottom by an applied pressure. The magnitude of the pressure is the product of the column height, the density of the fluid, and the acceleration due to gravity plus whatever pressure is applied to the top surface of the fluid column. Thus, the manometer is also a differential pressure measurement device and is used in the absolute mode when the space above the top surface of the field column is evacuated or in the gage mode when that space is

at ambient atmospheric pressure. Limitations in accuracy are due to the uncertainties in the density of the fluid and in the column height measurements. In general, at atmospheric pressure, a state-of-the-art manometer will have a lower uncertainty than a state-of-the-art primary standard piston gage.

The piston gage has two advantages over the manometer: portability and ease of use. These two properties coupled with the stability of the piston gage make it an excellent transfer standard. In order to meet the demand for reduced uncertainties, NIST has used the manometer that was developed at NIST for gas thermometry [2] as a primary standard to calibrate the two piston gages that serve as the reference standards for NIST piston gage calibration service. Calibration services are now offered through these transfer standard piston gages.

Herein we report the results of the calibration of the piston gage calibration reference standards using the manometer in the absolute mode.

2. Apparatus

A complete description of the gas thermometer manometer (GTM) and a thorough evaluation of its uncertainties at the 99 percent confidence level are found in the literature [2,3,4]. Recently, Edsinger and Schooley, as a part of their new gas thermometry measurements up to 933 K, have reconsidered the uncertainty of the manometer and have determined that the value given in [2] of 2 ppm at the 99 percent confidence level is satisfactory [5].

The two piston gages are commercial units, identical in make and model. They were modified in two ways: in an effort to eliminate every part having even a remote possibility of being hard to clean and thus becoming a source of dirt, we replaced the entire mechanism for the top and bottom stops with parts made of Kel-F. Also the rotative mechanism was modified such that the cylinder and the piston with its weight stack could be rotated together up to the desired angular velocity, on the order of 60 revolutions per minute (rpm), and then the piston was floated and the cylinder was stopped allowing the piston to continue. Pressure measurements were then made with the cylinder stationary and the piston coasting. The Kel-F bottom stop was coated with a robust conductive aluminum film which was grounded to the cylinder to prevent electrostatic charges from accumulating on the surface when the rotating weight hanger rubs on the bottom stop. Without the conductive

film, the resulting electrostatic forces can produce errors of several ppm at atmospheric pressure.

The temperature of the piston and cylinder assembly was monitored with an array of ten thermistors, connected in parallel, mounted on the stationary portion of the cylinder mount, and calibrated in situ.

Figure 1 is a schematic diagram of the experimental arrangement. Item A is a calibrated differential pressure transducer having a full range of 130 Pa and a sensitivity of 7×10^{-2} Pa. It was calibrated by using two piston gages, one supplying pressure to each pressure port of the transducer. The use of the transducer provides two advantages: it allows both instruments to work against a limited-volume pressure system which makes the apparatus easier to operate. The transducer was also used to read small differential pressures between the manometer and the piston gage which makes the establishment of a perfect equilibrium unnecessary. The zero was checked before each measurement by applying the identical pressure to both sides of the transducer via the bypass valve. Typically, the differential pressure for a given measurement was a fraction of a pascal.

Item B of figure 1 is another calibrated differential pressure transducer of the same make, model, range, and sensitivity as item A. It was used to measure the pressure in the bell jar surrounding the weights, which is evacuated for absolute mode operation.

The pistons and cylinders were examined for residual magnetism using a Hall-effect detector and were demagnetized as necessary.

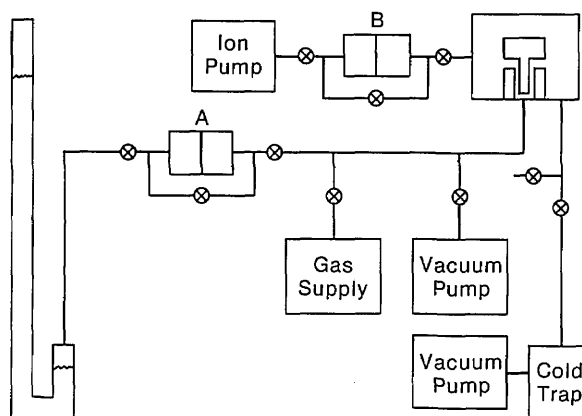


Figure 1. Schematic diagram of the pressure system connecting the manometer to the piston gage. The items marked A and B are calibrated differential pressure transducers. The circled X's are valves.

3. Results

Both gages were repeatedly calibrated with the manometer at 27 and 95 kPa in the absolute mode using nitrogen; a total of 107 measurements for PG 28 and 149 measurements for PG 29. The effective areas for the gages were calculated from the expression

$$A = \frac{Mg}{(P - P_b - \rho gh + \epsilon)[1 + (\alpha_p + \alpha_c)(T - T_R)]} \quad (1)$$

where

- M is the total mass supported by the pressure including the weights and piston
- g is the local acceleration due to gravity
- P is the pressure at the lower mercury surface in the manometer
- P_b is the pressure in the bell-jar surrounding the weights
- ρ is the density of the nitrogen
- h is the height between the reference level of the piston gage and the level of the lower mercury surface in the manometer
- ϵ is the differential pressure measured by transducer A
- α_p is the linear thermal expansion coefficient for the piston
- α_c is the linear thermal expansion coefficient for the cylinder
- T is the temperature of the operating piston gage
- T_R is the reference temperature and is defined to be 23 °C.

The effective area of each gage was found to be constant over this pressure range. Figures 2 and 3 are histograms showing the deviation from the average areas expressed in ppm. The measurements at 95 kPa are marked with a dot to distinguish them from the 27 kPa measurements. There is no apparent significant pressure dependence on the area of either gage. The areas and the tripled standard deviations are given in table 1.

Table 1. Areas and tripled standard deviations of PG 28 and PG 29

	PG 28	PG 29
Area, 10^{-4} m ²	3.3582249	3.3572390
Tripled standard deviation	1.89 ppm	3.42 ppm

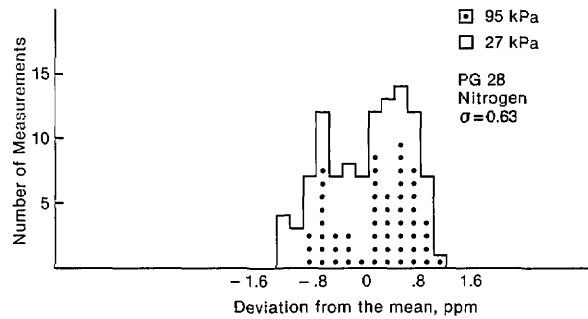


Figure 2. Histogram showing the deviation of the measured area from the mean for PG 28.

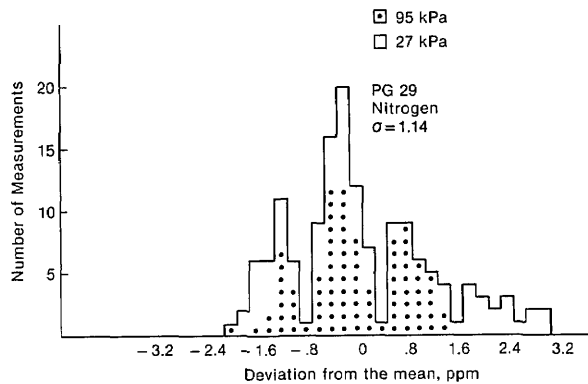


Figure 3. Histogram showing the deviation of the measured area from the mean for PG 29.

The uncertainty in the effective area of each piston gage arising from the uncertainties in the various parameters of eq (1) can be expressed as [6]

$$\frac{dA}{A} = \left[\sum \left(\frac{1}{A} \frac{\partial A}{\partial X_i} dX_i \right)^2 \right]^{1/2} \quad (2)$$

where the X_i are the parameters given in eq (1). These uncertainties are given in table 2. The tripled standard deviations about the means given for the areas of the two gages in table 1 are combined with the uncertainty given by eq (2) by the root-sum-square method; they are also listed in table 2.

The sources for the values listed under the heading “ dx_i ” in table 2 are as follows:

The value of dM is the result of calibration of the piston gage weights using NIST standards and is discussed elsewhere [7]. The value of dg is the result of on-site measurements. Reference 2 discusses the value of dP . The values of dP_b are based on calibration measurements. The value of $d\rho$ is based on an uncertainty in temperature measurement of 0.5 K

Table 2. Uncertainties in area for gages PG 28 and PG 29 calculated at a pressure of 100 kPa based on three standard deviations

Parameter			Parameter	Differential		$\frac{1}{A} \frac{\partial A}{\partial X_i} dX_i$
X_i	Units	Value	Uncertainty dX_i	$\frac{1}{A} \frac{\partial A}{\partial X_i}$	Value	ppm
M	kg	3.4	1.1×10^{-6}	$1/M$	3×10^{-1}	0.33
g	m/s ²	9.8	1.5×10^{-6}	$1/g$	1×10^{-1}	0.15
P	Pa	1×10^5	2.0×10^{-1}	$1/P$	1×10^{-5}	2.0
P_b	Pa	1.3	6×10^{-2}	$1/P$	1×10^{-5}	0.6
ρ	kg/m ³	1.2	1.8×10^{-3}	gh/P	5×10^{-4}	0.9
h	m	5	2.0×10^{-3}	$\rho g/P$	1.2×10^{-4}	0.24
ϵ	Pa	0.5	6×10^{-2}	$1/P$	1×10^{-5}	0.6
$(\alpha_p + \alpha_c)$	/° C	8.22×10^{-6}	1.5×10^{-8}	$T - T_R$	1	0.015
$T - T_R$	° C	$T_R = 23$	3×10^{-2}	$\alpha_p + \alpha_c$	8.22×10^{-6}	0.24
$\frac{dA}{A}$ arising from the parameters of eq (1)						2.40
				PG 28	PG 29	
Uncertainty in eq (1)				2.40	2.40	
Tripled standard deviation of area about the mean				1.89	3.42	
Combined total uncertainty				3.05	4.18	

along the tube connecting the manometer to the piston gage [2]. On-site height measurements produced the value of dh . Separate thermal expansion coefficient measurements on the materials from which the piston and cylinders were made result in the value of $d(\alpha_p + \alpha_c)$. The value for the uncertainty in the temperature measurements is based on calibration data of the thermistors.

The uncertainty in P includes the uncertainty in the head correction, ρgh , with the assumption that the gas is helium [2]. Since, in this case, nitrogen was used, we have explicitly included the uncertainty for the nitrogen head correction without removing the helium head correction uncertainty in the value of dP , a conservative approach.

The determination of effective areas of piston gages PG 28 and PG 29 as reported in this paper reflect state-of-the-art measurements and they provide an improved basis for NIST calibration services for the practical use of gas operated piston gages. It is recognized that reasonably frequent verification of the effective areas by the use of the GTM facility is important and necessary to establish a new body of control history to support improved levels of calibration service accuracy. The intrinsic stability of well constructed gas operated piston gages combined with the accuracy of the GTM provides a clear basis for significant improvement in the accuracy levels of practical pressure measurements.

About the authors: B. E. Welch and R. E. Edsinger are physicists who were in the Temperature and Pressure Division of the NIST Center for Chemical Technology. Both have retired. V. E. Bean and C. D. Ehrlich are physicists in that same division.

4. References

- [1] Maghzenani, R., Molinar, G. F., Marzola, L., and Kulshrestha, R. K., J. Phys. E: Sci. Instrum. 20, 1173 (1987).
- [2] Guildner, L. A., Stimson, H. F., Edsinger, R. E., and Anderson, R. L., Metrologia 6, 1 (1970).
- [3] Guildner, L. A., and Edsinger, R. E., J. Res. Natl. Bur. Stand. (U.S.) 80A, 703 (1976).
- [4] Schooley, J. F., Proceedings of the 1988 Workshop and Symposium of the National Conference of Standards Laboratories, p. 50-1, August 14-18, 1988.
- [5] Edsinger, R. E., and Schooley, J. F., Metrologia 26, 95 (1989).
- [6] Heydemann, P. L. M., and Welch, B. E., Piston Gages, in Experimental Thermodynamics, Volume II, edited by LeNeindre, B., and Vodar, B., Butterworths, London (1975) p. 183.
- [7] Davis, R. S., and Welch, B. E., J. Res. Natl. Bur. Stand. (U.S.) 93, 565 (1988).

Absolute Isotopic Abundance Ratios and Atomic Weight of a Reference Sample of Nickel

Volume 94

Number 6

November–December 1989

J. W. Gramlich, L. A. Machlan,
I. L. Barnes, and P. J. Paulsen

National Institute of Standards
and Technology,
Gaithersburg, MD 20899

Absolute values have been obtained for the isotopic abundance ratios of a reference sample of nickel (Standard Reference Material 986), using thermal ionization mass spectrometry. Samples of known isotopic composition, prepared from nearly isotopically pure separated nickel isotopes, were used to calibrate the mass spectrometers. The resulting absolute isotopic ratios are: $^{58}\text{Ni}/^{60}\text{Ni} = 2.596061 \pm 0.000728$, $^{61}\text{Ni}/^{60}\text{Ni} = 0.043469 \pm 0.000015$, $^{62}\text{Ni}/^{60}\text{Ni} = 0.138600 \pm 0.000045$, and $^{64}\text{Ni}/^{60}\text{Ni} = 0.035295 \pm 0.000024$, which yield atom percents of $^{58}\text{Ni} = 68.076886 \pm 0.005919$, $^{60}\text{Ni} = 26.223146 \pm 0.005144$,

$^{61}\text{Ni} = 1.139894 \pm 0.000433$, $^{62}\text{Ni} = 3.634528 \pm 0.001142$, and $^{64}\text{Ni} = 0.925546 \pm 0.000599$. The atomic weight calculated from this isotopic composition is 58.693353 ± 0.000147 . The indicated uncertainties are overall limits of error based on two standard deviations of the mean and allowances for the effects of known sources of possible systematic error.

Key words: absolute ratio; assay; atomic weight; dimethylglyoxime; isotopic abundance; mass spectrometry; nickel.

Accepted: August 28, 1989

1. Introduction

The Inorganic Analytical Research Division of the National Institute of Standards and Technology, has been conducting a long-term program of absolute isotopic abundance ratio and atomic weight determinations using high precision isotope ratio mass spectrometry. Previous atomic weight determinations include silver [1,2], chlorine [3], copper [4], bromine [5], chromium [6], magnesium [7], lead [8], boron [9], rubidium [10], rhenium [11], silicon [12], potassium [13], thallium [14], strontium [15], and gallium [16].

To obtain absolute isotopic ratios from the observed or relative measurements made on a mass spectrometer, it is necessary to calibrate the instrument using samples of accurately known isotopic ratios of the element under study. These synthetic isotopic standards, assayed and gravimetrically

prepared from chemically pure and nearly isotopically pure isotopes, provide a bias correction (calculated isotopic ratio/observed isotopic ratio) which, when applied to the observed isotopic ratios of the reference sample being calibrated, allows absolute ratios to be calculated for the sample. The atomic weight is then obtained by multiplying the fractional abundance of each isotope by its nucleic mass [17] and summing the resultant products. A more detailed description of the method used for the determination of isotopic abundance ratios and atomic weights at NIST is given elsewhere [2].

In 1961, the IUPAC Commission on Atomic Weights recommended a value of 58.71 for the atomic weight of nickel. That value was based on the isotopic abundance measurements of White and

Cameron [18]. The Commission noted in its report that all chemical determinations that had been reported and believed to be significant gave a mean value for the atomic weight of 58.69. The best chemical determinations appeared in a series of publications by Baxter and associates in the 1920s [19,20,21]. These measurements yielded an average atomic weight of 58.694, with credibility increased by proof of accuracy of parallel work on the atomic weight of cobalt [22] which is now known accurately because of its mononuclidic state.

In 1973 the Commission reexamined both the chemical and mass spectrometric measurements and so recommended a lower value of 58.70 for the atomic weight of nickel. Later that year, Barnes et al. [23] published a superior but not absolute mass spectrometric measurement which produced an atomic weight value of 58.688, in good agreement with the chemical determinations. After reexamination in 1979, the Commission recommended the present standard atomic weight value of 58.69 ± 0.01 [24]. Nickel is currently listed by the IUPAC Commission on Atomic Weights and Isotopic Abundances as one of the elements with an atomic weight with a large uncertainty [25].

Since no significant variations in the isotopic composition of nickel in nature have been observed, either in this study or in previous work, a high accuracy measurement of the atomic weight of a reference sample of nickel (SRM 986) will allow IUPAC to recommend a value with a much smaller uncertainty.

2. Experimental Procedure

2.1 Mass Spectrometry

Isotope ratio measurements were made on two different thermal ionization mass spectrometers with separate operators. One instrument was an NIST designed mass spectrometer equipped with a 30-cm radius of curvature, 90° magnetic sector (designated inst. #1, operator #1). The second instrument was a Finnigan-MAT 261 mass spectrometer¹ (designated inst. #2, operator #2). The NIST instrument employed a shielded Faraday cage collector with a double slit collimator. The remainder of the measurement circuitry consisted of a para-

metric electrometer [26], a precision voltmeter, and a computer. Timing, magnetic field switching, and data acquisition were controlled by the computer. The Finnagin-MAT 261 is a 23-cm radius, 90° magnetic sector instrument which uses a non-normal entry and exit ion path. This arrangement gives the dispersion of an instrument of 2.78 times (64 cm) the radius. It is equipped with seven deep Faraday cup collectors, six of which are externally adjustable. Each cup has an individual amplifier contained within an evacuated, thermally controlled chamber. The chamber temperature is maintained to ± 0.02 °C.

Nickel was thermally ionized from a platinum filament fabricated from 0.001×0.030 in (0.0025×0.076 cm) high purity platinum ribbon. Prior to filament fabrication, the platinum ribbon was heated for several hours in dilute hydrochloric acid to reduce any iron impurities that might cause isobaric interferences. After fabrication, the filaments were degassed for 1 h by passing a current of 3 A through them in a vacuum and under a potential field of 45 V. Filaments cleaned in this manner generally exhibited no detectable emissions for the nickel isotopes using blank filament loadings. The maximum background observed was 1.2×10^{-16} A at mass 58, which appeared to be a natural nickel background. This background would be insignificant for measurement of the natural standard and the point calibration mixes. Filaments used for measurements of the nickel separated isotopes were examined in the mass spectrometer prior to sample loading. Only those filaments which showed no detectable background were used for analysis of the separated isotopes.

All sample loadings were conducted in a Class 100 clean air hood. Pipets made of Pyrex tubing were used to transfer the samples from their containers to the filaments. The tubing was cleaned by heating in 8 mol/L HNO₃ for 24 h, rinsing with ultra-high purity water, heating in 6 mol/L HCl for 24 h, followed by several rinsings in ultra-high purity water.

Samples were loaded onto the filaments under the following conditions: approximately 5 μg of solution (5 μL of 1 mg/mL Ni as NiNO₃ in 1+49 HNO₃)² was added to the filament and dried for 5 min at 1 A. Five μL of a solution containing 17 mg

¹ Certain commercial equipment, instruments, or materials are identified in this paper to specify adequately the experimental procedure. Such identification does not imply recommendation or endorsement by the National Institute of Standards and Technology, nor does it imply that the materials or equipment identified are necessarily the best available for the purpose.

² A reagent dilution of (1+49) indicates 1 volume of concentrated reagent diluted with 49 volumes of pure water. If no dilution is specified, use of concentrated reagents is implied. The acids and water used for these dilutions were produced at NIST by sub-boiling distillation [26].

Aerosil 300 (Degussa, Frankfurt, FGR) powder/g of solution, 0.34 mg/g AlCl_3 /g solution, and 0.1 g of high purity H_3PO_4 /g of solution were added to the filament and dried at a current, through the filament, of 1, 1.3, and 1.5 A, each for a time period of 5 min. The filament was then slowly heated to fume off the excess H_3PO_4 and then heated for a few seconds at approximately 700 °C. After a 5 min cooling period, the filament was loaded into the mass spectrometer.

The analysis procedure for inst. #1 was as follows: the initial filament current was set to produce a filament temperature of 1000 °C. At 4 min intervals the filament temperature was increased by 50 °C until at 20 min a final temperature of 1250 °C was achieved. After measurement of baselines on both sides of each mass of interest, data were collected between 30 and 70 min into the analysis. For the reference material, 5 min sets of ratio measurements were made in the following order: 58/60, 61/60, 62/60, 64/60, 64/60, 62/60, 61/60, 58/60.

The analysis procedure for inst. #2 was slightly different. The heating pattern was the same with a maximum temperature of 1250 °C (as measured with a two color optical pyrometer) used. The six mass unit range covered by the nickel isotopes is just beyond the range of this instrument so that it was necessary to jump the magnetic field once to collect all of the ratios. Thus, the 58/60, 61/60, and 62/60 ratios were collected simultaneously during a 32 s integration, a jump of one mass unit was made and the 64/60 ratio was collected. Five sets of twenty such ratios were collected for each sample. The amplifiers were calibrated at the beginning of each sample run; baselines were collected at the beginning of each block of twenty ratios.

2.2 Purification of Separated Nickel Isotopes

Electromagnetically separated ^{58}Ni , ^{60}Ni , and ^{62}Ni isotopes were obtained from the Nuclear Division, Oak Ridge National Laboratory. The ^{58}Ni was designated sample 121426, the ^{60}Ni was designated sample 121501, and the ^{62}Ni was designated sample 158201. The certificate which accompanied each sample showed isotopic enrichment to approximately 99.8% for the ^{58}Ni material, 99.8% for the ^{60}Ni material, and 99.0% for the ^{62}Ni material. The certificates included a semi-quantitative spectrographic analysis which showed that the principal impurities were Cu and Zn at the 0.1% level and several other elements at the 0.05% level.

To reduce these impurities to a level low enough so that they would not cause a significant error in

either the assay procedure or the mass spectrometric ratio measurements, the separated isotopes were purified by a combination of cation exchange chromatography, ammonium hydroxide precipitation, electrodeposition and anion exchange chromatography.

Each separated isotope was treated as follows: the nickel (approximately 2 g of ^{58}Ni and ^{60}Ni , and 1.8 g of ^{62}Ni) was dissolved in 20 mL of HNO_3 (1+1), evaporated to dryness and then 25 g of HClO_4 were added. The solution was evaporated to HClO_4 fumes, and after cooling, 5 g of 10 mol/L HCl was added. This step was used to help eliminate any Cr that was present. The sample solution was evaporated to dryness and the residue was dissolved in 50 g of H_2O . This solution was passed through two cation exchange columns (a single column of the necessary length was not available) in series (each column, 19×1.6 cm, was filled with AG 50×8, 100–200 mesh resin and cleaned with 120 g of 4 mol/L HCl followed with H_2O until the eluate was neutral). After adding the nickel, some impurities were eluted from the columns with 200 g of 0.4 mol/L HCl. The nickel was eluted with 120 g of 3 mol/L HCl and this solution was evaporated to dryness. The residue was dissolved in 50 g of H_2O , an excess of NH_4OH was added (approximately 20 mL) and the solution was filtered to remove insoluble hydroxides. The solution was evaporated to dryness, 25 g of H_2O were added and then 25 g of H_2SO_4 were slowly added. The solution was evaporated to fumes of H_2SO_4 and, after cooling, 5 g of HNO_3 were added. The beaker was covered and heated, then the cover was removed and the solution evaporated to fumes of H_2SO_4 . The sides of the beaker were rinsed down with H_2O and the solution again evaporated to fumes of H_2SO_4 . The solution was diluted to 150 mL with H_2O , two clean platinum gauze electrodes were placed in the solution and a 2 V dc potential was applied between the electrodes for 16 h. The electrodes were removed from the solution and re-cleaned in HNO_3 (1+1). The electrodes were placed back into the separated isotope solution, NH_4OH was added to approximately 20 mL excess and a 2.0 V dc potential was applied until the nickel color had disappeared from the solution (this required up to three days, with an additional 5 mL of NH_4OH being added each day). The electrode with the nickel deposit was removed from the solution, rinsed with H_2O and the nickel was dissolved by heating in 40 g of 10 mol/L HNO_3 . The nickel solution was evaporated to dryness, 20 g of 5 mol/L HCl were added and the solution was again

evaporated to dryness. The 5 mol/L HCl addition and evaporation to dryness was repeated. The residue was dissolved in 10 g of 5 mol/L HCl and all but 4 g of this was evaporated. Thirty g of 9.5 mol/L HCl were added and the resulting solution was passed through two anion exchange columns in series (each column consisted of a 5-mL plastic syringe filled to 5 mL with AG1×8, 100-200 mesh resin and cleaned with 40 g of 9 mol/L HCl, 50 g of H₂O, and 10 g of 9 mol/L HCl). Ten g of 9 mol/L HCl were used to rinse the beaker and complete the elution of the nickel from the column. The sample was converted to the nitrate form by adding sequentially 20, 15, and 10 g portions of HNO₃ to the beaker and evaporating the sample to dryness between each addition of acid.

2.3 Preparation and Analysis of Separated Isotope Solutions

The purified ⁵⁸Ni and ⁶⁰Ni were transferred to 500-mL Teflon bottles and diluted to approximately 400 g with HNO₃ (1+49). The purified ⁶²Ni was transferred to a 2-L Teflon bottle and diluted to approximately 1700 g with HNO₃ (1+49).

A preliminary assay of the nickel concentration of each separated isotope solution was accomplished by isotope dilution mass spectrometry. Two weighed portions of the ⁶⁰Ni separated isotope solution were spiked with known amounts of natural nickel. Two weighed portions of each of the other two separated isotopes (⁵⁸Ni and ⁶²Ni) were spiked with weighed portions of the ⁶⁰Ni separated isotope. After mixing, evaporation and dilution to 1 mg Ni/g of solution with HNO₃ (1+49), the ⁵⁸Ni/⁶⁰Ni or ⁶²Ni/⁶⁰Ni ratios were determined by thermal ionization mass spectrometry. The concentration of nickel was then calculated for each solution and used to determine the amount of each separated isotope solution required for the calibration mixes. Samples of the three separated isotope solutions were analyzed for impurity elements by inductively coupled plasma mass spectrometry (ICP-MS).

Samples, equivalent to approximately 1.5 mg of Ni, were spiked with 1.5×10^{-8} g each of ²⁰⁶Pb, ²⁰³Tl, ²⁰¹Hg, ¹⁹⁵Pt, ¹⁸³W, ¹⁴⁵Nd, ¹⁴²Ce, ¹³⁷Ba, ¹²⁵Te, ¹²³Sb, ¹¹³In, ¹¹¹Cd, ¹¹⁰Pd, ⁹⁷Mo, ⁹¹Zr, ⁸⁷Rb, ⁸⁶Sr, ⁷³Ge, ⁷¹Ga, ⁶⁷Zn, ⁶⁵Cu, ⁵⁷Fe, ⁵³Cr, ⁵⁰V, ⁴⁷Ti, ²⁶Mg, and ⁶Li. The solutions were diluted to 1 mg Ni/mL with HNO₃ (1+49). Table 1 shows the results of these isotope dilution analyses as well as concentrations estimated from relative sensitivity factors (rsf). The rsf values are derived from a mass vs sensitivity

response curve obtained from an external standard containing 20 elements spaced across the mass scale from Li to Hg. Table 2 shows the results of the ICP-MS analyses of SRM 986 and the same

Table 1. Analysis of impurities in the nickel separated isotopes

Element	Spike isotope	⁵⁸ Ni	⁶⁰ Ni	⁶² Ni
Concentrations in µg/g, determined by isotope dilution				
Pb	²⁰⁶ Pb	1.3	2.2	3.1
Tl	²⁰³ Tl	0.1	0.1	0.3
Hg	²⁰¹ Hg	6	2	2
Pt	¹⁹⁵ Pt	6.5	9.4	15
W	¹⁸³ W	0.9	2	1
Nd	¹⁴⁵ Nd	0.1	1	0.1
Ce	¹⁴² Ce	0.1	0.2	0.3
Ba	¹³⁷ Ba	0.1	0.2	0.2
Te	¹²⁵ Te	0.6	0.5	2
Sb	¹²³ Sb	0.9	1	0.1
In	¹¹³ In	0.1	0.5	0.1
Cd	¹¹¹ Cd	0.9	2	3
Pd	¹¹⁰ Pd	1.6	2	2
Mo	⁹⁷ Mo	1.5	0.5	0.7
Zr	⁹¹ Zr	2	2	0.5
Sr	⁸⁶ Sr	0.1	0.2	0.2
Rb	⁸⁷ Rb	0.3	0.4	0.2
Ga	⁷¹ Ga	0.3	1	0.4
Ge	⁷³ Ge	2	2	1
Zn	⁶⁷ Zn	0.3	≤5	1
Cu	⁶⁵ Cu	2	≤12	^a
Fe	⁵⁷ Fe	^a	≤35	≤16
Cr	⁵³ Cr	0.7	0.4	0.6
V	⁵⁰ V	3	1	1
Ti	⁴⁷ Ti	3	3	3
Mg	²⁶ Mg	3	4	1
Li	⁶ Li	≤14	≤15	≤20
Concentrations in µg/g, determined by rsf and/or external std				
U		0.1	0.1	0.1
Th		0.1	0.1	0.1
Bi		0.1	0.1	0.1
Au		0.2	0.2	0.2
Ir-I		0.3	0.3	0.3
Sn		0.2	0.9	0.8
Ag		0.3	0.1	0.1
Rh		0.3	0.1	0.1
Ru		0.3	0.3	0.3
Y		0.3	0.1	0.1
Se		1	4	1
As		1	1	1
Co ^b		≤240	≤2000	13
Mn		1	2	1
Sc		1	1	0.1
Al		≤3	≤3	≤3
Na		≤10	≤10	≤10
B		1	1	1
Be		1	1	1

^a Matrix interference.

^b ⁵⁸Ni and ⁶⁰Ni tails at ⁵⁹Co.

Table 2. Analysis of impurities in the pure nickel (SRM 986) and the doped and purified nickel standard

Element	Pure nickel	Doped and purified Ni
	Isotope dilution	External standard in Ni
Pb	<0.4	2
Tl	<0.2	<0.2
Nd	<0.8	<0.7
Ba	<0.4	9
Te	<0.6	<0.5
Sn	2	0.6
Cd	<0.3	<0.2
Pd	9	<0.1
Sr	<0.1	<0.1
Se	<2	<2
Zn	<0.7	<0.7
Cu	<3	<1
Cr	0.7	76
Mg	<0.1	4
External standard in Ni		
Au	<2	<2
Pt	<0.8	17
Co	<4	<4
Mn	0.4	9
Ca	<4	<4
Al	4	11

nickel material doped with 0.1% of natural Pb, Au, Pt, Ba, Cd, Pb, Zn, Cu, Co, Fe, Mn, Cr, Ca, Al, and Mg, and then cleaned up with the same separation procedure developed for the separated nickel isotopes. The pure nickel was analyzed by a combination of stable isotope dilution and comparison to an external standard. The doped and cleaned sample was analyzed only by comparison to the external standard. The external standard was made by adding 10 ppm (10 $\mu\text{g/g}$ Ni) of each of the doping elements to the pure nickel solution, thus producing a matrix matched standard.

2.4 Assay of Separated Isotope Solutions

Four weighed portions containing approximately 1.7 mmol of nickel were withdrawn from each separated isotope solution in the following manner: a polyethylene stopper with a 20-cm Teflon needle inserted through it was used to replace the cap on the bottle. A 20-mL all polypropylene—polyethylene syringe was attached to the hub of the needle and the desired amount of solution was withdrawn. The syringe was then disconnected from the hub and the tip was capped with a plastic cap. Any static charge that might be

present on the plastic syringe was dissipated by wiping it with a damp lintless towel and placing it on the balance pan that was surrounded by several polonium anti-static sources. The syringe and contents were weighed on a semimicro balance to ± 0.02 mg. The solution was then delivered from the syringe into a 600-mL pyrex beaker and the syringe was again capped, wiped and weighed. The weight of the sample was determined from the weight of the syringe before and after the delivery of the sample. Two assay samples were withdrawn from each solution before after the calibration samples and two after to ensure that no change in concentration occurred during the time interval (about 6 h) required for the aliquanting. Each weighed sample was assayed as follows: the sample was evaporated to dryness and converted to the chloride by adding 10 mL of 4 mol/L HCl and evaporating slowly to dryness. The addition of 10 mL of 4 mol/L HCl and the evaporation were repeated two more times. Two g of 4 mol/L HCl, 4 g of ammonium citrate solution (prepared by dissolving 25 g of $(\text{NH}_4)_2\text{HC}_2\text{H}_3\text{O}_7$ in 200 mL of water, filtering and diluting with water to 250 mL) and 250 mL of water were added to the sample. A weighed portion of dimethylglyoxime reagent solution (prepared by dissolving 10 g of dimethylglyoxime in n-propanol, filtering and diluting with n-propanol to 1 L) equal to the amount required to form nickel dimethylglyoxime and 10 g excess was added to each assay sample. Ten g of dimethylglyoxime reagent solution and 30 g of n-propanol were added to each blank. The sample was heated in a water bath maintained at 65 ± 2 °C. Five drops of 4 mol/L NH_4OH were added, the sample was stirred with a glass stirring rod and after 5 min the addition of ammonia and stirring were repeated. The addition of 4M NH_4OH was repeated, gradually increasing the number of drops to ten, until the Ni was completely precipitated as determined by the solution remaining colorless with the addition of NH_4OH . Three more additions of ten drops of ammonia were made to ensure the precipitation of the nickel. The sample was removed from the water bath 30 min after the last ammonia addition. A total time of approximately 3 h was required for the precipitation. The nickel dimethylglyoxime crystals that are formed by this procedure are relatively large when compared to the usual method of precipitation.

The sample was allowed to stand approximately 48 h and then was filtered through a tared 15 mL glass filtering crucible of medium porosity. As much of the nickel dimethylglyoxime crystals as

possible was transferred to the crucible using a water wash. The material in the crucible was washed three times with water (a total of 55–60 g of water was used for transfer and washing). The crucible and contents were dried at 150 °C for 16 h. The filtrate was transferred back to the original beaker and reserved for the determination of dissolved and untransferred nickel.

The filtering crucible and contents were cooled in a desiccator, transferred to the case of a microbalance and allowed to stand for at least 2 h. The crucible and contents were weighed to ± 0.002 mg. A combination blank and buoyancy correction was made by averaging three crucibles that had been used to filter blank samples which had been carried through the procedure. The crucible and contents were dried an additional 3 h at 150 °C and the cooling and weighing were repeated. The additional drying, cooling and weighing were repeated until constant weight was reached. The air weight of the nickel dimethylglyoxime was then determined and converted to vacuum weight using 1.606 for the density of $^{58}\text{NiC}_8\text{H}_{14}\text{O}_4\text{N}_4$, 1.617 for the density of $^{60}\text{NiC}_8\text{H}_{14}\text{O}_4\text{N}_4$, and 1.628 for the density of $^{62}\text{NiC}_8\text{H}_{14}\text{O}_4\text{N}_4$. These densities were calculated by assuming that they were proportional to the density of natural $\text{NiC}_8\text{H}_{14}\text{O}_4\text{N}_4$, 1.611, in the same relationship as their molecular weight. The vacuum weight of the nickel dimethylglyoxime was converted to millimoles of nickel using a calculated atomic weight for nickel and the 1987 atomic weight values for carbon, hydrogen, oxygen, and nitrogen. The formula weights used were 288.1616 for the $^{58}\text{NiC}_8\text{H}_{14}\text{O}_4\text{N}_4$, 290.1511 for $^{60}\text{NiC}_8\text{H}_{14}\text{O}_4\text{N}_4$, and 292.1279 for $^{62}\text{NiC}_8\text{H}_{14}\text{O}_4\text{N}_4$.

The filtrate from the precipitation of the $^{62}\text{NiC}_8\text{H}_{14}\text{O}_4\text{N}_4$ was spiked with approximately 0.5 μmol of ^{60}Ni and the filtrate from the ^{58}Ni and ^{60}Ni precipitation were spiked for determining soluble and untransferred nickel by isotope dilution mass spectrometry with approximately 0.5 μmol of ^{62}Ni . After adding the spike, the pH of the filtrate solution was adjusted to 1.65 ± 0.05 with 4 mol/L HCl. The solution was heated for 2 h to ensure equilibration of the spike and sample nickel. After cooling, this solution was passed through a cation exchange column (7.0 \times 0.45 cm filled to 4.5 cm with AG 50 \times 8, 100–200 mesh cation exchange resin and cleaned with 25 g of 4 mol/L HCl and H_2O until the eluate was neutral), washed with a few mL of H_2O and then 150 mL of 0.25 mol/L HCl. The nickel was eluted with 18 g of 4 mol/L HCl and the eluate was evaporated to dryness on a hot

plate. A few drops of HNO_3 and HClO_4 were added to the residue and it was heated to help decompose the organic material. The sample was evaporated to dryness, cooled and the residue dissolved in 10 g of H_2O . This solution was passed through the same cation exchange column after cleaning the column as before and washed with a few mL of H_2O and 20 g of 0.25 mol/L HCl. The nickel was eluted with 18 g of 4 mol/L HCl and the eluate was evaporated to dryness on a hot plate. A few drops of HNO_3 and HClO_4 were added to the residue and it was heated to dryness. The residue was dissolved in a few drops of HNO_3 (1+49) and the nickel isotopic ratios were determined by thermal ionization mass spectrometry. The nickel found as soluble Ni was added to the nickel determined by gravimetry to yield the total nickel in the sample. Table 3 shows the results of these analyses.

This method of determining the concentration of nickel solutions was previously tested on solutions containing known amounts of nickel. Solutions were prepared from high purity nickel metal. The nickel concentration in five sets of four samples, each containing 1.58 to 1.79 mmol of nickel was determined as described above. Comparison of the calculated and measured concentrations detected a positive bias of about 0.03 percent, but this would have a negligible effect on ratios.

2.5 Isotopic Analysis of the Separated Isotope Solutions

Each of the three separated isotope solutions was analyzed eight times by operator #1 on instrument #1. The ion source was cleaned between analyses of the solutions as a precaution against the possibility of cross-contamination from the source parts. Preliminary measurements showed that the different separated isotope solutions could be analyzed back-to-back on the same source with no detectable cross-contamination.

As mentioned in section 2.1, preliminary measurements to evaluate possible sources of systematic errors indicated that a small natural nickel background could be present on some filaments. Acid leaching of the filaments and optimized filament outgassing procedures minimized the magnitude and frequency of this problem. This optimization was achieved by monitoring the ^{58}Ni on increasingly smaller sample sizes of the ^{60}Ni separated isotope, and measuring the nickel signal from filaments cleaned and degassed under various conditions using an ion counting detection system.

Table 3. Concentration of nickel in separated isotope solutions

Solution	Sample no.	Weight NiDMG ^a (g)	Ni from NiDMG (mmol)	Ni from filtrate (mmol)	Total Ni (mmol)	Weight sample (g)	Concentration (mmol Ni/g)
"Ni-58"	1	0.487793	1.692775	0.000444	1.693219	19.64900	0.0861733
	2	0.492528	1.709207	0.000480	1.709687	19.83881	0.0861789
	3	0.486624	1.688720	0.000494	1.689214	19.60097	0.0861801
	4	0.488016	1.693550	0.000544	1.694094	19.65837	0.0861767
						Total	0.0861773
					SD	0.0000030	
"Ni-60"	1	0.506874	1.746931	0.000449	1.747380	20.31729	0.0860046
	2	0.497094	1.713225	0.000559	1.713784	19.92565	0.0860089
	3	0.501435	1.728185	0.000451	1.728636	20.09839	0.0860087
	4	0.599604	1.725323	0.000563	1.725323	20.06610	0.0860100
						Total	0.0860081
					SD	0.0000024	
"Ni-62"	1	0.509754	1.744969	0.000397	1.745366	101.53728	0.01711267
	2	0.512447	1.754186	0.000465	1.754651	102.53728	0.01711232
	3	0.510848	1.748713	0.000458	1.749171	102.21630	0.01711245
	4	0.511917	1.752374	0.000497	1.752871	102.43149	0.01711264
						Total	0.01711253
					SD	0.00000017	

^a NiDMG = nickel dimethylglyoxime.

All filaments used for measurement of the separated isotopes were examined in the mass spectrometer prior to sample loading. In addition to monitoring all nickel masses for contamination, ⁵⁶Fe and ⁶⁶Zn were examined to insure the absence of isobaric interferences. Only those filaments which showed no detectable ($<1 \times 10^{-16}$ A) signal were used for the measurement of the separated isotopes.

The corrected isotopic compositions of the separated isotopes are given in Table 4.

2.6 Preparation of Calibration Samples

Five calibration samples were prepared by mixing weighed portions of "Ni-58", "Ni-60", and "Ni-62" solutions. The portions were withdrawn from the bottles and weighed in the manner previously described for the assay of the solutions. The portions weighed from 4.9 to 110 g and each was weighed to ± 0.05 mg. It is therefore estimated that the weighing error for each mix should not exceed two parts in 10^5 . To minimize any significant possibility of change in concentration of the isotope solutions with time, the portions for the calibration mixes were withdrawn from the bottles between the samples taken for assay, over a period of about 6 h.

Each calibration mix was thoroughly mixed, the sides of the beaker were washed with H₂O and 0.3

mol/L HNO₃ and evaporated to dryness on a hot plate. The residue was dissolved and diluted with HNO₃ (1+49) to 5 mg Ni per gram of solution. After thorough mixing, a portion of this solution was diluted with HNO₃ (1+49) to 1 mg Ni per gram of solution and transferred to a small Teflon bottle. The isotopic compositions of the calibration mixes are given in table 5.

Table 4. Isotopic composition of separated nickel isotopes used in calibration samples

Separated isotope	Isotopic composition		
	Atom percent	2-sigma uncertainty	
"Ni-58"	58	99.873684	0.000478
	60	0.116721	0.000308
	61	0.002126	0.000156
	62	0.005364	0.000238
	64	0.002105	0.000164
"Ni-60"	58	0.226876	0.000700
	60	99.702709	0.001176
	61	0.027175	0.000528
	62	0.033806	0.000256
	64	0.009434	0.000456
"Ni-62"	58	0.355954	0.000454
	60	0.478222	0.000698
	61	0.096433	0.000438
	62	99.007380	0.001272
	64	0.062011	0.000152

Table 5. Isotopic composition of calibration samples

Solution no.	Isotope solution	Weight solution (g)	Ni				Total ⁵⁸ Ni (mmol)	Total ⁶⁰ Ni (mmol)	Total ⁶² Ni (mmol)	Ratio ⁵⁸ Ni/ ⁶⁰ Ni	Ratio ⁶² Ni/ ⁶⁰ Ni
			from solution (mmol)	⁵⁸ Ni from solution (mmol)	⁶⁰ Ni from solution (mmol)	⁶² Ni from solution (mmol)					
1	"Ni-58"	19.16757	1.651809	1.649723	0.001928	0.000089	1.651439	0.622292	0.085107	2.653798	0.136764
	"Ni-60"	7.22959	0.621803	0.001411	0.619955	0.000210					
	"Ni-62"	5.00563	0.085659	0.000305	0.000410	0.084809					
2	"Ni-58"	18.41320	1.586800	1.584795	0.001852	0.000085	1.586476	0.605063	0.086241	2.622002	0.142532
	"Ni-60"	7.02949	0.604593	0.001372	0.602796	0.000204					
	"Ni-62"	5.07309	0.086813	0.000309	0.000415	0.085951					
3	"Ni-58"	18.46549	1.591306	1.589296	0.001857	0.000085	1.590991	0.613132	0.085139	2.594858	0.138859
	"Ni-60"	7.12359	0.612686	0.001390	0.610865	0.000207					
	"Ni-62"	5.00786	0.085697	0.000305	0.000410	0.084846					
4	"Ni-58"	18.42601	1.587904	1.585898	0.001853	0.000085	1.587603	0.619467	0.083950	2.562852	0.135520
	"Ni-60"	7.19758	0.619050	0.001404	0.617210	0.000209					
	"Ni-62"	4.93759	0.084494	0.000301	0.000404	0.083656					
5	"Ni-58"	18.11755	1.561322	1.559349	0.001822	0.000084	1.561054	0.615253	0.086466	2.537254	0.140536
	"Ni-60"	7.14866	0.614843	0.001395	0.613015	0.000208					
	"Ni-62"	5.08622	0.087038	0.000310	0.000416	0.086174					

2.7 Isotopic Analyses of the Calibration Mixes and the Reference Sample

Two sets of analyses of the calibration mixes and reference sample were performed on instrument #1 and instrument #2. Instrument #1 was used to measure 28 samples of the reference material and 4 samples each of mixes 1–5. Instrument #2 was used to measure 21 samples of the reference material and 6 samples of mixes 1–5. The samples were analyzed in a random pattern of mixes and the reference sample. Deviations from a totally random pattern were the initial successive analyses of the reference material to insure instrument and statistical control and the requirement that the same mix solution not be analyzed in succession.

3. Results and Discussion

The results of the measurements of the calibration mixes are shown in Table 6. Table 7 summarizes the observed and corrected nickel isotopic ratios for the reference sample for operators 1 and 2 respectively, as well as the absolute isotopic abundance ratios for nickel and their uncertainties.

Table 8 gives summary calculations for the reference sample. The atomic weight is calculated from the absolute isotopic abundance by summing the product of the nuclidic masses [17] and the corresponding atom fractions.

As mentioned in the introduction, the presently recommended atomic weight of nickel is 58.69 ± 0.01 . The IUPAC Commission on Atomic

Table 6. Determination of mass spectrometer bias

Calibration sample no.	Calculated		Isotopic ratios				Correction factors			
	⁵⁸ Ni/ ⁶⁰ Ni	⁶² Ni/ ⁶⁰ Ni	Operator 1		Operator 2		Operator 1		Operator 2	
			⁵⁸ Ni/ ⁶⁰ Ni	⁶² Ni/ ⁶⁰ Ni	⁵⁸ Ni/ ⁶⁰ Ni	⁶² Ni/ ⁶⁰ Ni	⁵⁸ Ni/ ⁶⁰ Ni	⁶² Ni/ ⁶⁰ Ni	⁵⁸ Ni/ ⁶⁰ Ni	⁶² Ni/ ⁶⁰ Ni
1	2.653798	0.136764	2.695878	0.134686	2.694002	0.134730	0.984391	1.015430	0.985077	1.015102
2	2.622002	0.142532	2.663804	0.140356	2.659318	0.140512	0.984307	1.015506	0.985968	1.014378
3	2.594858	0.138859	2.635760	0.136696	2.633919	0.136854	0.984483	1.015826	0.985170	1.014651
4	2.562852	0.135520	2.604370	0.133421	2.600775	0.133575	0.984056	1.015734	0.985419	1.014563
5	2.537254	0.140536	2.577182	0.138349	2.575263	0.138502	0.984508	1.015817	0.985241	1.014687
Average correction factors							0.984349	1.015663	0.985375	1.014676
Correction factor standard deviations							0.000182	0.000183	0.000354	0.000267

Table 7. Corrected isotopic ratios of the SRM

Ratio	Operator 1	Operator 2	Average ratio
$^{58}\text{Ni}/^{60}\text{Ni}$	2.5961255	2.5959968	2.5960612
$^{61}\text{Ni}/^{60}\text{Ni}$	0.0434680	0.0434703	0.0434691
$^{62}\text{Ni}/^{60}\text{Ni}$	0.1385976	0.1386025	0.1386001
$^{64}\text{Ni}/^{60}\text{Ni}$	0.0353113	0.0352784	0.0352949

Table 8. Atomic weight, atom percent, and isotopic ratios of nickel

	Value	Total uncertainty (2-sigma)	Due to uncertainty in assay (2-sigma)	Due to uncertainty in mass spectrometry (2-sigma)	Due to uncertainty in mix preparation (2-sigma)	Due to uncertainty in nuclidic mass (2-sigma)
Atomic weight	58.693353	0.000147	0.000091	0.000104	0.000049	0.000002
Atom percent						
^{58}Ni	68.076886	0.005919	0.004045	0.003762	0.002125	
^{60}Ni	26.223146	0.005144	0.003776	0.002724	0.002186	
^{61}Ni	1.139894	0.000433	0.000138	0.000402	0.000083	
^{62}Ni	3.634528	0.001142	0.000615	0.000817	0.000508	
^{64}Ni	0.925546	0.000599	0.000317	0.000420	0.000287	
Isotopic ratios						
$^{58}\text{Ni}/^{60}\text{Ni}$	2.596061	0.000728	0.000525	0.000410	0.000293	
$^{61}\text{Ni}/^{60}\text{Ni}$	0.043469	0.000015	0.000004	0.000014	0.000004	
$^{62}\text{Ni}/^{60}\text{Ni}$	0.138600	0.000045	0.000028	0.000025	0.000025	
$^{64}\text{Ni}/^{60}\text{Ni}$	0.035295	0.000024	0.000014	0.000015	0.000013	

Weights and Isotopic Abundances lists this as one of the least well known atomic weights and also one of the few remaining elements where the atomic weight is based, at least in part, on chemical determinations made in the early 1920s. Based on this work, a value of 58.6934 ± 0.0002 will be recommended which is two orders of magnitude more precise and, more importantly, is now known on an absolute scale.

The reference material is issued by the NIST Office of Standard Reference Materials as SRM 986, Nickel Metal Isotopic Standard, and is certified for isotopic composition.

4. Acknowledgments

We are greatly indebted to Keith R. Eberhardt and Susannah B. Shiller of the Statistical Engineering Division, who spent more time than they had available on the statistical analysis of the data and to William A. Bowman III, Ronald W. Shideler, and the late George M. Lambert for instrumental

maintenance support. We are especially grateful to Professor John De Laeter of Curtin University who shared with us his experiences and those of his colleagues with the Aerosil procedure and provided the material used in this research.

About the authors: J. W. Gramlich was associated with the High Accuracy Measurement Program in the Inorganic Analytical Research Division of NBS for many years as a research chemist. He is currently with the U.S. Department of Energy, New Brunswick Laboratory, Argonne IL 60439. L. A. Machlan was associated as a research chemist with the Atomic Weights Program in the Inorganic Analytical Research Division of NBS for many years. He is currently retired but continues to serve NIST as a contractor. I. L. Barnes is a research chemist with the Inorganic Analytical Research Division in the NIST Center for Analytical Chemistry. P. J. Paulsen is a research chemist in the Inorganic Analytical Research Division in the NIST Center for Analytical Chemistry.

5. References

- [1] Shields, W. R., Garner, E. L., and Dibeler, V. H., *J. Res. Natl. Bur. Stand. (U.S.)* **66A**, 1 (1962).
- [2] Powell, L. J., Murphy, T. J., and Gramlich, J. W., *J. Res. Natl. Bur. Stand. (U.S.)* **87**, 9 (1982).
- [3] Shields, W. R., Murphy, T. J., Garner, E. L., and Dibeler, V. H., *J. Amer. Chem. Soc.* **84**, 1519 (1962).
- [4] Shields, W. R., Murphy, T. J., and Garner, E. L., *J. Res. Natl. Bur. Stand. (U.S.)* **68A**, 589 (1964).
- [5] Catanzaro, E. J., Murphy, T. J., Garner, E. L., and Shields, W. R., *J. Res. Natl. Bur. Stand. (U.S.)* **68A**, 593 (1964).
- [6] Shields, W. R., Murphy, T. J., Catanzaro, E. J., and Garner, E. L., *J. Res. Natl. Bur. Stand. (U.S.)* **70A**, 193 (1966).
- [7] Catanzaro, E. J., Murphy, T. J., Garner, E. L., and Shields, W. R., *J. Res. Natl. Bur. Stand. (U.S.)* **70A**, 453 (1966).
- [8] Catanzaro, E. J., Murphy, T. J., Shields, W. R., and Garner, E. L., *J. Res. Natl. Bur. Stand. (U.S.)* **72A**, 261 (1968).
- [9] Catanzaro, E. J., Champion, C. E., Garner, E. L., Marinenko, G., Sappenfield, K. M., and Shields, W. R., *Natl. Bur. Stand. (U.S.) Spec. Publ. 260-17*; 1970 February, 60 pp.
- [10] Catanzaro, E. J., Murphy, T. L., Garner, E. L., and Shields, W. R., *J. Res. Natl. Bur. Stand. (U.S.)* **73A**, 511 (1969).
- [11] Gramlich, J. W., Murphy, T. J., Garner, E. L., and Shields, W. R., *J. Res. Natl. Bur. Stand. (U.S.)* **77A**, 691 (1973).
- [12] Barnes, I. L., Moore, L. J., Machlan, L. A., Murphy, T. J., and Shields, W. R., *J. Res. Natl. Bur. Stand. (U.S.)* **79A**, 727 (1975).
- [13] Garner, E. L., Murphy, T. J., Gramlich, J. W., Paulsen, P. J., and Barnes, I. L., *J. Res. Natl. Bur. Stand. (U.S.)* **79A**, 713 (1975).
- [14] Dunstan, L. P., Gramlich, J. W., Barnes, I. L., and Purdy, W. C., *J. Res. Natl. Bur. Stand. (U.S.)* **85**, 1 (1980).
- [15] Moore, L. J., Murphy, T. J., and Barnes, I. L., *J. Res. Natl. Bur. Stand. (U.S.)* **87**, 1 (1982).
- [16] Machlan, L. A., Gramlich, J. W., Powell, L. J., and Lambert, G. M., *J. Res. Natl. Bur. Stand. (U.S.)* **91**, 323 (1986).
- [17] Wapstra, A. H., and Audi, G., *Nucl. Phys.* **A432**, 1 (1985).
- [18] White, J. R., and Cameron, A. E., *Phys. Rev.* **74**, 991 (1948).
- [19] Baxter, G. P., and Parsons, L. W., *J. Amer. Chem. Soc.* **43**, 507 (1921).
- [20] Baxter, G. P., and Hilton, F. A., Jr., *J. Amer. Chem. Soc.* **45**, 694 (1923).
- [21] Baxter, G. P., and Ishimaru, S., *J. Amer. Chem. Soc.* **51**, 1729 (1929).
- [22] Baxter, G. P., and Dorcas, M. J., *J. Amer. Chem. Soc.* **46**, 357 (1924).
- [23] Barnes, I. L., Garner, E. L., Gramlich, J. W., Machlan, L. A., Moody, J. R., Moore, L. J., Murphy, T. J., and Shields, W. R., *Geochim. Cosmochim. Acta Suppl.* **4**, 2, 1197 (1973).
- [24] Atomic weights of the elements 1987. *Pure Appl. Chem.* **60**, 841 (1988).
- [25] Peiser, H. S., *Anal. Chem.* **57**, 511A (1985).
- [26] Kuehner, E. C., Alvarez, R. A., Paulsen, P. J., and Murphy, T. J., *Anal. Chem.* **44**, 2050 (1972).
- [27] Shideler, R. W., and Gramlich, J. W., in preparation.

The Absolute Isotopic Composition and Atomic Weight of Terrestrial Nickel

Volume 94

Number 6

November–December 1989

**J. W. Gramlich, E. S. Beary,
L. A. Machlan, and I. L. Barnes**

National Institute of Standards
and Technology,
Gaithersburg, MD 20899

Twenty-nine samples of high-purity nickel metals, reagent salts and minerals, collected from worldwide sources, have been examined by high-precision isotope ratio mass spectrometry for their nickel isotopic composition. These materials were compared directly with SRM 986, certified isotopic standard for nickel, using identical measurement techniques and the same instrumentation. This survey shows no statistically significant variations among the samples investigated, indicating that the certified atomic weight and associated uncer-

tainty for SRM 986 is applicable to terrestrial nickel samples. The atomic weight calculated for SRM 986 is 58.69335 ± 0.00015 [2]. The currently recommended IUPAC value for terrestrial nickel is 58.69 ± 0.01 .

Key words: absolute ratio; atomic weight; isotopic abundance; mass spectrometry; nickel; SRM 986; Standard Reference Materials; terrestrial samples.

Accepted: September 1, 1989

1. Introduction

For several decades, the Inorganic Analytical Research Division of the National Institute of Standards and Technology has conducted a continuing program of absolute isotopic abundance and atomic weight determinations using high-precision isotope ratio mass spectrometry. Although this program has yielded extremely accurate atomic weights for reference samples, the uncertainty associated with a generally useful atomic weight is limited by the isotopic variations among materials readily available to the scientific community or by a lack of knowledge regarding such variations. This work compares the isotopic composition and atomic weight of nickel from a global population of terrestrial nickel sources, and samples that have been purified industrially into nickel metal and reagent salts, to a Standard Reference Material (SRM 986) of accurately known isotopic composition and atomic weight [1]. This reference sample

is pure nickel powder, lot F-3625 obtained from Atomergic Chemicals Corporation¹ and is available from the Office of Standard Reference Materials at NIST.

2. Experimental Procedure

2.1 Chemical Purification of the Samples

Nickel ores, such as niccolite, linnaeite, gersdorffite, and carrollite, were obtained from the U.S. National Museum. These samples were representative of ores from mines in North America, South

¹ Certain commercial equipment, instruments, or materials are identified in this paper to specify adequately the experimental procedure. Such identification does not imply recommendation or endorsement by the National Institute of Standards and Technology, nor does it imply that the materials or equipment identified are necessarily the best available for the purpose.

America, Europe, Asia, and Africa (table 1). Also listed in table 1 are commercially purified nickel metal and nickel compounds from European and American sources which were procured for this study. The reagent nickel compounds required little pretreatment, while the ores required extensive chemical separations to obtain nickel essentially free of contamination, as required for this high-precision mass spectrometric technique.

Samples of nickel ore weighing 200–600 mg were treated with about 10 g of aqua regia (3:1 HCl, HNO₃), covered and heated until the reaction subsided. Although some undissolved material remained, the samples were evaporated to dryness, and then taken up in 10 g of HCl (1+2). The samples were then filtered into 400-mL beakers and the precipitate was discarded. Ten to fifteen g of ammonium citrate solution (400 g/L) were added to each sample filtrate to complex the Fe, and the resulting mixture was diluted to 250 mL. Thirty-five g of 1% dimethylglyoxime solution in *n*-propanol were added to each beaker and heated slowly to about 70 °C while adding NH₄OH until the pH was between 8 and 9. The samples were heated for 30 min while maintaining the temperature at 70 °C, then cooled and filtered. The precipitate was redissolved in 4 g HNO₃ (1+3), covered and heated until all the nickel dimethylglyoxime was dissolved. Twenty-five g of water were added to the samples as a preparation for cation exchange chromatography. Five mL of AG 50×8, 100–200 mesh cation exchange resin were placed in plastic columns about 1 cm in diameter, and the resin was cleaned using 25 g of 3 *N* HNO₃ and then H₂O until the eluate was neutral. After the sample was loaded onto the column the impurities were eluted using 25 g of 0.3 *N* HNO₃. The Ni was eluted with 15 g of 3 *N* HNO₃, and evaporated to a small volume (about 1 mL). Four g of 9 *N* HCl were added as a preparation for anion exchange chromatography. Five mL of AG 1×8, 100–200 mesh anion exchange resin was added to plastic columns 1 cm in diameter, and the resin was cleaned using 9 *N* HCl, then neutralized with water. The Ni was eluted using 12–15 g of 9 *N* HCl, while impurities remained on the column. The purified Ni solution was evaporated to dryness and redissolved in 4 g of 5 *N* HCl. The dissolved sample was then diluted to a 35-mL volume and neutralized with NH₄OH, followed by 2 mL excess NH₄OH. This solution was then electrolyzed at 2–2.5 V using platinum gauze electrodes until the Ni color disappeared from the solution. The electrode with the Ni deposit was removed from the solution and rinsed with H₂O,

allowed to air dry, and the electrode was weighed. The Ni was removed using concentrated HNO₃, and the electrode was air dried and reweighed. Typically, 50–150 mg of Ni metal were recovered from each ore. Sample solutions using the purified Ni were prepared in HNO₃ (1+49), at a concentration of 1 mg Ni/g.

The four nickel metal samples and four nickel compounds were simply dissolved, converted to the nitrate, and sample solutions were prepared as 1 mg Ni/g in HNO₃.

2.2 Mass Spectrometry

Isotope ratio measurements were performed on the same NIST designed mass spectrometer that was used to determine the absolute isotopic abundance and atomic weight of a reference sample of nickel (SRM 986) [1]. The measurements on terrestrial nickel materials, reported in this paper, were conducted in conjunction with, but following the mass spectrometric measurement associated with the certification of SRM 986. Analyses of SRM 986 that were used to assure measurement control and to correct for isotopic fractionation in this experiment, were also used in the calculations used to certify SRM 986. The bias-corrected isotopic ratios reported in this paper are thus based on the extensive measurements made on SRM 986 both to certify the SRM and in this work.

Samples containing approximately 5 μg of nickel (as NiNO₃ in 2% HNO₃) were loaded onto a platinum filament with a mixture of silica gel- AlCl₃-H₃PO₄ as an ionization enhancement agent. Samples were analyzed by thermal ionization mass spectrometry using procedures and parameters identical to those used for the certification of SRM 986. The details of filament preparation, sample loading and the analysis procedures have been published [1].

3. Results and Discussion

The corrected abundance ratios for the 29 samples are given in table 2. The same correction factors as used for SRM 986 were used. In the design of the survey both mineral type and geographic origin were considered to obtain the widest possible distribution.

The isotopic abundances reported in this work indicate no significant trend or variation in the isotopic composition of nickel in terrestrial sources.

Table 1. Nickel reagent-mineral survey (description of samples)

NIST no.	Description of sample	Source
0	NIST SRM 986 (reference sample)	
1	Linnaeite (with tetrahedraite) U.S. Natl. Museum no. B2981	Schwabengrobe (near Mussen), Germany
2	Millerite U.S. Natl. Museum no. 66501	Gap Mine, Lancaster County, PA
3	Pentlandite U.S. Natl. Museum no. 96387	Worthington Mine, Sudbury, Canada
4	Gersdorffite U.S. Natl. Museum no. 113044	Temagamy Island, Ontario, Canada
5	Gersdorffite U.S. Natl. Museum no. B3310	Merkur Mine, Ems, Germany
6	Carrollite U.S. Natl. Museum no. 122349	Kambove, Congo
7	Rammelsbergite U.S. Natl. Museum no. C693	Eisleben, Saxony, Germany
8	Gersdorffite U.S. Natl. Museum no. 120381	Ait Ahmane, Bou Azzer, Morocco
9	Millerite (with gaspeite and polydimitite) U.S. Natl. Museum no. 121729	Pqfuri Native Trust, Transvaal, S. Africa
10	Millerite U.S. Natl. Museum no. B1596	Victoria Mine, Littfeld, Germany
11	Millerite U.S. Natl. Museum no. 113065	Temagami, Ontario, Canada
12	Niccolite (and vaesite) U.S. Natl. Museum no. 86655	Green-Meehan Mine, Cobalt, Ontario, Canada
13	Niccolite U.S. Natl. Museum no. 105150	Alistos, Sinaloa, Mexico
14	Niccolite U.S. Natl. Museum no. 121284	Iran
15	Niccolite and Chalcantite U.S. Natl. Museum no. 103642	Schneeberg, Saxony, Germany
16	Siegenite U.S. Natl. Museum no. B3169	Schwaben Mine, Siegerland, Germany
17	Niccolite (with rammelsbergite) U.S. Natl. Museum no. 114458	La Sorpresa Mine, Tapacari, Bolivia
18	Rammelsbergite U.S. Natl. Museum no. 117334	Mohawk #2 Mine, Keweenaw County, Michigan
19	Rammelsbergite U.S. Natl. Museum no. 94556	Hudson Bay Mine, Cobalt, Ontario, Canada
20	Heazlewoodite U.S. Natl. Museum no. 115427	Lord Brassey Mine, Heazlewood, Tasmania
21	Pentlandite in Pyrrhotite U.S. Natl. Museum no. R11297	Stare Ransko Near-Chotebor, Bohemia, Czechoslovakia
22	Linnaeite U.S. Natl. Museum no. 96797	Mineral Hill Mine, Sykesville, Maryland
23	NIST SRM 772 (magnetic moment std.) Ni metal, 99.999% pure	Leico Industries Inc., New York, NY 10019
24	Ni metal, wire	Jarrell Ash
25	Ni metal, rod lot no. 02801	Spex
26	NiO, 99.999% pure lot no. N121G0541	Atomergic Chemicals, Inc.
27	NiCl ₂ ·6H ₂ O lot no. 634B740817	Merck
28	NiCl ₂ ·6H ₂ O lot no. 631216/1	Union Chimique, Belge, SA
29	NiSO ₄ ·6H ₂ O lot no. 1453	Union Chimique, Belge, SA

Table 2. Isotope ratios for the mineral samples corrected to SRM 986

No.	Identification	$^{58}\text{Ni}/^{60}\text{Ni}$	$^{61}\text{Ni}/^{60}\text{Ni}$	$^{62}\text{Ni}/^{60}\text{Ni}$	$^{64}\text{Ni}/^{60}\text{Ni}$
1	SI-B2981	2.596679	0.043485	0.138603	0.035355
2	SI-66501	2.596233	0.043458	0.138551	0.035327
3	SI-96387	2.596016	0.043460	0.138632	0.035327
4	SI-113044	2.596500	0.043472	0.138551	0.035359
5	SI-B3310	2.595810	0.043469	0.138649	0.035352
6	SI-122349	2.596492	0.043473	0.138555	0.035282
7	SI-C693	2.596163	0.043451	0.138559	0.035295
8	SI-120381	2.596368	0.043470	0.138571	0.035308
9	SI-121729	2.595924	0.043463	0.138598	0.035286
10	SI-B1596	2.596326	0.043469	0.138597	0.035326
11	SI-113065	2.596410	0.043493	0.138616	0.035338
12	SI-86655	2.596075	0.043468	0.138628	0.035293
13	SI-105150	2.596513	0.043467	0.138584	0.035331
14	SI-121284	2.596502	0.043477	0.138634	0.035301
15	SI-103642	2.596470	0.043469	0.138607	0.035337
16	SI-B3169	2.596537	0.043458	0.138604	0.035339
17	SI-114458	2.596135	0.043460	0.138559	0.035290
18	SI-117334	2.596225	0.043461	0.138599	0.035326
19	SI-94556	2.596113	0.043458	0.138603	0.035293
20	SI-115427	2.596205	0.043486	0.138602	0.035368
21	SI-R11297	2.596508	0.043451	0.138625	0.035358
21	SI-R11297	2.595943	0.043479	0.138570	0.035305
22	SI-96797	2.596204	0.043478	0.138595	0.035320
22	SI-96797	2.595841	0.043478	0.138556	0.035353
23	SRM 772	2.595992	0.043487	0.138606	0.035338
24	Jarrell Ash	2.595953	0.043487	0.138617	0.035329
25	Spex Ni rod	2.595996	0.043478	0.138634	0.035322
26	Atomergic	2.596071	0.043467	0.138615	0.035324
27	NiCl ₂ ·6H ₂ O	2.596036	0.043479	0.138614	0.035320
28	NiCl ₂ ·6H ₂ O	2.596096	0.043476	0.138589	0.035319
29	NiSO ₄ ·6H ₂ O	2.596310	0.043480	0.138587	0.035319

To evaluate formally the data for constancy of isotopic composition, we used an analysis of variance (ANOVA) procedure to conduct a statistical test of the hypothesis that the materials have identical isotopic ratios. The ANOVA procedure was carried out in two ways: both including and excluding the SRM 986 data obtained from the two different instruments used in the absolute abundance ratio work. This was done to be sure that any differences between the two instruments would not affect the conclusions.

For each of the four isotope ratios, the ANOVA tests showed that the variability among the measured ratios for the minerals survey samples is never significantly greater than variability of the measurements of the SRM 986 material. Thus, the conclusion of this statistical test is that there is no evidence of real variation in the isotopic ratios for the nickel samples surveyed. The ANOVA results are summarized in Table 3.

Table 3. Results of ANOVA tests of the hypothesis of equality of isotopic ratios for SRM 986 and the other nickel samples

Isotope ratio	ANOVA <i>F</i> -ratio	Significance probability ^a
All data (including instrument #2):		
$^{58}\text{Ni}/^{60}\text{Ni}$	0.184	1.00
$^{61}\text{Ni}/^{60}\text{Ni}$	0.067	1.00
$^{62}\text{Ni}/^{60}\text{Ni}$	0.433	0.99
$^{64}\text{Ni}/^{60}\text{Ni}$	1.157	0.32
Instrument #1 data only:		
$^{58}\text{Ni}/^{60}\text{Ni}$	0.113	1.00
$^{61}\text{Ni}/^{60}\text{Ni}$	0.032	1.00
$^{62}\text{Ni}/^{60}\text{Ni}$	0.288	1.00
$^{64}\text{Ni}/^{60}\text{Ni}$	0.649	0.87

^a The significance probability is the probability of obtaining an *F*-ratio as large or larger than the observed value assuming that the null hypothesis (equality of isotope ratios) is true. The results of the ANOVA test are generally considered not to show significant evidence of a difference unless the significance probability is less than 0.05.

Graphical summaries of these results, in a somewhat different form, are shown in figures 1-4. These figures, called "bihistograms," provide a visual comparison of the measured isotope ratio data for the SRM 986 material (as measured by instrument #1, see reference [1]) with the corresponding ratios for the other nickel samples surveyed. In each figure the isotope ratios for SRM 986 are represented in the "upside-down" histogram, with the histogram of the mineral survey ratios shown on

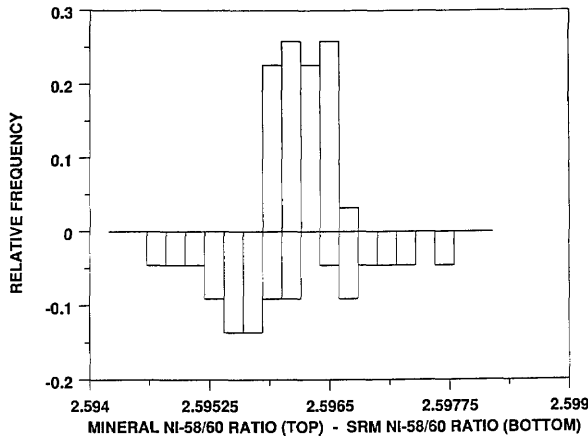


Figure 1. A bihistogram showing the values obtained for the $^{58}\text{Ni}/^{60}\text{Ni}$ ratios (corrected to the absolute values of the ratios obtained for SRM 986) vs those values. Shown on the top is a histogram of the mineral $^{58}\text{Ni}/^{60}\text{Ni}$ ratios and on the bottom (inverted) is a histogram of the same ratios obtained for SRM 986.

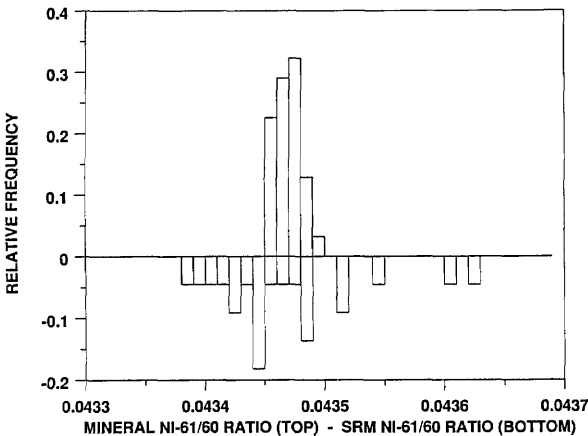


Figure 2. A bihistogram showing the values obtained for the $^{61}\text{Ni}/^{60}\text{Ni}$ ratios (corrected to the absolute values of the ratios obtained for SRM 986) vs those values. Shown on the top is a histogram of the mineral $^{61}\text{Ni}/^{60}\text{Ni}$ ratios and on the bottom (inverted) is a histogram of the same ratios obtained for SRM 986.

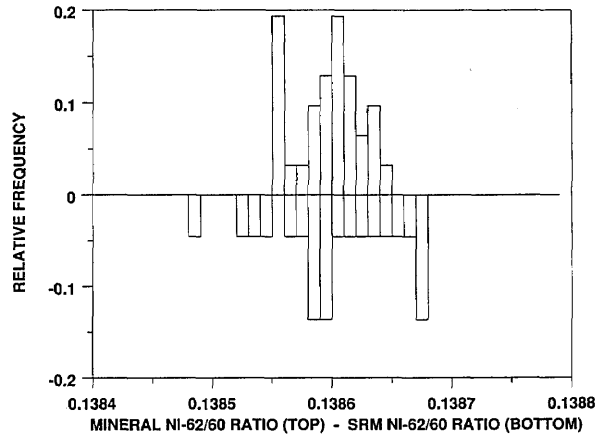


Figure 3. A bihistogram showing the values obtained for the $^{62}\text{Ni}/^{60}\text{Ni}$ ratios (corrected to the absolute values of the ratios obtained for SRM 986) vs those values. Shown on the top is a histogram of the mineral $^{62}\text{Ni}/^{60}\text{Ni}$ ratios and on the bottom (inverted) is a histogram of the same ratios obtained for SRM 986.

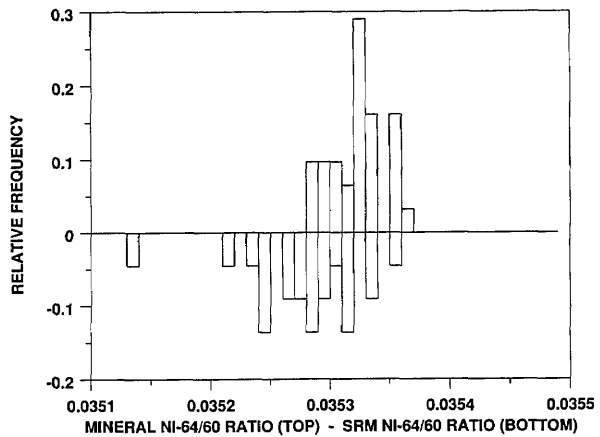


Figure 4. A bihistogram showing the values obtained for the $^{64}\text{Ni}/^{60}\text{Ni}$ ratios (corrected to the absolute values of the ratios obtained for SRM 986) vs those values. Shown on the top is a histogram of the mineral $^{64}\text{Ni}/^{60}\text{Ni}$ ratios and on the bottom (inverted) is a histogram of the same ratios obtained for SRM 986.

top. The SRM 986 data always show at least as much variability as do the mineral survey data. This fact indicates that the observed variation in the survey nickel samples is readily accounted for by measurement variability, and therefore it supports the conclusion that there is no real variation in the isotopic composition of the nickel samples. It appears in these figures that the data for the minerals actually show less variation than that of the SRM. We believe that this is only an indication that

the procedure for the analyses was even more tightly controlled by the time that these samples were analyzed.

Evidence in the literature also indicates no identifiable variations in the atomic weight of nickel among terrestrial sources [2]. However, many of the previous measurements are far less precise than this study, and thus many have not been able to identify small isotopic variations. Further support of isotopic homogeneity is supplied by a limited study of the isotopic composition of lunar samples, directly compared to SRM 986, which also showed no significant variations relative to the SRM [3].

4. Acknowledgments

The authors are indebted to the staff of the U.S. National Museum for assistance in selecting the minerals used in this study. S. Goldich also provided valuable help in the selection of these materials. We gratefully acknowledge the help of Keith Eberhardt of the Statistical Engineering Division with the statistical analysis of the data. We thank W. J. Barnes for his assistance in typing the manuscript.

About the authors: J. W. Gramlich was associated with the High Accuracy Measurement Program in the Inorganic Analytical Research Division of NBS for many years as a research chemist. He is currently with the U.S. Department of Energy, New Brunswick Laboratory, Argonne IL 60439. E. S. Beary is a research chemist with the NIST Inorganic Analytical Research Division in the Center for Analytical Chemistry. L. A. Machlan was associated as a research chemist with the Atomic Weights Program in the Inorganic Analytical Research Division of NBS for many years. He is currently retired but continues to serve NIST as a contractor. I. L. Barnes is a research chemist with the Inorganic Analytical Research Division in the NIST Center for Analytical Chemistry.

5. References

- [1] Gramlich, J. W., Machlan, L. A., Barnes, I. L., and Paulsen, P. J., *J. Res. Natl. Inst. Sci. Technol.* **94**, 347 (1989).
- [2] Element by element review of their atomic weights, *Pure Appl. Chem.* **58**, 695 (1984).
- [3] Barnes, I. L., Garner, E. L., Gramlich, J. W., Machlan, L. A., Moody, J. R., Moore, L. J., Murphy, T. J., and Shields, W. R., *Geochim. Cosmochim. Acta Suppl.* **4**, 2, 1197 (1973).

Special Report on Standards for Radioactivity

*Report on the 1989 Meeting of the
Radionuclide Measurements Section of the
Consultative Committee on Standards for the
Measurement of Ionizing Radiations*

Volume 94

Number 6

November–December 1989

Dale D. Hoppes

National Institute of Standards
and Technology,
Gaithersburg, MD 20899

This report describes the activities discussed at the 10th meeting of Section II of the Consultative Committee on Standards for the Measurement of Ionizing Radiations (Comité Consultatif pour les Etalons de Mesure des Rayonnements Ionisants, CCEMRI) held in May 1989 at Sèvres (France). Topics included present and future international comparisons of activity measurements, the status and possible extension of the International reference system for activity measurements of gamma-ray emitting nuclides, reports from other working groups, accomplishments at the Interna-

tional Bureau of Weights and Measures (Bureau International des Poids et Mesures, BIPM), and progress at member laboratories.

Key words: becquerel; comparisons of activity measurements; ^{109}Cd ; Consultative Committee on Standards for the Measurement of Ionizing Radiations; ^{125}I ; International Reference System for radionuclides; radioactivity standards; ^{75}Se .

Accepted: August 16, 1989

1. Background

One of the consultative committees of the International Committee of Weights and Measures (Comité International des Poids et Mesures, CIPM) which guides and assists the International Bureau of Weights and Measures (Bureau International des Poids et Mesures, BIPM) in ensuring the uniformity of physical measurements is the Consultative Committee on Standards for the Measurement of Ionizing Radiations (Comité Consultatif pour les Etalons de Mesure des Rayonnements Ionisants, CCEMRI) [1]. The variety of measurement types in the field led to the committee being set up with three sections. Section II, with the responsibility for radioactivity measurements, met on March 29–

31, 1989, with selected representatives from 11 countries and the European community laboratory participating.

The challenge in radioactivity standards is as much quantity as quality. Although the accuracy required and achieved for specifying the activity of a sample of a radionuclide is usually only of one percent, a standard must be developed for *each* pertinent radionuclide. Currently the National Institute of Standards and Technology has received justified requests for over 130 radionuclides, for example [2]. There is no official international standard for any radionuclide; rather, the standardizing laboratory in each country develops an appropriate

measuring method which would allow a sample of the particular radionuclide to be measured with a known uncertainty.

Almost all countries have adopted the International System (SI) unit, the becquerel (Bq), specifying the activity of a sample in decays per second (s^{-1}). Goals of the Radionuclides Section of CCEMRI are to improve measuring methods and better define their uncertainties, to compare results obtained in different countries, and to bring these results into congruence. The 10th meeting made considerable progress towards these goals.

2. Section Activities

The agenda of the meeting emphasized actions coordinated through the BIPM, the accomplishments of working groups, and the significant activities of the small BIPM group.

2.1 Comparisons of Activity Measurement

One mechanism with which national standardizing laboratories can compare results for a radionuclide is through simultaneous measurements of quantitative mass aliquants of a common solution. Twenty-eight such comparisons have been completed since 1961. The status of the three following current exercises was reported.

A 1986 comparison of ^{109}Cd had been reported at the previous session in 1987, with satisfactory agreement on the activity [3]. However, 10 of the 18 laboratories participating also measured the 88-keV gamma-ray emission rate, which is the desired quantity when the radionuclide is used to calibrate the counting efficiency of gamma-ray spectrometry systems at that energy. It was pointed out that the combined result probably offers the most reliable measurement of the gamma-ray probability per decay for this radiation. The value obtained was $P_\gamma = 0.03614 \pm 0.00012$, where the uncertainty is the combined standard deviation of the means for activity and emission rate. It was recognized at the session that simply quoting this uncertainty might lead to an unrealistically small value being carried forth in evaluations, for uncertainties common to all measurements had not been considered. The BIPM staff was given the challenging task of making a realistic appraisal of the uncertainty before preparing an article describing the comparison for publication. This exercise emphasizes that nuclear data can be significant in the application of radionuclidic standards, that cooperative measure-

ments can provide an incidental dividend of good nuclear data, and that standardizing laboratories should lead the way in demonstrating meaningful analyses of the uncertainties of such data.

The comparison in 1988 of solutions of ^{125}I [4] also led to session reports of the measurements of another important nuclear datum, the half life, by 5 of the 19 laboratories participating. The value suggested for the comparison, (59.4 ± 0.5) d, perhaps carried such a large uncertainty because of chemical instability or detection problems for the low-energy radiations in past measurements. These factors also can cause difficulties in activity measurements, as demonstrated by one laboratory in the comparison. Three ingenious methods gave very consistent results in-house with small estimated uncertainties—but were conspicuously 1.5% deviant from the average of measurement results from other laboratories. Sources had been prepared from a dilution of the solution supplied; a subsequent recheck with the main solution produced a result in agreement with the average of other participants. One important function of the comparisons is to alert all laboratories to potential problems; another is to test the variations observed against the combined uncertainties explicitly given in detail.

The third comparison discussed was that of ^{75}Se , a radionuclide with a 16-ms delayed state in the daughter ^{75}As . This radionuclide had been distributed only to five members of a working group for a “trial” comparison, a precaution which has revealed unexpected problems in some past comparisons. Only one result was reported at the session due to a delay in distributing the solution because of a high radionuclidic impurity level in the first material received from the commercial supplier. While impurities must always be considered in activity measurements, some effort is made to minimize the possibility of their beclouding the accuracy of the basic direct methods being compared.

As the above three examples show, comparisons are made only of radionuclides selected because of some special challenge. The same was true of those considered as possible candidates for future comparisons, once the ^{75}Se exercise is completed. ^{99}Tc emits only beta particles and has a half life sufficiently long that the thin solid sources required for some methods must be of low activity; ^{210}Pb may have chemical problems; ^{144}Ce — ^{144}Pr has shown discrepancies in measurements with different ionization chambers, perhaps because of the proportion of response due to bremsstrahlung; ^{147}Pm is a beta-ray-emitting radionuclide with a gamma ray

of low probability; and ^{237}Np would be the first high-atomic-number nuclide measured recently. Availability of suitable material of the first three radionuclides is being checked by section members.

2.2 The International Reference System (Système International de Référence, SIR) for Gamma-Ray Emitting Radionuclides

Comparisons are time-consuming activities which require a concentrated action by all participants at the same time. Obviously comparisons can only address a small fraction of the required radionuclides, even supposing that national capability for accurate measurement of a radionuclide can be maintained, once demonstrated.

Several years ago a more general comparison method was established at BIPM for gamma-ray-emitting radionuclides [5]. Samples of any suitable radionuclide are submitted at a convenient time as a specified volume of solution in uniform ampoules. The response for a stated amount of activity in two re-entrant ionization chambers is compared with that of a radium reference source, and the ratio per becquerel is registered on tables for that radionuclide containing the same information for samples from other laboratories.

At the present time 373 results for 48 radionuclides from 25 laboratories have been registered. The scheme allows not only a comparison of standards between nations, but also provides a back-up repository of measurements of a given nation with time, in case similar ionization chambers used to retain standards in the national laboratory become inoperable.

The success of the present SIR, and the demand for demonstrated international agreement for radionuclides not emitting suitable gamma rays, led to the formation of a working group at the ninth Radionuclides-Section session to investigate extension. A survey of possible users indicated that demand for three further types of desired radionuclides might be satisfied in a straightforward manner, albeit with considerable testing to determine reliability and comparison uncertainty.

Gaseous radionuclides which emit suitable gamma rays can be compared in the present chambers, once a suitable ampoule is selected. One possible ampoule is being studied.

Measurements in some member laboratories suggest that the bremsstrahlung from radionuclides emitting only beta particles with maximum energy greater than 600 keV can probably be compared with the present BIPM chambers, and this can be

tested. For radionuclides emitting photons which are highly absorbed by the well walls of the present BIPM chambers, thinner-walled chambers are suggested. Members were asked to submit specifications of suitable chambers by the end of 1989.

For radionuclides emitting even lower-energy photons or only beta-particles, two possibilities were suggested. Calorimetry [6] would not require opening of sealed containers supplied by participants, but required activity levels are much greater than most laboratories wanted to supply.

Another possibility, of potentially universal application, is liquid-scintillation counting. Previous bilateral comparisons using this method involved the preparation of extensive sets of samples. However, one laboratory proposed a system using calculated response functions for each radionuclide in a system comparing the coincidences between two and three phototubes viewing the same scintillator [6]. This possibility, which might allow each laboratory to prepare sealed samples, is to be further discussed and possibly tested in a working group.

2.3 Other Working Group Actions

Although they cannot be discussed here in detail, several other actions involving techniques or specific topics were discussed.

2.3.1 Principles of the Coincidence Methods Several of the direct activity measurement methods [6] make use of the time relation between the initial and subsequent radiations in a decay. Nineteen drafts of papers, reports, or working party notes were circulated between the 1987 and 1989 sessions. Many were concerned with the corrections for detector pulses lost in the time a counting system is insensitive due to a previous pulse [7].

2.3.2 High-Count-Rate Measurements Some of the corrections which generate the major uncertainties in activity measurements are better tested with rates beyond those normally used. Several techniques have been developed since the last working group test, but questionnaire results suggested that other section actions should be carried out first while the best testing scheme is devised.

2.3.3 ^{226}Ra Standards “Radium” is unique in that international standards, by mass, do exist. A set was prepared by Hönigschmid in 1934. Two laboratories in countries where large radium sources find extensive use suggested a repackaging of the original set from glass to metal tubes. However, great difficulty in opening a similar source prepared in 1924 showed that fears of breakage due to pressure buildup and glass deterioration are

probably not warranted. Laboratories who no longer use or desire the Hönigschmid standards they have were requested to supply them to the two laboratories that use them.

2.3.4 High-Efficiency NaI(Tl) Techniques If each decay of a radionuclide results in a cascade of x rays or gamma rays, a well-type NaI(Tl) detector can detect at least one radiation most of the time, and the fraction lost can be calculated accurately if the efficiency for different energies is known. A report on experiences in member laboratories is to be published.

3. BIPM Activities

In addition to maintaining the SIR, and investigating its extension, the BIPM staff participates in the general comparisons and prepares the detailed reports describing the results. They also make fundamental contributions to the development of measuring techniques and their analysis.

Examples presented at this session were the measurement of the half life of a metastable state following the decay of ^{75}Se , with a preliminary value of (16.3 ± 0.3) ms; the development of corrections for circuit dead times in series, with possible mixtures of the two types which further extend when a second pulse arrives during a dead period, or not [8]; and possible applications of modulo-2 counting for identifying dead times.

4. Laboratory Reports

A final portion of this session, and all recent ones, has been the presentation of written and oral reports from each attending laboratory covering topics of possible general interest not discussed elsewhere in the agenda. These cover not only discoveries and new data, but also trends in the demands and delivery of standards to users.

5. Discussion

The unusual nature of radioactivity standardization makes international cooperation especially significant. The interchange of ideas about basic standardization during the sessions of the Radionuclides Section of the CCEMRI at BIPM, and about applied radioactivity measurements at associated meetings of the International Committee for Radionuclide Metrology, contributes to both the effi-

ciency and accuracy of such measurements. The examples displayed in this article from the 10th session of the Radionuclides Section illustrate the scope and range of these activities.

About the author: Dale D. Hoppes is a physicist and leader of the group for radioactivity measurements in the Ionizing Radiation Division, Center for Radiation Research, NIST National Measurement Laboratory.

6. References

- [1] BIPM Com. Cons. Etalons Mes. Ray. Ionisants **11**, R 109 (1985).
- [2] Hoppes, D. D., *Env. Intl.* **10**, 99 (1984).
- [3] Ratel, G., International Comparison of Activity Measurements of a Solution of ^{109}Cd (March 1986), Rapport BIPM-88/4, Sèvres, France, 1988.
- [4] Ratel, G., International Comparison of Activity Measurements of a Solution of ^{125}I (May 1988), Draft Rapport CCEMRI(II)/89-2, Sèvres, France, 1989.
- [5] Rytz, A., *Int. J. Appl. Radiat. Isot.* **34**, 1047 (1983).
- [6] Mann, W. B., Rytz, A., and Spagnol, A., *Appl. Radiat. Isotopes* **38**, 717 (1988), chapter 5.
- [7] Chauvenet, B., Bouchard, J., and Vatin, R., *Appl. Radiat. Isotopes* **38**, 10 (1988).
- [8] Müller, J. W., The transmission factor $T_1(N,N)$ revisited, Rapport BIPM-88/12 (1988); and some series expansions of T_1 , Rapport BIPM 88/13 (1988) (BIPM, Sèvres, France).

On Measuring the Root-Mean-Square Value of a Finite Record Length Periodic Waveform

Volume 94

Number 6

November–December 1989

E. Clayton Teague

National Institute of Standards and Technology,
Gaithersburg, MD 20899

An analysis of the uncertainty in measuring the root-mean-square, rms or R_q , value of a periodic waveform which results from the use of a finite record length is presented. Even though the results of the analysis are somewhat as expected, i.e., that the uncertainty is inversely proportional to the number of periods in the record, the explicit relationship between the magnitude of the uncertainty and properties of the waveform does not appear to be available in the literature. The paper first presents an introductory example in terms of the reasonably well known case of band-

width limited Gaussian waveform to introduce definitions. Following this is an analysis of the periodic waveform using the same approach. It is shown that for a large number of periods, n , in the record length, the normalized three standard deviation of the rms value is given by $3/(8\pi n)$.

Key words: periodic surface profile; periodic waveform; random error; root-mean-square value; surface roughness; uncertainty.

Accepted: August 22, 1989

1. Introduction

This paper presents a discussion of the uncertainty in measuring the root-mean-square, rms, value of a periodic waveform which results from the use of a finite record length. The analysis was motivated by seeking to understand the source of a random uncertainty component which was present in some measurements of the absolute arithmetic average, R_a , deviation from a mean line of profiles of precision roughness specimens. The profiles of these specimens had an approximately triangular waveform with two wavelengths and amplitudes. For the longer wavelength specimens the random phasing of the waveform with respect to the recording interval proved to be a major source of uncertainty in the measurements. In this case the record length included 40 periods of the waveform. Even though the results of the analysis are somewhat as expected, i.e., that the uncertainty is

inversely proportional to the number of periods in the record, the explicit relationship between the magnitude of the uncertainty and properties of the waveform does not appear to be available in the literature. The discussion first presents an example in terms of the reasonably well known case of a bandwidth limited Gaussian waveform to introduce some definitions and relationships. Following this is an analysis of the periodic waveform which uses a similar approach.

2. Bandwidth Limited Gaussian Waveform

By definition the mean square value, q^2 , calculated from a finite length L of the waveform $y(x)$ is given by the equation:

$$q^2 = 1/L \int_0^L y^2(x) dx. \tag{1}$$

For convenience and brevity in the following discussion, the definitions listed below will be used [1].

Sample space ≡ the set of points representing the possible outcomes of a measurement.

$\phi(k)$ ≡ a real number, called the random variable, which represents the outcome of a measurement indexed by k .

$p(\phi)$ ≡ $\lim_{\Delta\phi \rightarrow 0} \text{Probability} [\phi < \phi(k) < \phi + \Delta\phi]$

$E\{g[\phi(k)]\}$ ≡ the expected value of any real single-valued continuous function $g(\phi)$ of the random variable $\phi(k)$. It is given by:

$$E\{g[\phi(k)]\} = \int_{-\infty}^{+\infty} g(\phi)p(\phi) d\phi.$$

As an example, the mean square value of $y(x)$ is given by:

$$E[y^2(x)] = \int_{-\infty}^{+\infty} y^2(x)p(x) dx.$$

$E[y^2(x)]$ will be defined as \bar{q}^2 which is that value approached by q^2 as the record length L approaches infinity. Also \bar{q}^2 is the limiting value for the mean q^2 as the number of samplings gets large. The variance of $y(x)$ is defined by:

$$\text{var}\{y\} = E[(y - \bar{y})^2] = \int_{-\infty}^{+\infty} (y - \bar{y})^2 p(x) dx.$$

Similarly the variance in q^2 is defined by:

$$\text{var}\{q^2\} = E[(q^2 - \bar{q}^2)^2].$$

For the special case when $y(x)$ is a bandwidth limited Gaussian waveform with zero mean, Bendat and Piersol [1] show that

$$\frac{\text{var}\{q^2\}}{\bar{q}^4} = \frac{2L^*}{L} \left[1 - e^{-2L/L^*} \right] + \frac{L^*}{L} \left[\left(2 \frac{L}{L^*} + 1 \right) e^{-2L/L^*} - 1 \right],$$

where L^* is the shift distance required for the auto-correlation function to drop by 63% of its zero shift value. If $L \gg L^*$ the relation reduces to

$$\frac{\text{var}\{q^2\}}{\bar{q}^4} = 2 \frac{L^*}{L}.$$

The propagation of error formulae discussed by Ku [2] may be used to relate the variance of the root-mean-square value = $\text{rms} = \sqrt{q^2}$ to this variance of q^2 . Results given in table 1 of this reference show that if

$$\frac{\text{var}\{q^2\}}{\bar{q}^4} = \epsilon, \text{ then } \frac{\text{var}\{\text{rms}\}}{\bar{q}^2} = \frac{\epsilon}{4}.$$

Thus, the normalized three-standard-deviations limit, 3SD, in the root-mean-square values calculated from randomly sampled lengths, L , of a Gaussian profile with a correlation length L^* is given by:

$$3\text{SD limit of } \frac{\text{rms}}{\bar{q}} = \frac{3}{2} \frac{\sqrt{2L^*}}{L} = 2.1 \frac{\sqrt{L^*}}{L}.$$

Whitehouse and Archard [3] report reasonable confirmation of this result for their test specimens which had approximately Gaussian profiles. The importance of this result is stated very clearly by Whitehouse and Archard [3]. "The variance of measured rms or R_a values for the roughness of a surface may be found easily if one knows the standard deviation of a large number of such measurements made upon the same surface. Alternatively one may predict the variance from a knowledge of the correlation length of a typical profile of the test surface." The argument just given for the 3SD limit partially fulfills the "it can be shown" statement by Whitehouse and Archard.

3. Periodic Waveforms

Unfortunately these results do not apply for periodic waveforms such as that of many precision roughness specimens. However, the principles of calculation are still applicable. Consider the example of the sinusoidal waveform:

$$y(x) = A \sin(\omega x + \theta). \tag{2}$$

The waveform is sampled for a length L with the phase angle θ considered as the random variable of

the sample space. The angle θ will be considered as having a uniform distribution over values from 0 to 2π , i.e.,

$$p(\theta) = \frac{1}{2\pi}, \quad 0 < \theta < 2\pi \quad \text{and} \quad p(\theta) = 0, \quad \text{for all other values of } \theta$$

According to definitions in eqs (1) and (2):

$$q^2 = \frac{1}{L} \int_0^L A^2 \sin^2(\omega x + \theta) dx.$$

Evaluation of the integral yields

$$q^2 = \frac{A^2}{2} \left[1 - \frac{\sin 2(\delta + \theta)}{2\omega L} + \frac{\sin 2\theta}{2\omega L} \right],$$

where $\delta = \omega L - 2n\pi$. The conditional variance of q^2 , given δ , is (noting that $\bar{q}^2 = A^2/2$):

$$\begin{aligned} \text{Var}(q^2 | \delta) &= E[(q^2 - \bar{q}^2)^2] = \frac{1}{2\pi} \\ &\times \int_0^{2\pi} \left[\frac{A^2}{2} \left(1 - \frac{\sin 2(\delta + \theta)}{2\omega L} + \frac{\sin 2\theta}{2\omega L} - \frac{A^2}{2} \right)^2 d\theta. \end{aligned}$$

Evaluation of the integral yields:

$$\text{var}(q^2 | \delta) = \frac{A^4 (1 - \cos 2\delta)}{16 \omega^2 L^2}.$$

Thus, if the record length happens to include an integral number of periods, $\text{var } q^2 = 0$. But if we take the more likely case in which δ has a distribution of values like that of θ due either to variations in the measured wavelength, ω^{-1} , or in the record length, L , the result integrated with respect to δ is obtained as follows.

$$\begin{aligned} \text{var}(q^2)_\delta &= \frac{1}{2\pi} \int_0^{2\pi} \text{var}(q^2 | \delta) d\delta \\ &= \frac{1}{2\pi} \int_0^{2\pi} \frac{A^4 (1 - \cos 2\delta)}{16 \omega^2 L^2} d\delta. \end{aligned}$$

Substituting $\omega L = \delta + 2n\pi$ followed by the introduction of dummy variables x and y reduces the integral to:

$$\begin{aligned} \text{var}(q^2)_\delta &= \frac{1}{2\pi} \int_{2n\pi}^{2(n+1)\pi} x^{-2} dx \\ &\quad - \frac{1}{\pi} \int_{4n\pi}^{4(n+1)\pi} (\cos y / y^2) dy. \end{aligned}$$

Solving these integrals yields:

$$\begin{aligned} (\text{var } q^2)_\delta &= \frac{A^4}{16} \frac{1}{4\pi^2 n(n+1)} \quad \text{or} \quad \frac{(\text{var } q^2)_\delta}{\bar{q}^4} \\ &= \frac{1}{16\pi^2 n(n+1)} \end{aligned}$$

where n is again defined by the equation $\delta = \omega L - 2n\pi$. This result for $(\text{var } q^2)_\delta$ does account for the relationship between ωL and δ . Use of the same relationships between $\text{var } q^2$ and var rms given earlier yields:

$$\frac{(\text{var rms})_\delta}{\bar{q}^2} = \frac{1}{64\pi^2 n(n+1)}.$$

An *averaged* normalized three-standard-deviation limit for variations of the rms values is then given by:

$$3\text{SD}\left(\frac{\text{rms}}{\bar{q}}\right) = \frac{3}{8\pi\sqrt{n(n+1)}}, \quad (3)$$

or for large n ,

$$3\text{SD}\left(\frac{\text{rms}}{\bar{q}}\right) = \frac{3}{8\pi n}. \quad (4)$$

Finally, if the record length L and measured wavelengths, ω^{-1} , are stable and such that δ has a narrow distribution about $\pi/2$ or $3\pi/2$ the $3\text{SD}(\text{rms}/\bar{q})$ could be as much as twice this average value.

4. Comparison with Variations of Roughness Measurements

For surface profiles obtained from roughness measurements, one would expect that the normalized 3SD of a set of measured R_a values would be approximately equal to that computed for the R_q (rms) values since both quantities are similar measures of the sampled profile's empirical probability density function. The measurements of R_a values which initiated this analysis should therefore be understandable in terms of the results just derived.

For the measurements, two types of specimens were used; one set had an R_a value of $3.2 \mu\text{m}$ and a wavelength such that $n = 40$; the other set had an R_a value of $0.5 \mu\text{m}$ and a wavelength such that $n = 250$. Record lengths for the measurements were approximately 3.8 mm. Predicted uncertainties for

the variations of a measured value about the mean R_a are therefore:

$$3SD_{3.2 \mu m} = 0.3\% \text{ of mean } R_a,$$

and

$$3SD_{0.5 \mu m} = 0.05\% \text{ of mean } R_a,$$

if one assumes the *averaged* three standard deviations limit. The *maximum* values for the analytical uncertainties are 0.6 and 0.1% of the mean R_a values for the 3.2 and 0.5 μm specimens, respectively.

In a series of 80 sets of three R_a measurements, the uncertainty (3 standard deviations) of these triplicate measurements with respect to their average values was:

$$3SD_{3.2} = 1.0\% \text{ of mean } R_a,$$

and

$$3SD_{0.5} = 0.7\% \text{ of mean } R_a.$$

The intent of this comparison between the analytical and experimental values is not that of justifying the theoretical analysis. However, in terms of understanding the experimental variations the agreement is sufficient to confirm that, for the longer wavelength specimen, a major source of uncertainty for the roughness measurements results from the finite sampling length.

The imperfect waveforms of the precision roughness specimens are the most likely sources of the residual uncertainty. As illustrated in figure 1 the specimen waveforms have distortions which are produced by either an additive random function together with phase modulation or by the

combination of random amplitude and phase modulation. The effect of an additive random function is the only one which can be readily analyzed. For this case the rms value of the sum of two uncorrelated waveforms adds in a rms manner. Assume that the waveforms can be represented by the sum of a random component, with an rms value of q_R and a correlation length of L^* , and a periodic component, with an rms value of q_P and angular frequency ω . Then the use of propagation of error formulae derived by Ku [2] yields:

$$3SD\left(\frac{\text{rms}}{\bar{q}}\right) = 1.5 \left[2a \frac{L^*}{L} + \frac{b}{16n^2\pi^2} \right]$$

where n and L are as defined earlier and

$$a = \left(1 + \frac{q_R^2}{q_P^2} \right)^{-2}, \quad b = \left(1 + \frac{q_P^2}{q_R^2} \right)^{-2}.$$

Estimates of q_R^2 and L^* from the calculation of autocorrelation functions of the waveforms for the 0.5 $\mu m - R_a$ specimen are: $L^* = 0.05 L$ and $q_R = 0.01 q_P^2$. Effects of random amplitude and phase modulation are not accounted for in these estimates. With these values of q_R^2 and L^* the dominant source of uncertainty for the waveform sampled for 250 periods is the random additive component which increases the uncertainty limits to 0.3% of the mean value. Approximately the same values for L^* and q_R^2 were obtained from studies of the 3.17 $\mu m - R_a$ specimen. Since $q_R^2 = 2.8 \times 10^{-4} q_P^2$, in this instance, the uncertainty produced by the random component is insignificant for measurements on this specimen.

5. Conclusion

The uncertainty in measuring the root-mean-square value of a finite record length of a periodic waveform has been obtained and is given in eqs (3) and (4). The theoretical results were compared with data obtained from surface profile measurements of precision roughness specimens. However, eqs (3) and (4) are quite general and will apply to rms measurements of the amplitude of periodic waveforms arising from other areas.

During customary announcements of this paper to NIST staff, an analysis of the errors of measurement due to variations in sampling interval length, (complimentary to that presented here), was brought to the author's attention. The effects of

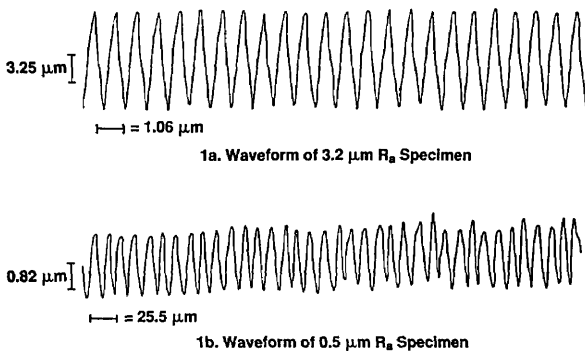


Figure 1. Waveforms of roughness specimens which were used for statistical studies.

adjusting the sample interval length relative to an integral number of cycles of the test waveform are determined and applied to measurements of electrical power with a wattmeter [4].

6. Acknowledgments

The author gratefully acknowledges helpful discussions with Charles P. Reeve of the Statistical Engineering Division. His suggestions clarified many of the ideas presented in the paper; in particular, the use of the concept of conditional variance enabled the basic calculation to be expressed in more conventional statistical terminology.

About the author: Dr. E. Clayton Teague is Group Leader of Micrometrology in the NIST Precision Engineering Division of the Center for Manufacturing Engineering, National Engineering Laboratory. He has worked in the area of surface texture measurement for 18 years.

7. References

- [1] Bendat, Julian S., and Piersol, Allan G., *Random Data: Analysis and Measurement Procedures*, Chapters 3 and 6, Wiley Interscience (1971).
- [2] *Precision Measurement and Calibration*, Edited by Ku, H. H.; pp. 331–341, NBS Special Publication 300, Volume 1, U.S. Government Printing Office, Superintendent of Documents, 1969.
- [3] Whitehouse, D. J., and Archard, J. F., *Proc. Roy. Soc. London* **A316**, 97 (1970).
- [4] Stenbakken, G. N., *IEEE Trans. on Power Apparatus and Systems* **PAS-103**, 2919 (1984).

A Search for Optical Molasses in a Vapor Cell: General Analysis and Experimental Attempt

Volume 94

Number 6

November–December 1989

A. L. Migdall

National Institute of Standards
and Technology,
Gaithersburg, MD 20899

We analyze the application of optical molasses to a thermal vapor cell to make and collect cold atoms. Such an arrangement would simplify the production of cold atoms by eliminating the difficulty of first having to produce and slow an atomic beam. We present the results of our calculations, computer models, and experimental work. As a guide for future work, general results

are given to illustrate which fundamental parameters are most important in the production of cold atoms in a vapor cell.

Key words: laser cooling; optical molasses; vapor cell.

Accepted: August 25, 1989

1. Introduction

We have proposed using the technique of laser cooling to directly cool and collect gas atoms in a thermal vapor cell. This allows a high density region of very cold atoms to be built up [1]. This eliminates the difficulty of first having to produce and slow an atomic beam, and thus holds the promise of greatly simplifying the production of cold atoms. We present here an analysis of the processes involved in this proposal, as a guide for future work, and give the results of our attempts to realize it experimentally.

The proposal is to set up a region of optical molasses directly in an atomic vapor cell, allowing the accretion of a high density of cold atoms. The molasses consists of three pairs of counterpropagating laser beams tuned below resonance in an atomic vapor cell. This arrangement [2] of opposing light beams provides a strong damping or viscous force for slow atoms. This effect, which was first demonstrated with a cooled atomic beam several years ago [3], is well described in the literature [4,5] and

so will only be discussed briefly here. Atoms that enter the molasses region with slow enough velocities have a high probability of being slowed and viscously captured before exiting the other side. The motion of these captured atoms becomes diffusive, because any velocity the atoms acquire in a particular direction (due to random scattering of photons) is quickly damped by the viscous force [3]. Because of this random walk type motion, these atoms remain in the molasses region for much longer times than they would have under ballistic motion at their original thermal velocities or even their ultimate cooled velocity (hence the term optical molasses). After a time, all the atoms in the cell with "catchable" velocities (most probably those with velocities less than some critical value) become mired in the molasses region. Thus the density of cold atoms in the molasses region builds up, as the lowest velocity atoms in the rest of the cell are depleted. The density of cold atoms continues to increase as the low velocity tail of the thermal

distribution is replenished by processes that move the velocity distribution back toward thermal equilibrium. It is the fluorescence of the accumulated cold atoms that would be observed.

2. Theoretical Analysis

We calculate how fast the cold atom density should increase with time and estimate the processes limiting residence time in classical two-state molasses [5]. This is done with the help of computer models of the cooling process for the specific case of a sodium atom in a vapor cell containing a molasses region. In addition, we calculate the visibility of the effect by comparing the fluorescence signal expected from the cold atoms to the background signal that is also present. We also examine the general dependences of the signal size on the atomic parameters, so that comparisons can be made of the relative merits of trying to cool other atoms in a vapor cell or using other transitions.

The initial rate of increase of the cold atom density is governed by the rate at which capturable atoms enter the molasses region. The rate of entry (and subsequent capture) of atoms is just the flux Φ ,

$$\Phi = \frac{1}{4} n_c V_{\text{cavg}} \quad (1)$$

integrated over the surface area of the molasses volume, where n_c is the density of catchable atoms and V_{cavg} is the average velocity of those atoms. The probability of capture versus velocity for a two-state atom entering the molasses region was determined by a Monte Carlo simulation. The use of this simple two-state model is justified in this situation, because during most of the capture process, the velocities correspond to detunings that are large relative to atomic linewidth. (It is important to note that it is the capture rate that is more important in estimating the final signal rather than the ultimate temperature of the molasses, since the residence time in the molasses is limited by other processes.) A 1-cm region of 3-D molasses is modeled, where each beam has a saturation parameter of one (defined as I/I_0 , where I is the light intensity and I_0 is the on-resonance intensity which power broadens the natural transition width by a factor of $\sqrt{2}$). The laser frequency is tuned $\Gamma_n/2$ below resonance, where Γ_n is the natural width of the cooling transition. For this model, the result shows that the catchable atoms are simply those atoms with velocities less than some maximum cutoff value, V_c . In

this case, the catchable density, n_c found by integrating the Maxwell-Boltzmann distribution from $V=0$ to V_c (for $V_c \ll \sqrt{(k_B T/M)}$, where k_B is the Boltzmann constant, T is the gas temperature, and M is the atomic mass) is given by:

$$n_c = \frac{4}{3\sqrt{\pi}} n_0 \left(\frac{M}{2k_B T}\right)^{3/2} V_c^3, \quad (2)$$

where n_0 is the total density of the thermal atoms in the cell. The average velocity of these atoms, found by performing a similar integration, is just equal to $(3/4) V_c$. The fractional increase in the total density with time, $F(t)$ (for t much less than the average time for leaving the molasses) equals the rate of new atoms getting caught in the region times t divided by the volume of a sphere of radius R and the original density, n_0 :

$$F(t) = \frac{\frac{1}{4} n_c V_{\text{cavg}} 4\pi R^2}{n_0 \frac{4}{3} \pi R^3} t = \frac{9 n_c V_c}{16 n_0 R} t. \quad (3)$$

To estimate this increase, we use the results of our computer simulations, including those shown in figure 1. This figure shows the general result that the average distance needed to snag an Na

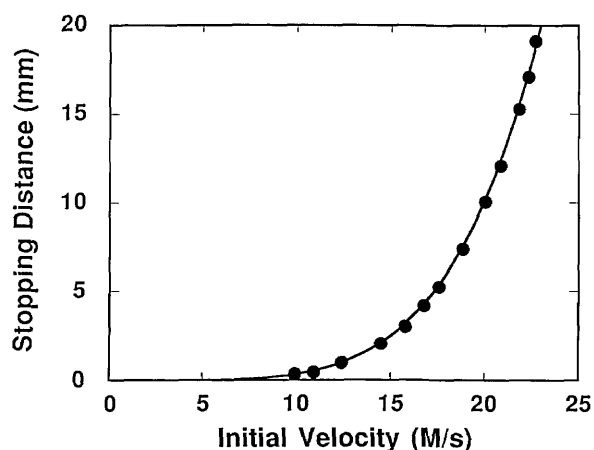


Figure 1. The distance required to bring a Na atom from its initial velocity to the point where its motion is completely diffusive. The points are the result of a model of 3-D molasses with each beam having a saturation parameter of one. The size of the molasses region needed to hold an atom for an extended time must be somewhat larger than the stopping distance, because the atom must stop away from the boundary of the region to remain caught for an appreciable time. The line is a fit to a power law, aV^b . The best fit parameters are $a = 4.7 \times 10^{-6}$ and $b = 4.87$, very nearly the expected 5th power form.

atom in uniform molasses is proportional to the 5th power of the initial velocity. (Note that the size of the molasses region required to catch and hold an atom would be somewhat larger than these stopping distances, since the atom must not stop right on the boundary if it is to remain caught for an appreciable length of time.) This velocity dependence agrees with the calculated dependence obtained by expanding to first order, the velocity dependence of the damping force for a red detuning of $\Gamma_n/2$ and $kV > \Gamma_n$, where k is the wave vector in wavenumbers of the laser. By integrating, we get the stopping distance, D as a function of velocity. The result of this calculation has the form

$$D \approx \frac{Mk^2 V_c^5}{5\hbar\Gamma_n^4}. \quad (4)$$

According to our simulations for Na atoms on typical trajectories traversing a molasses region consisting of the intersection of three 1-cm diameter beams, 20 m/s is roughly the critical velocity, below which the probability of stopping before exiting the other side is nearly unity. The fraction of atoms with velocities less than 20 m/s, as given by eq (2), is 5×10^{-5} of the total Na density at 75 °C.

We also investigated how the capture rate is affected by having 1-D molasses surrounding the central 3-D molasses region [6]. This is important because, before an atom enters the central region it is likely to pass through a region of only one pair of counterpropagating beams. In this region, only one component of velocity is damped, but it is just the component of velocity needed to reach the central region. Thus some atoms headed for the central region may be, in effect, deflected away, thereby reducing the velocity capture range. This process is modeled and found to produce a minimum velocity below which atoms on certain trajectories cannot reach the central volume. The circles in figure 2 show an example of a trajectory where only those atoms with velocities between 17 and 19 m/s are stopped in the molasses region. The triangular points in figure 2 represent a nearly equivalent case to that of no surrounding 1-D molasses for reasons to be described later. 1-D molasses surrounding the central 3-D region should also produce a slight increase in the maximum catchable velocity, due to the extra length of the cooling region. Some effect of this is seen on those velocities just slightly too fast to be caught. The circular points show significant cooling of velocities in the 20 to 23 m/s range, whereas the triangular points show minimal cooling in that range. The number of atoms within

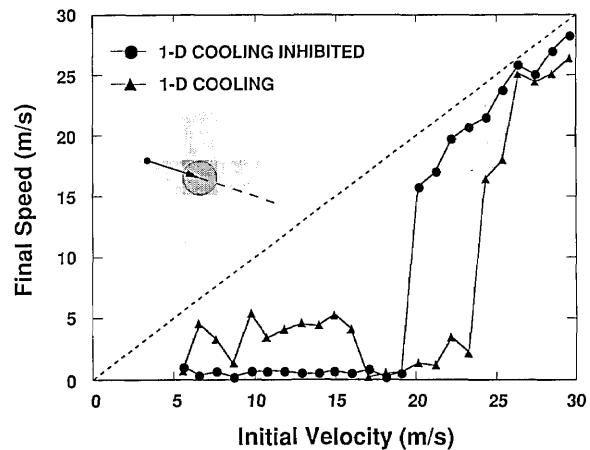


Figure 2. The final speed of Na atoms incident on the molasses region vs starting velocity. The molasses region has a central volume of 3-D damping surrounded by 1-D damping due to a single pair of beams. The insert shows the particular trajectory used, which passes through the 1-D region before entering the 3-D region. The circles are for the configuration with both laser frequencies in all beams. The triangles indicate that one laser frequency is in one pair of beams and the second frequency in the other two pairs. For this curve, only atoms with velocities in the range between 17 and 19 m/s were caught. Atoms in the range from 20 to 23 m/s were greatly slowed but did not in fact stop in the 3-D molasses region. The difference between the dashed line and the data points is the total slowing experienced by the atom.

this band of capturable velocities is about one-third of the number that is caught in the central 3-D molasses without the surrounding 1-D molasses. We describe a means to reduce this effect later.

What ultimately limits the maximum density that can be built up are the processes that remove cold atoms from the molasses. Atoms leave the region by diffusion, by acquiring a drift velocity due to imbalance of opposing beams [5], and by collisions with the thermal gas atoms which transfer a relatively large amount of kinetic energy. Here we estimate the time for each of these processes, assuming classical two-state optical molasses damping.

The time for an atom to random walk out of the molasses is proportional to R^2 , where R is a characteristic radius of the molasses region. Assuming for Na a random walk with a time step size equal to the velocity correlation time of 4×10^{-5} s and a velocity equal to the simple Doppler cooling limit of 50 cm/s, the average time to leave is long, about 0.45 s for a 1-cm diameter region. The calculated time [5] for an atom to drift out due to a beam intensity imbalance is also long, 0.25 s for a 1% intensity imbalance, $I/I_0=1$, and a detuning of

$\Gamma_n/2$. Our final estimate is not hurt by using such a simple model of molasses since it is known to underestimate these times which, in our case, are already long enough not to be the process limiting the final density buildup.

The time for a cold atom to be knocked out of the molasses depends on the density of the thermal gas atoms and their collision cross sections. The dominant cross section for this is the elastic cross section for collisions between ground-state and excited-state atoms. We estimate this cross section to be on the order of 10^{-13} to 10^{-12} cm², which for Na at 75 °C, gives a time to be knocked out of the molasses of 1.0 to 0.1 s, assuming that half the atoms are in the excited state.

The visibility of the cold atom signal depends on the size of that signal relative to any background signal. A background signal exists because each of the laser beams is in resonance with a fraction of the uncooled atoms. This fraction is approximately equal to Γ_n/Γ_D where Γ_D is the Doppler width of the resonance transition at the cell temperature. This will produce a sizable background fluorescence signal. The total background fluorescence signal will be about three to six times the signal due to a single beam, since the three pairs of beams are orthogonal, and the tuning is such that the six beams interact with nearly distinct velocity classes.

3. Signal Estimate

To understand better how cell molasses works, it is useful to estimate the signal size in terms of fundamental atomic parameters so that the estimate can easily be extended to an arbitrary atom. In this way, we can see best how to maximize the cold atom signal. To do this, we eliminate V_c and n_c from eq (3) by writing them in terms of the mass and transition width of the atom. Substituting eqs (2) and (4) into eq (3) and using $D=2R$ we get

$$F(t) = 3 \left(\frac{M}{2k_B T} \right)^{3/2} \frac{\left[\frac{10\hbar\Gamma_n^4}{Mk^2} \right]^{4/5}}{4\sqrt{\pi} R^{1/5}} t \quad (5)$$

To determine the size of the signal expected from the increase in density of the cold atoms, we take the ratio of this density to the density of the hot atoms that are also fluorescing. The total fraction of hot atoms that are on resonance with any of the laser beams is estimated to be $\sim 5\Gamma_n/\Gamma_D$, for a laser tuned $\Gamma_n/2$ below resonance. Since Γ_D is proportional to the thermal velocity of the atoms, the ra-

tio S of the cold atom signal to the background fluorescence can be written as:

$$S(t) = \frac{F(t)}{5\Gamma_n \left[2k \left(\frac{2k_B T}{M} \ln 2 \right)^{1/2} \right]}. \quad (6)$$

Substituting eq (5) into eq (6) and extracting just the proportionalities with respect to the atomic parameters and cell conditions, we find

$$S(t) \propto M^{0.2} \Gamma_n^{2.2} R^{-0.2} T^{-1}. \quad (7)$$

From this form we can see that $S(t)$ depends only weakly on such parameters as M , R , and T but is strongly dependent on Γ_n . Thus, to enhance the density gain and signal visibility in cell molasses it is important to select an atom with a large transition width. Alternately, it may be possible to achieve this artificially, possibly by power broadening the transition, if this can be done without greatly degrading the cooling process.

The above analysis has assumed a two-state atom. In actuality since Na has two ground states ($F=1$ and $F=2$), two frequencies are necessary to prevent optically pumping the atom to the other ground state and losing it to the cooling process. The two-state ideal can be approximated by having both frequencies present in the molasses region. This can be accomplished by two different arrangements. The first uses both frequencies in all beams. This is the usual arrangement for optical molasses in beam experiments. The second arrangement uses one frequency in two pairs of beams with the other frequency in the third pair of beams. This second optical arrangement, by separating the frequencies, nearly eliminates the effect of the surrounding 1-D molasses region while possibly enhancing the signal-to-background fluorescence ratio [7]. One particular arrangement might be to have only light resonant with the $F=2$ to $F'=2$ transition in two pairs of counter propagating beams, while the third pair contains only light resonant with the $F=1$ to $F'=2$ transition. With this setup, the cooling in the 1-D molasses regions would be effectively turned off after only a few transitions as the atom is optically pumped to the other ground state. Only in the intersection of the beams would both frequencies be present to prevent optical pumping out of the cooling process. The triangular points of figure 2 show the result of optical pumping, the lower velocities become catchable again as the effect of the 1-D molasses region is nearly eliminated. For this arrangement,

the cooling in the intersection region will proceed at a reduced rate (since cooling on the $F=2$ to $F'=2$ transition is not as effective for not clearly understood reasons), but 3-D cooling will still occur.

The big advantage with this technique is that the visibility should be greatly enhanced. While both the cold atom signal would be smaller (due to less effective damping using these transitions) and the background signal would be smaller (due to optical pumping), it is expected that the background signal reduction would be greater than the cold atom signal reduction. The rms thermal velocity of the atoms in the cell is about 6×10^4 cm/s. This gives a transit time across the 1 cm beams of 1.6×10^{-5} s. Using either the $F=1$ to $F'=2$ or $F=2$ to $F'=2$ frequency alone will optically pump the atoms after only a few transitions or about 100 ns. Since a hot atom is in the beam for 160 times as long as this optical pumping time, the background fluorescence should be reduced by nearly this factor.

4. Experiment

To look for evidence of molasses experimentally, we set up a Na vapor cell with a base pressure at room temperature of 2×10^{-10} Torr. The cell was operated at 75 °C. An effort was made to make the temperature distribution as uniform as possible. This uniformity was important to prevent a non-Maxwell-Boltzmann velocity distribution resulting from local hot spots in the cell. The Na vapor pressure at this temperature was measured to be in the range of 1 to 3×10^{-8} Torr. The cell windows were antireflection coated to reflect less than 0.25% per surface. High reflectivity ($R > 99.85\%$) mirrors were used to retroreflect the beams. Each of the three mutually orthogonal pairs of counterpropagating beams were linearly polarized with their polarizations mutually orthogonal. The Na D₂ line was used for the cooling transition. The power in each beam was varied from about 1 to 10 mW with the beams apertured from 0.5 to 1 cm in diameter. The collimation of the molasses beams were set using a shearing interferometer. With this interferometer, we were able to set the radius of curvature of the wavefront to be greater than 100 m. A photomultiplier tube was used to collect the light from the region of intersection of the beams.

In setting up this experiment, there is the practical problem of finding the initial evidence of a signal in the presence of the background fluorescence. It is our experience that in a beam experiment, mo-

lasses lifetimes of about 100 ms can be set up blind (i.e., with no need to see the signal). For molasses in a cell, the maximum lifetime may be somewhat smaller than this due to collisions with background atoms, so we need a signal that is visible at this lifetime to observe the effect. Our calculations of density buildup are valid when the rate of increase is greatest, that is, for times much less than any of the limiting lifetimes. Therefore, we chose to look for density buildups on a time scale of less than about 50 ms. We attempted to observe the signal (with both frequencies in all beams) using a lock-in amplifier and modulating the $F=1$ to $F=2$ laser frequency on the order of 10 MHz at a 20 Hz rate while slowly scanning the $F=2$ to $F=3$ laser. This would allow the cold atom signal to build up for 25 ms. According to our calculations, using $V_c=20$ m/s, a 1-cm region, and allowing for the reduction due to 1-D molasses surrounding the central 3-D region, the initial rate of density increase for the above parameters is about 3.5% per second. Since the background signal results from the fluorescence of about 3.6% of the total number of atoms (for our Na cell at 75 °C, the natural width is $\sim 0.7\%$ of the Doppler width), the rate of increase in cold atom fluorescence signal is predicted to be about 100% of the background signal per second. For the 25 ms build up time, the expected fluorescence increase due to laser cooled atoms is approximately 2.5% over the background fluorescence. The signature of this signal should be a peak with a frequency width on the order of the natural width of the transition and located just to the red of the $F=2$ to $F=3$ transition. The signal should, of course, disappear when one of the six beams is blocked. We estimate that our sensitivity is roughly at the 1% level, which is comparable to our expected signal. We saw no evidence of laser cooled atoms in the cell using the above setup, or the alternate arrangement of separate frequencies in separate beams, so we are only able to conclude that our signal estimates give a limit to the size of the cold atom density buildup.

5. Discussion

One important assumption in our calculations is that the velocity distribution is quickly rethermalized as the low velocity atoms are caught in the molasses. In our cell, the temperature and density are such that, for thermalization purposes, there are essentially no collisions between atoms in the gas phase. In addition, the sticking coefficient for Na

atoms hitting the walls should be nearly unity. This means that any atom in the gas is a fresh atom emitted from the wall with no memory of any previous velocity. As a result, our calculations depend on the velocity distribution of the atoms emitted from the walls being Maxwell-Boltzmann. This should be a valid assumption since, at the low densities of our cell, the low-velocity end of the distribution should not be suppressed. This is in contrast to beam experiments, where the low velocity atoms can be depleted by collisions with a large flux of faster atoms [8]. We mention here, for completeness, that there may be other mechanisms that could drastically reduce the rate of emission of slow atoms from the walls, such as a surface barrier potential. If such a barrier did exist, the slowest atoms emitted by the wall would not make it over the hill to enter the molasses volume. In this case, rethermalization would occur through inelastic interactions between the atom and the barrier. This could be a very slow process which would reduce the cold atom density that could be achieved. Also, if for some reason the sticking coefficient was anomalously low, the rate of rethermalization would be slow, reducing the rate of cold atom buildup.

6. Conclusions

We have estimated the processes relevant to laser cooling atoms in a thermal vapor cell. We have shown which parameters are important in attempting to observe such cooling. This should be a useful guide when considering the relative merits of trying to cool other atoms or trying to cool on other transitions. Our experimental results give an upper limit on the size of the cold atom density buildup that can be expected for optical molasses in a thermal vapor cell. In particular, we have seen that it is most important to have a large width for the cooling transition. It is left open whether an appropriate system can be found with a broader transition or one that can be broadened artificially by some means, such as power broadening, which will improve the cold atom density increase and allow cell molasses to achieve its promise as a convenient source of cold atoms.

7. Acknowledgments

We would like to thank P. Gould and P. Lett who helped with the experimental part of this pro-

ject. We also thank all the members of the NIST laser cooling and trapping project for their useful suggestions on this work. The support of the Office of Naval Research is gratefully acknowledged.

About the author: Alan L. Migdall is a physicist in the Radiometric Division of the Center for Radiation Research at the National Institute of Standards and Technology, Gaithersburg, MD.

8. References

- [1] Migdall, A. L., Metcalf, H., and Phillips, W. D., *J. Opt. Soc. Amer. A* 2 (13) P51 (1985).
- [2] Hansch, T. W., and Schawlow, A. L., *Opt. Comm.* 13 68 (1975).
- [3] Chu, S., Hollberg, L., Bjorkholm, J. E., Cable, A., and Ashkin, A., *Phys. Rev. Lett.* 55 48 (1985).
- [4] Gould, P. L., Lett, P. D., and Phillips, W. D., in *Laser Spectroscopy VIII*, Persson, W. and Svanberg, S., eds., Springer, Berlin (1987) p. 58.
- [5] Lett, P., et al., submitted to *J. Opt. Soc. Amer. B*.
- [6] Migdall, A. L., Phillips, W. D., and Metcalf, H. J., *Bull. Amer. Phys. Soc.* 31 973 (1987).
- [7] Migdall, A. L., Metcalf, H. J., Phillips, W. D., and Gould, P. L., *Bull. Amer. Phys. Soc.* 32 281 (1987).
- [8] Ramsey, N. F., *Molecular Beams*, Oxford Science Publications, New York (1985) p. 24 and references therein.

News Briefs

General Developments

GRAVIMETERS USED SUCCESSFULLY

Highly sensitive and portable instruments to measure the acceleration of gravity, developed by the NIST-University of Colorado Joint Institute for Laboratory Astrophysics (JILA), have performed successfully at various sites around the country in field tests by the National Geodetic Survey. The results of this initial year of field testing pave the way for a network of measurements made with these instruments, both in the United States and abroad. They will be used to monitor local variations in gravity, study vertical ground motions for earthquake detection, and assist in the determination of sea level changes. A paper describing the field test is available from Jo Emery, NIST, Division 104, Boulder, CO 80303.

DUCTILE-TO-BRITTLE FRACTURE BEHAVIOR OF STEEL STUDIED

Although the fracture behavior of steels is understood at high and at very low temperatures, the behavior at intermediate temperatures has been hard to characterize. In this ductile-to-brittle transition region, measurements of the fracture toughness as a function of temperature show a large scatter, and measurements of different-sized specimens at different loading rates give different results. A NIST guest scientist from West Germany has clarified the cause of this variability on a quenched and tempered pressure vessel steel (DIN 20 MnMoNi 55, similar to ASTM A533B). Four different types of fracture initiation sites have been identified, including cleavage facets, inclusions, clusters of inclusions, and local zones of ductile tearing. The fracture toughness depends on the distance from the crack tip to the initiation site. The

study results are published in *Fracture Behavior of a Pressure Vessel Steel in the Ductile-to-Brittle Transition Region* (NISTIR 88-3099), available from the National Technical Information Service, Springfield, VA 22161 for \$13.95, prepaid. Order by PB #89-189195.

CERTIFICATION OF ALUMINUM IN SERUM ALBUMIN FOR FDA

NIST scientists recently developed methods for the determination of aluminum in serum albumin. The serum albumin was provided by the Center for Biologics Evaluation and Research Division of the Food and Drug Administration (FDA) and will be used by FDA as a quality assurance material. The analytical procedures involve the use of atomic absorption spectrometry with electrothermal atomization, molecular fluorescence, and inductively coupled plasma atomic emission spectrometry.

The serum albumin will be used for quality control in the manufacture and analysis of parenteral materials. Parenteral materials enter the body through means other than the digestive tract, e.g., injections or implants. Aluminum levels in parenteral solutions are of increasing concern because trace quantities of aluminum have been correlated to diseases affecting nerve tissue and bone. One of the greatest impacts has been on patients with renal impairment or patients receiving large or frequent amounts of albumin. It is expected that this research will greatly aid the FDA regulatory program for parenterals.

CAC QA PROGRAM IMPROVES THE QUALITY OF MEASUREMENTS MADE IN CANCER CHEMOPREVENTION STUDIES

For the past 5 years, the Center for Analytical Chemistry has operated a quality assurance program for more than 40 laboratories that measure serum and plasma levels of selected fat-soluble vita-

mins as part of National Cancer Institute (NCI) supported investigations to determine the cancer-prevention benefits of selected micronutrients in human populations at high risk of contracting certain forms of cancer.

The QA program developed at NIST to support analytical measurements made in these studies has three main components: (1) development and critical evaluation of analytical methods for the determination of retinol (vitamin A), α -tocopherol (vitamin E) and β -carotene in serum; (2) interlaboratory measurement proficiency testing; and (3) development of serum based reference materials to serve as accuracy benchmarks.

By the spring of 1988 the first two components were well under way and a pilot batch of serum-based reference materials with assigned values for the concentrations of the three fat-soluble vitamins was developed and distributed to laboratories participating in the QA program. In 3 years prior to their development, interlaboratory precision improved from ~ 50 to ~ 25 percent in a regular fashion. With reference materials available for laboratories to validate and trouble shoot their methods, there has been a three-fold improvement in interlaboratory precision, to the point where the precision today is less than 8 percent.

NIST efforts are now being channeled toward improving measurement comparability for five new agents. A program is also being developed to transfer NIST measurement capabilities in two-dimensional electrophoresis to NCI grantee laboratories for measuring the appearance/disappearance of selected proteins as a function of the progress of various forms of carcinoma. This technology has the potential for use as a diagnostic tool as well as a means for screening prospective chemopreventive agents.

ATOMIC LIQUID AND SOLID BEHAVIOR OBSERVED IN PLASMAS

NIST scientists have made the first confirmation of the existence of condensed states in a plasma system. Their nonneutral plasmas consisted of up to 15,000 positive beryllium ions contained in an ion trap and cooled to a temperature below 10 mK. At sufficiently high density and low temperature the system undergoes a transition from a gaseous ion cloud to a set of concentric shells of ions. In this state, ions move freely within a given shell, but motion between shells is constrained. The system is liquid-like within a shell and solid-like between shells, as in a smectic liquid crystal.

There is high interest in this type of system. First, certain internal atomic transitions in the trapped ions may be used as the basis for a very high quality frequency standard. Second, the trapped beryllium-ion plasmas at low temperature may serve as a model of other interesting systems that exhibit similar behavior but are less amenable to systematic study. Some examples are dense, ionized states of matter found in astrophysical objects such as neutron stars, conduction electrons in semiconductors, and charged particles confined in high-energy storage rings.

NIST SERVICE FOR SETTING COMPUTER CLOCKS

The Time and Frequency Division of the Center for Atomic, Molecular and Optical Physics has just completed its first year of operation of a new service which provides computer and other digital systems with telephone access to NIST time at accuracies approaching 1 ms. Features of the service include automatic compensation for telephone-line delay, advanced (48-day) alert for changes to and from daylight savings time, and advanced (1-month) notice of insertion of leap seconds. Although the main application of this system is to set computer clocks, simple hardware can also be developed to set noncomputer clock systems. The NIST system, entitled Automated Computer Time Service (ACTS), involves transmission of a time signal, which is then echoed by the user, so that the telephone time delay can be measured by NIST. The system adjusts for this delay and advances the transmission so that the signal arrives at the user on time. User software for the service is sold through the SRM program as RM8101.

PROPOSED REVISION OF STANDARD FOR POSIX: PORTABLE OPERATING SYSTEM INTERFACE FOR COMPUTER ENVIRONMENTS

A proposed revision to Federal Information Processing Standard (FIPS) 151, POSIX, was announced in the Federal Register. The revision will adopt IEEE Standard 1003.1-1988, Standard for Portable Operating System Interface for Computer Environments which defines a C language source interface to an operating system environment. FIPS 151 was adopted on an interim basis, pending completion of the technical specifications by the IEEE standards committee, to enable federal agencies to begin specifying POSIX in procurements. The standard will assist agencies in achieving a more open software environment.

PRESENCE OF TOXIC S₂F₁₀ CONFIRMED FOR FIRST TIME IN SF₆ EXPOSED TO DISCHARGE

NIST scientists have confirmed for the first time by direct measurement that the toxic gas disulfur-decafluoride (S₂F₁₀) is formed by corona discharges in compressed sulfur hexafluoride (SF₆), a gas increasingly used as an electrical insulation and current-interruption medium in power transmission and distribution equipment. The team of scientists also found that the observed formation rate of S₂F₁₀ is consistent with predictions of a theoretical model for the discharge chemistry developed by NIST scientists. When SF₆ is subjected to an electrical discharge it decomposes to form various corrosive and/or toxic byproducts which are of concern in assessing the reliability and safety of power systems that use it. The suspicion, not proven until this work, had been that S₂F₁₀ would be among these products.

NCWM TRAINING MODULE PUBLISHED

The National Conference on Weights and Measures (NCWM) has published the twelfth module of a planned set of training programs for state and local weights and measures officials that the NCWM is developing under a grant from NIST.

Module 24, Introduction to NIST Handbook 44, provides an overview of NIST Handbook 44, Specifications, Tolerances, and Other Technical Requirements for Weighing and Measuring Devices, which has been adopted by all 50 states as the basis for regulation of these devices. The module includes information on the history of the handbook, its organization and format, and how to use it. It discusses some of the basic principles underlying the handbook, for example, the factors that are considered in establishing tolerances for weighing and measuring devices.

This module is the first to be issued by the NCWM in a self-study format. Earlier modules are intended to be taught by an instructor. Each training module includes an inspector's or student's manual and an instructor's manual or a course administrator's guide.

Copies of Module 24 have been distributed to each state weights and measures program. The NCWM also will have copies of the module available for sale.

HIGH-SPEED METALLIZING OF FIBERS

A small-scale pilot plant designed to test new experimental concepts in high-speed electrodeposition of metals and alloys on monofilament

high-strength fibers is now complete and in operation to produce small quantities of metallized fiber for evaluation. This technology, developed at NIST, makes use of triaxial impinging jets of electrolyte to increase the deposition rate. Deposition of metals such as copper, nickel, and cobalt tungsten have been demonstrated. This experimental apparatus has allowed cost estimates to be made, and these indicate that metal and/or metallic composite precursors can be produced for about \$130/kg. Currently available technology is more than an order of magnitude more expensive.

ELECTROCHEMICAL DEPOSITION OF Al-Mn QUASICRYSTALS AND INTERMETALLICS

Electrodeposition of aluminum alloys and intermetallics from molten salt electrolytes offers several advantages over other metals processing techniques. The span of operating temperatures possible with molten salt electrolytes (120–500 °C) allows for the deposition of a variety of structures. In addition, since the solidification is isothermal and alloy composition is rigorously controlled by the melt composition, the microstructure and composition of electrodeposited alloys are quite uniform and predictable. Amorphous, quasicrystalline as well as metastable and stable crystalline structures have been observed in binary aluminum-manganese alloys electrodeposited from an electrolyte containing AlCl₃ and NaCl with controlled additions of MnCl₂. Electrodeposited alloys can be formed under conditions far from equilibria where the deviation from equilibrium, as well as the degree of ordering, is defined by the concurrent processes of new layer formation and surface diffusion.

The metastable amorphous phase has been formed by low-temperature electrodeposition. The direct formation of quasicrystals, having a level of free energy between that of an amorphous and a stable crystalline phase, can be achieved by an increase in deposition temperature in a manner somewhat analogous to that reported for sputter deposition. A further increase in electrolyte temperature results in the formation of the stable intermetallic phases which appear on the equilibrium phase diagram. The ability to electrodeposit thick, uniform films of the icosahedral and decagonal phases, for instance, may lead to the first mechanical property measurements of these very important binary alloys.

STRUCTURAL CERAMICS DATABASE DEVELOPED

A prototype structural ceramics database has been developed in the Ceramics Division to provide materials property data for advanced applications of ceramics. The goal of the project is to provide a critical link between the development of new materials in laboratory research studies and the use of these materials in competitive product applications. Providing this link will accelerate the development of advanced technologies that require structural ceramics for higher temperature operation or greater durability. The project is funded in part by the Gas Research Institute, the Standard Reference Data, and the Ceramics Division.

The prototype is designed for DOS-based personal computers and emphasizes user-friendliness, flexible design, and evaluated data. Property values in the system are supplemented with measures of quality, method and procedures information, and significant cautions. Materials are described in considerable detail using a modification of the ASTM Committee E-49 recommendations, and a complete bibliography of the sources of data is included.

Currently, the prototype contains thermal and mechanical property data for monolithic silicon carbides and silicon nitrides. Preparations are now under way to test the prototype at selected industrial sites.

MAGNETIC ORDER OBSERVED IN ARTIFICIAL SUPERLATTICES

NIST scientists and guest researchers from the University of Notre Dame, have recently made the first neutron diffraction determination of magnetic order in artificial metallic superlattices. The specimens consisted of layers of dilute magnetic semiconductor materials and were produced by molecular beam epitaxy techniques which yielded 100-200 alternate layers of MnSe and ZnSe, each of thickness approximately 2-5 nm. The results of the neutron measurements clearly identified long-range antiferromagnetic order within the MnSe layers. In the direction perpendicular to the atomic planes the ordering is limited in extent by the interface with the nonmagnetic ZnSe layer. No evidence of magnetic propagation between MnSe layers was found, a result consistent with predictions of current magnetism theory.

COLLABORATIVE RESEARCH EFFORT ON MATERIALS RESEARCH RENEWED

A major manufacturer of semiconductor devices, has begun its fourth year of collaborative research

with NIST on the study of materials used in the production of semiconductors. Using the neutron depth profiling facility (NDP) operated by the Center for Analytical Chemistry (CAC), researchers will continue investigations on the thin films that form the passivation layers on semiconductor devices. Elemental depth profiles are being determined to better understand and control the effects of processing in device fabrication. NDP, a quantitative and nondestructive technique, provides a means to make repetitive analyses of a single sample at various processing stages. Other techniques also can be used in conjunction with NDP on the same sample volume. Key experiments are now being designed to take advantage of both the improved detection limits for the technique and the improved research facilities being constructed as part of the Cold Neutron Research Facility.

NY FIRM JOINS WITH NIST TO INVESTIGATE CID SENSORS

A Liverpool, NY, firm has begun a twofold research program with researchers at NIST. One objective of the program is to improve chemical analysis accuracy and detection limits through the use of charge injection device (CID) sensors in analytical instrumentation. The second goal is to identify and investigate the effects of various forms of nuclear irradiation on the CID sensors and their associated camera systems.

The CID sensor is an imaging device that offers numerous technical advantages over related devices, such as the more commonly known Charge Coupled Device (CCD). For example, CID cameras typically allow excellent exposure control in low-light situations, and they also are more tolerant to intense light, producing accurate image detail even under extreme lighting conditions. This has made the devices ideal for purposes such as missile tracking, semiconductor pattern recognition, and factory process line inspection.

Scientists from industry and NIST will use the NBSR 20-MW reactor and other intense sources of radiation to expose the sensors and associated CID components to x-ray, gamma, beta, neutron, and charged particle environments to determine "radiation hardness" of the materials. The electronic characteristics of the devices will be gauged before, during, and after radiation exposure. The researchers will also explore the analytical instrumental uses of CIDs in a variety of spectroscopy applications where the signal intensity may vary greatly in magnitude during the analysis of a sample.

COLD NEUTRON WORKSHOP ON ANALYTICAL MEASUREMENTS WITH COLD NEUTRON BEAMS

The Center for Analytical Chemistry and the Reactor Radiation Division hosted the third in a series of meetings on the Cold Neutron Research Facility (CNRF). The recent meeting was held to inform the scientific community of this national facility and to solicit recommendations on the instruments being built. Two analytical measurement techniques, prompt gamma neutron activation analysis (PGNAA) and neutron depth profiling (NDP), were specifically highlighted for scientists, managers, and students from universities, industry, and other agencies from across the United States. Through invited talks and open discussions, the potential of the new instruments was explored. The participants reviewed the basics of the two techniques and discussed applications in a variety of areas, including semiconductors, polymers, metals, superconductors, biological materials, environmental monitoring, and fundamental physics. Additionally, the users policy for the CNRF was described, including required procedures for submitting proposals to gain access to the new instruments.

HIGH EFFICIENCIES OF SOFT X-RAY MIRRORS MEASURED AT SURF II

NIST scientists in collaboration with researchers from the University of Arizona, Goddard Space Flight Center, Lawrence Berkeley Laboratory, and Lawrence Livermore Laboratory, have recently measured the reflectivity of soft x-ray optical devices at angles of the incident radiation near normal to the surface and at wavelengths from 150-250 Å at SURF II. Reflectivities up to 47 percent were measured. The soft x-ray optics beamline at SURF II is one of the few facilities in the world capable of making these measurements. By working interactively with the few laboratories capable of making efficient soft x-ray mirrors, we are helping to develop the emerging technology of soft x-ray optics.

This high reflectivity at normal incidence allows scientists to make high-quality soft x-ray imaging systems used in the remote sensing and imaging of objects that emit strongly in this spectral region, e.g., the Sun and stars, with unprecedented spatial resolution. Because these devices are also wavelength selective, they act as "monochromatic" filters and discriminate against other wavelengths.

These wavelength selective, stigmatic mirrors are also being used to make efficient optical cavities for experimental soft x-ray laser systems. Other

applications include: soft x-ray lithography to obtain linewidths on semiconductor chips substantially smaller than now attainable and soft x-ray microscopy to make real-time observations of living cells in the so-called "water window" between 24 and 45Å.

LASER ABLATION SOURCE FOR STRUCTURAL STUDIES

Recently, NIST scientists completed the development of a novel molecular beam source to be used in conjunction with a pulsed-beam Fourier transform microwave spectrometer for molecular structure studies. This new capability now makes it possible to examine the technologically important refractory materials and low vapor pressure metals for which very few studies have been possible. Perhaps even more exotic molecules, e.g., mixed metal compounds and metal-molecule clusters, can be investigated with this new method.

The laser ablation beam source uses a Nd-YAG laser to vaporize solid materials into a rare gas pulsed jet, which is then examined for rotational spectra by the Fourier transform spectrometer. This method for forming vapor phase refractory molecules for spectroscopic studies overcomes substantial limitations in the conventional method of brute force heating of solid samples of the starting materials. One of the most problematic limitations of the conventional approach is a materials problem, i.e., the ability to find high-temperature inert materials as a container for substances heated in excess of 2000 °C. The laser ablation method requires no container and heats only a small area of material, $\sim 0.1 \text{ mm}^3$. The vapor is then entrained in a supersonic pulse of inert gas for delivery to the spectroscopic chamber. The initial studies with this instrument have included the examination of the rotational spectra from SiC_2 , an important circumstellar molecular species, and the oxides of the transition elements Y, La, Zr, and Hf. The rotational transition frequencies are used to determine the bond distance between the metal and oxygen atom. Measurements of the shifts in these frequencies, when an external electric field is applied, yield the molecular dipole moment and provide important information on the electronic nature of the molecular bonding.

FREQUENCY TABLES FOR CARBON MONOXIDE LASERS

In collaborative work with the University of Bonn, NIST scientists have obtained new, highly

accurate values for the molecular constants of carbon monoxide. This was done by measuring the frequencies of spectral lines of a stabilized CO laser. Frequency-measured transitions are some thousand times more accurate than wavelength-measured ones. While some of the spectral lines are well-known from earlier, isolated experiments, most of them have been improved by about a factor of 1,000 in this work. The results contribute substantially to the list of unified wave number standards used by the scientific community to calibrate spectrometers. The increasing use of Michelson interferometers has increased the need for such standards in all parts of the spectrum. The results are also useful for spectroscopic studies of important molecules in space and in the upper atmosphere. The measurements were in the region from 1140 to 2100 wave numbers, i.e., 34–62 THz, or 4.7–8.7 μm .

NEW RECORD BEAM CURRENT, 300 mA, ACCELERATED TO FULL ENERGY IN SURF-II, THE NIST ELECTRON STORAGE RING

The performance of the Synchrotron Ultraviolet Radiation Facility's (SURF-II) electron storage ring has been improved. Electron beams exceeding 250 mA are being accelerated to operating energy on a regular basis, and a new record of 300 mA has been achieved. The light intensity at all wavelengths radiated by the relativistic electron beam is directly proportional to the beam current. The higher radiation output achieved results in improved signal-to-noise for the surface science, atomic and molecular physics, and optical properties measurements that are investigated at the facility. These investigations are done by various groups from NIST, other government agencies, universities, and private industry. The storage ring also serves as a primary irradiance standard in the far ultraviolet (4–300 nm) and this improvement has extended the dynamic range of spectral irradiance that is provided to groups who use the facility to make absolute calibrations of monochromators or spectrometers.

AGREEMENTS OF OPEN SYSTEMS INTERCONNECTION (OSI) PROTOCOLS PUBLISHED

A new National Computer Systems Laboratory (NCSL) publication records working implementation specification agreements of OSI protocols among the organizations participating in the NIST Workshop for Implementors of OSI. Issued as NISTIR 89-4082, the document is based on the

proceedings of the NIST Workshop Plenary Assembly held March 17, 1989. While work described in this document is not advanced enough for use in product development or procurement reference, the work is intended as a basis for future stable agreements. As each protocol specification is completed and becomes technically stable, it is moved from this working document to the stable companion document, which records mature agreements. NIST Special Publication 500-162, Stable Implementation Agreements for Open Systems Interconnection Protocols, Version 2, Edition 1, is the current version of these mature agreements.

The NIST Workshop for Implementors of OSI accepts the specifications of emerging standards for protocols and produces agreements on the implementation and testing particulars of these protocols. This process expedites the development of OSI protocols and promotes interoperability of independently manufactured data communications equipment.

NCSL RELEASES REVISED STRUCTURED QUERY LANGUAGE (SQL) TEST SUITE

National Computer Systems Laboratory (NCSL) released Version 1.2 of the SQL Test Suite which helps users and vendors determine compliance with FIPS 127, Database Language SQL. The revised test suite adds the programming language interface Pascal and includes tests for features to be available in the next revision of FIPS 127, expected to be approved later in 1989. Version 1.2 replaces the original version of the SQL Test Suite released in August 1988. Over 30 companies presently utilize the SQL Test Suite.

OPTIONAL MODULE FOR INFORMATION RESOURCE DICTIONARY SYSTEM (IRDS) STANDARD TO BE DEVELOPED

In June 1989, ANSI's Technical Subcommittee X3 approved the development of an optional module for the IRDS standard in the area of Naming Convention Verification and assigned responsibility for the X3 Technical Report to Task Group X3H4.3, IRDS Naming Convention Verification. Approved in March as FIPS 156, the IRDS is a software system that records, stores, and processes information about an organization's data and data processing resources. NCSL's Special Publication 500-149, Guide on Data Entity Naming Conventions, is being used as the basis for developing the report.

NSF GRANT FOR NIST SENIOR RESEARCH FELLOWSHIP

National Science Foundation (NSF) has awarded a grant to the American Statistical Association for the support of a research fellowship program at NIST in the Center for Computing and Applied Mathematics. The research fellow will be selected competitively based on recommendations from an advisory group of leading industrial engineers and statisticians. The fellow will be a guest worker in the Statistical Engineering Division, leading a team effort in cross disciplinary research in process modeling and optimization as a basic approach to quality. NSF has approved this program for 3 years. During this period, several fellows are expected to collaborate with other NIST centers on a number of different processing research projects.

FIRST DEMONSTRATION OF SOLITON-LIKE COMPRESSION OF PULSES FROM OPTICAL FIBER LASER

NIST scientists have demonstrated for the first time that pulses from fiber lasers have the necessary power and spectral purity to produce soliton-like compression in external fibers. This soliton-like reduction in pulse width has previously been observed only in pulses from large, high-power lasers. An application of the work is the development of ultra-high-bit-rate lightwave communications systems. The team mode-locked an erbium fiber laser, formed by optically pumping various lengths of erbium-doped fiber. For a fiber cavity length of 20 m, the resulting pulses are 18 ps wide at a wavelength of 1536 nm and a peak power of 0.5 W. Using a streak camera, the team then measured the width of pulses from the erbium laser that had traversed 14 km of ordinary telecommunications-grade optical fiber and found that they were compressed to 5 ps. At the 0.5-W power level, the nonlinear component of the fiber refractive index is large enough to cause a "chirp" or variation of optical frequency during the pulse. At a wavelength of 1536 nm the group velocity dispersion in most fibers is negative, with the result that the trailing edge of the pulse travels faster than the leading edge, and pulse compression can result from propagation through a fiber.

EIA COMMITTEE ASKS NIST TO DEVELOP STANDARDS FOR FIBER GEOMETRY

Electronic Industries Association Committee FO6.6 on Fibers and Materials has expressed concern over the adequacy of present methods for fiber geometry and asked NIST to develop traceable standards. This request is a result of the committee's preliminary analysis of data from an international comparison of relevant measurement methods. NIST and the British Telecom Research Laboratories (BTRL) carried out an evaluation of the current state of methods for determining the geometry of optical fiber in response to a movement in the lightwave industry to reduce tolerances for physical dimensions of optical fibers. NIST administered the comparisons among U.S. and Japanese laboratories, while BTRL interacted with European laboratories. Twelve single-mode fibers were measured for outside diameter, ovality, and concentricity error. In total, 6 different techniques were evaluated, including microscopy with image processing, image shearing, microscopic interferometry, and Fizeau interferometry. Committees of the Electronic Industries Association (EIA) and the International Telegraph and Telephone Consultative Committee are now studying the results, which will be the subject of a joint NIST-BTRL report following a full analysis of the data.

GMAP SYSTEM ARCHITECTURE INSTALLED AT THE NATIONAL PDES TESTBED

In support of the National Product Data Exchange Specification (PDES) testbed project within the Factory Automation Systems Division of NIST, a guest worker from private industry, has installed the Geometric Modeling Applications Interface Program (GMAP) system architecture for supporting product data technology on the AMRF VAX 11/785. This work was done as part of the technology transfer tasks under the U.S. Air Force. Software tools to facilitate the testing of the current PDES specification are part of the GMAP system architecture and will be made available to the PDES community at large as part of the national PDES testbed.

The GMAP system architecture as installed at NIST supports every entity in the PDES/STEP Version 1.0 draft proposal, available from NTIS as document number PB 89-144794. However, the schema upon which the system currently operates

can be removed and replaced with future versions of PDES/STEP, utilizing the ability of the GMAP system architecture to maintain schema independence. PDES models and application programs can be created under the GMAP system to aid in testing the current draft proposal.

NIST QUALITY-IN-AUTOMATION PROJECT DRAWS MACHINE-TOOL COMPANY COLLABORATORS

The "Quality-in-Automation" project of NIST's Automated Manufacturing Research Facility (AMRF) has brought together senior engineers from a machine-tool company and a measurement-probe company to confer on a new measurement technique being developed within the AMRF.

As part of the AMRF project, CME researchers have developed an architecture for quality control in automated manufacturing, one aspect of which involves on-machine process-intermittent gaging, that is, high-speed automatic measurement of the dimensions of parts between the stages of the machining operations. The senior engineers conferred with CME researchers on configuring probes for machine tools to allow CME research on a generic technique for process-intermittent gaging. Both companies view the work of CME as invaluable in developing such advanced measurement techniques and demonstrating their feasibility on commercially available equipment such as theirs.

CBT DEVELOPS NEW DESIGN PROCEDURE FOR HEAT LOSSES FROM UNDERGROUND PIPING SYSTEMS

CBT has developed a new finite element computer model to estimate heat loss along structural supports for underground insulated steam and hot water pipes enclosed in shallow concrete trenches. Structural supports for these underground pipes are often in direct contact with the hot carrier pipes and form highly conductive heat flow paths through the pipe insulation to the concrete trench and the surrounding earth. The CBT model is based on two-dimensional steady-state heat conduction assuming a rectangular trench containing two insulated pipes with and without pipe supports. Two different configurations of typical structural supports were modelled. Sample calculations showed that heat loss per unit length in the vicinity of these structural supports could be as high as 17 times the value of the insulated pipe alone.

CBT MONITORS THE SOURCE STRENGTHS OF VOLATILE ORGANIC COMPOUNDS IN A MAJOR NEW FEDERAL OFFICE BUILDING

Volatile organic compounds (VOC) emitted into the air of modern office buildings that often lead to "sick building syndrome" are typically thought to be outgas from new materials when a building is first constructed or newly remodelled. CBT has discovered that this observation is not true for at least one new building. Over the last 14 months, CBT researchers have been monitoring the indoor air quality in a newly constructed 10-story federal office building in Portland, OR, beginning with the day of occupancy. They measured VOCs along with CO, CO₂, respirable particulates, formaldehyde, and radon. In addition, they made measurements of air infiltration, ventilation rates, and interzone air movement. The study indicated that the level of VOCs did not decrease over the monitoring period as would be expected if the predominant source had been building and interior finish materials. The levels remained relatively constant and could be clearly related to occupant activities. The dominant compounds found were C₁₀-C₁₁ branched alkanes emitted by 26 liquid process photocopiers and three liquid process plotters. In addition, a number of light hydrocarbons characteristic of vehicle exhaust were found and were traced to vehicles on the loading dock and in three levels of the underground garage. Although the concentration of some of these compounds was relatively high, the level of total organic carbon was three orders of magnitude below specified occupational threshold limit values for exposure to these carbon compounds. The potential for the measured concentrations of these carbon compounds to produce symptoms characteristic of the "sick building syndrome" (i.e., mucous membrane irritation, headache, nausea, and dizziness) is unknown and requires further study by health scientists.

X-RAY METHOD REMOVES AIDS VIRUS FROM EVIDENCE

Researchers at NIST, working with the Federal Bureau of Investigation and the National Cancer Institute, have tested an x-ray technique that wipes out the AIDS virus on criminal evidence without destroying important biological components. Workers in crime laboratories face a potential risk of accidental AIDS infection from exposure to criminal evidence—bloodstained clothing, for example—that may contain body fluids contaminated with the AIDS virus. Though steam

sterilization and related procedures can effectively inactivate the virus, these methods also can destroy important biological components, lessening or even canceling the value of the samples as criminal evidence. The researchers used an industrial radiographic instrument to produce the x rays and bombarded virus-tainted samples with varying intensities of x-ray radiation to determine the smallest amount needed to inactivate the AIDS virus at the lowest detectable concentration of the virus. They arrived at a dose that is about 25,000 times larger than a typical chest x ray but concluded that higher viral concentrations would require even larger radiation doses. The FBI is incorporating the new technique into its forensic labs, and other law enforcement agencies will likely follow suit.

BALDRIGE QUALITY AWARD PROGRAM SEEKS EXAMINERS

The Malcolm Baldrige National Quality Award Program currently seeks applications from individuals who can qualify as examiners. The award is offered annually to American companies that demonstrate the highest levels of total quality management. Information on the program and applications to serve as an examiner are available from the Malcolm Baldrige National Quality Award, NIST, A1123 Administration Bldg., Gaithersburg, MD 20899. As an examiner, the individual is responsible for reviewing and evaluating applications submitted for the award. Those chosen meet the highest standards of qualification and peer recognition and must participate in a preparation course based on the examination items, the scoring criteria, and the examination process. The Board of Examiners now numbers over 130 leading quality experts selected from industry, professional and trade organizations, and universities.

INTERNATIONAL DIRECTORY OF STANDARDS GROUPS UPDATED

The newly revised Directory of International and Regional Organizations Conducting Standards-Related Activities (NIST SP 767) provides information on 338 groups that conduct standardization, certification, and laboratory accreditation activities. The directory is designed to serve the federal agencies, standards writers, manufacturers, exporters, and others concerned with U.S. participation in international standards. With more than 60 new listings, the volume is one in a series to provide information on multinational standards-related endeavors. International and regional organi-

zations are listed in alphabetical order. Information includes acronyms, national affiliations, U.S. participants, membership restrictions, scope of interest, and availability of standards in English. Copies of NIST SP 767 are available from the Superintendent of Documents, U.S. Government Printing Office, Washington, DC 20402. Order by stock no. 003-003-02937-8 for \$22 prepaid. For a list of other NIST standards-related and certification directories, contact: Office of Standards Code and Information, NIST, A629 Administration Bldg., Gaithersburg, MD 20899; telephone: 301/975-4031.

EQUATION DEVELOPED FOR PREDICTING STEEL BEHAVIOR IN FIRE

NIST scientists have developed an equation for predicting the performance of ASTM A36 structural steel during and after a fire. Designed for personal computers (PCs), the equation predicts the performance of the most commonly used steel in the United States when the material is exposed to fire for periods from 2 min to 8 h over a temperature range from 350 to 650 °C. To assess deformation, an analysis of the various stresses, temperatures, and times involved are required in order to calculate the resulting strains. Each type of strain—elastic, recoverable; plastic, time-independent; and creep, time-dependent—has its own formula. The equation also can be used to construct “deformation mechanism” maps to show the dominant behavior of steel at any given temperature, time, and stress, and to compare the performance of A36 to foreign steels. A report, Elevated Temperature Deformation of Structural Steel (NISTIR 88-3899), with the new equation and information on the correlations between measured and predicted strains for ASTM A36, Australian AS A149, and Japanese SS41 structural steel steels, is available from the National Technical Information Service, Springfield, VA 22161. Order by PB# 89-172621/AS for \$21.95 prepaid.

HIGH-QUALITY AMORPHOUS SILICON FILMS PRODUCED

Government, industry, and academia are working to develop an inexpensive source of solar electricity—amorphous silicon photovoltaic solar cells. NIST and University of Colorado researchers at the Joint Institute for Laboratory Astrophysics have produced high-quality hydrogenated amorphous silicon films by decomposing silane gas on a very hot surface and depositing it on a nearby relatively cool 210 °C substrate. The technique uses a

low-pressure feed gas that offers great potential for high deposition rates, above 1 nm/s. The results obtained in this work demonstrate a low incidence of defects, which interfere with the photovoltaic efficiency and electron transport mechanisms. While high deposition rates were not the goal of the research, a low-pressure feed gas can be efficiently dissociated into a large flux of depositing radicals so that the technique looks promising for more efficient production of solar cells. The low pressure also avoids the undesirable production of dust which introduces defects into the deposited layers. A paper describing the process is available from Jo Emery, NIST, Division 104, Boulder, CO 80303; telephone: 303/497-3237.

NON-TOXIC ACIDS ARE BASIS FOR NEW CLASS OF CEMENTS

A new family of nonaqueous dental cements have been developed based on nontoxic dimer and trimer acids. They can be used in temporary fillings, liners, and as a foundation for other restorative materials. The new patented formulations, developed by a NIST scientist, use a dimer and/or a trimer acid derived from the partial polymerization of simple unsaturated fatty acids. These liquids can be mixed with a variety of basic powders used in restorative materials such as zinc oxide and calcium hydroxide. When mixed with powders, the bulky, flexible, hydrophobic nature of the dimer and trimer acids with their relatively low carboxylic acid content produce cements that are tough, low shrinking, water resistant, hydrolytically stable, and nonirritating. These new materials can be replacements for the eugenol cements that are mechanically and hydrolytically weak. For information on the new nonaqueous dental cements, contact: Dr. Joseph M. Antonucci, NIST, A143 Polymers Bldg., Gaithersburg, MD 20899; telephone: 301/975-6794.

QUICK WAY TO MEASURE HEAT CONDUCTION

Researchers from the NIST Center for Building Technology and the Virginia Polytechnic Institute and State University have investigated a quick technique for measuring on-site the heat-conducting properties of building insulation materials. Generally, this information is obtained through laboratory testing. Once in place, however, the material can settle or accumulate moisture and lose some of its insulation value. The new technique uses a thermistor, a semiconductor device, as a probe along with a computer which controls the system and

gathers data. Once inserted into the insulation, the probe acts both as a heater and a sensor to measure how the heat is being dissipated through the insulation over time. While the technique does have advantages, it also has limitations—primarily, a lack of suitable calibration materials. A report, *Development of an Automated Probe for Thermal Conductivity Measurements (NIST-GCR-89-563)*, is available from the National Technical Information Service, Springfield, VA 22161. Order by PB# 89-209324 for \$21.95 prepaid.

IS THERE A ROBOT IN YOUR FUTURE?

If you work in a federal building, there might be. The use of robotics in factories has exploded within the past decade with over 30,000 robots in use in the United States and more than 200,000 worldwide. Outside factories, using robots to perform tasks such as building operations and maintenance is receiving increased attention. In a study for the General Services Administration (GSA), which constructs, operates, and maintains federal buildings, the NIST Center for Building Technology conducted a state-of-the-art survey of robotic technology. The NIST researchers also identified potential barriers to using service robots in GSA buildings and suggested some changes to GSA's handbook of facility standards to accommodate robotic technology. *Assessment of Robotics for Improved Building Operations and Maintenance (NISTIR 88-4006)* is available from the National Technical Information Service, Springfield, VA 22161. Order by PB# 89-189237/AS for \$15.95 prepaid.

PROPERTIES OF METHANE DEVELOPED

The thermophysical properties of methane have been tabulated by NIST for a large range of fluid states based on recently formulated correlations. The use of improved correlations is important economically because methane is the major constituent of natural gas. The tables include: thermodynamic properties at temperatures from 91 to 600 K and pressures less than 100 MPa, viscosity at temperatures from 91 to 400 K and pressures to 55 MPa, and thermal conductivity from 91 to 600 K and pressures to 100 MPa. Algebraic expressions and associated tables of coefficients are given to permit additional property calculations. A FORTRAN program is listed for the evaluation of methane thermophysical properties using the Schmidt-Wagner equation of state with separate correlations for the viscosity and thermal conductivity. Copies of *Tables for the Thermophysical Properties of*

Methane (TN 1325) are available from the Superintendent of Documents, U.S. Government Printing Office, Washington, DC 20402. Order by stock number 003-003-02947-5 for \$23.00 prepaid.

FIBER LASER RESEARCH PROGRESSING

NIST researchers are investigating a laser consisting of a 90-cm length of optical fiber made of glass doped with erbium. The fiber, which has an 11- μm core, is pumped with green continuous-wave (CW) argon laser light at 528 nm. It produces CW infrared laser light at 1540 nm, suitable for transmission through optical fiber networks. NIST's work is aimed at reducing the linewidth of the infrared output to about 1 MHz, from the current 5 to 10 GHz, to realize a wavelength standard in this spectral range. A narrow bandwidth fiber laser could be used as a reference, or possibly the communication source, in a coherent communications system with increased channel capacity. Conventional pulse modulated communications over optical fibers require that the signal be amplified and reconditioned by repeaters at intervals of 30 to 60 km. Coherent communications, on the other hand, do not use wide bandwidth pulses to carry information but can use other techniques, such as closely spaced frequency modulation (FM) channels. Coherent communication signals are less affected by dispersion and do not need reconditioning as often. This means the repeaters could be spaced farther apart, which would reduce the cost of the network.

HAZARD I RELEASED TO HELP REDUCE FIRE DEATHS, COST

NIST released HAZARD I, a unique analysis method and computer program that promises to revolutionize fire safety practices and lead to marked reductions in fire losses and costs. HAZARD I can be used on a personal computer to predict the hazards to occupants in a burning building and the relative contribution of products, such as furniture, to those hazards. It is the first such comprehensive use of fire modeling in the world. HAZARD I can be used in a variety of ways in fields ranging from fire investigation and reconstruction and fire protection engineering to those concerned with product development, manufacturing, and marketing and architectural design. Also, it can be used to help building and fire codes officials evaluate new materials or design and construction techniques. A three-volume report and a set of computer disks are available for \$225 from the National Fire Protection Association, One Stop

Data Shop, Batterymarch Park, Quincy, MA 02269 or the National Technical Information Service, Springfield, VA 22161. Use PB# 89-215404 when ordering from NTIS.

NIST LAUNCHES CONSORTIUM TO DEVELOP FUTURISTIC LAB

With the goal of pooling the resources of industry, government, and academia to develop a totally automated analytical chemistry laboratory, NIST has instituted the Consortium on Automated Analytical Laboratory Systems (CAALS). Industry will likely welcome this futuristic laboratory, where automated devices—including robots—will perform the entire analytical procedure under the control of a sophisticated computer system. Analytical laboratory work often is labor intensive, performed by high-cost employees using expensive equipment. This makes the millions of yearly chemical analyses quite costly to industry and underscores the potential benefits of an automated laboratory. CAALS will pool the resources of a variety of experts to create a world-class team that will produce a viable robotics system that can be freely adapted. NIST welcomes consortium participants. For more information, contact Dr. H.M. (Skip) Kingston, NIST, A353 Chemistry Bldg., Gaithersburg, MD 20899; telephone: 301/975-4136.

INDUSTRY TO STUDY WEAR OF CERAMICS AT NIST

Private industry is sponsoring a Research Associate Program at NIST to study the tribological characteristics of ceramics and ceramic composites under various temperatures. Researchers will use a NIST high-temperature wear test facility and other special equipment to conduct studies on the friction, wear, and mechanical behavior of advanced ceramic materials. NIST currently is conducting a tribology research program that includes advanced ceramics, coatings, and composites as well as the lubrication requirements of these materials. For further information, contact: Dr. Said Jahanmir, NIST, A215 Metrology Bldg., Gaithersburg, MD 20899; telephone: 301/975-3671.

EVALUATION OF HIGH-FREQUENCY POWER METERS

Accurate power measurements are fundamental to assessing the performance of almost all radiofrequency, microwave, and millimeter wave equipment. Power considerations are also crucial for the design of efficient, cost-effective, and safe systems.

Measurements at these higher frequencies are affected by many factors. Impedance mismatch, interference, leakage, nonlinear effects, and other sources of error must be assessed and minimized. A NIST publication, Performance Evaluation of Radiofrequency, Microwave, and Millimeter Wave Power Meters (NIST TN 1310), describes measurement techniques for evaluating the electrical performance of certain commercially available power meters that use bolometric sensors and operate typically from 10 MHz to 26.5 GHz. TN 1310 is available from the Superintendent of Documents, U.S. Government Printing Office, Washington, DC 20402. Order by stock number 003-003-02931-9 for \$8.50 prepaid.

PORTLAND CEMENT CLINKER MATERIALS AVAILABLE

Producers of Portland cement have three new cement clinker reference materials (RMs) for assessing the quality of materials during processing. Portland cements produced in the United States are evaluated by ASTM C150, "Standard Specification for Portland Cement" comprising chemical composition, fineness, and performance in physical tests. The materials selected for the RMs differ widely in phase abundance, crystal sizes, and distribution crystals. The phase abundances in weight percent, in RMs 8486, 8487, and 8488, respectively, are 58.47, 73.39, and 64.97 alite; 23.18, 7.75, and 18.51 belite; 1.15, 12.09, and 4.34 aluminate; and 13.68, 3.27, and 12.12 ferrite; along with concentrations of free calcium/oxide, periclase, and alkali sulfate. The phases were determined by point counting using reflected light microscopy. The other properties were determined by chemical analysis. Each RM consists of three hermetically sealed glass vials with approximately 10 grams of crushed clinker. For information on RMs 8486, 8487, and 8488, available for \$96 each, contact the Office of Standard Reference Materials, NIST, B311 Chemistry Bldg., Gaithersburg, MD 20899; telephone: 301/975-OSRM (6776).

OH, SAY CAN YOU SEE?

Lighting can be soft or harsh or too dim or too bright or even just right. But, no matter how it is perceived, lighting greatly influences not only our ability to see but also our feelings and even our health. In an effort to understand how lighting affects human performance, researchers at NIST and the Lighting Research Institute studied energy consumption, brightness, and peoples' perceptions

of their lighting systems. The researchers used data from 912 workstations in 13 office buildings. Among the findings: About 70 percent of the occupants surveyed were satisfied with their lighting. Of those who were dissatisfied, 37 percent had furniture-integrated task lighting combined with an indirect ambient lighting system. Energy consumption also was higher for this system. Dissatisfaction was related to the patterns of brightness—workstations with lower brightness were less successful. Copies of the report, Evaluating Office Lighting Environments: Second Level Analysis (NISTIR 89-4069), are available from the National Technical Information Service, Springfield, VA 22161. Order by PB# 89-189153 for \$21.95 prepaid.

NEW NIST STANDARD REFERENCE DATABASE

NIST Standard Reference Database 17—NIST Chemical Kinetics, released earlier of this year, provides rapid access to kinetics data for gas phase reactions. The database contains more than 8,000 data items on 2,000 separate reactions. Searchable by reactants or by reference, retrievals provide surveys of the literature on a particular reaction, all or subsets of the reactions of a specific species, and the data available from a given paper. NIST Chemical Kinetics, which can function on any MS-DOS or PC-DOS, has rapidly become a best-seller.

CERAMIC POWDERS SYNTHESIS—MAGNETIC MEDIA

The Ceramics and Metallurgy Divisions are examining a new class of magnetic composite materials. These materials consist of ultrafine magnetic particles of less than 20 nm, and offer considerable potential for ultradense magnetic recording media.

Information transmission, storage, and retrieval technologies have experienced phenomenal growth within the past two decades. Thus, there exists a continuing need for new or improved approaches to support this expanding field. For example, the area of magnetic recording is highly dependent on magnetic particulate media.

Magnetic composite materials are generated using sol-gel techniques appropriate to the formation of diphasic iron-silica xerogels. These composites are synthesized by room temperature polymerization and curing of gels derived from solutions of tetraethylorthosilicate, ferric nitrate, and water. The hydrofluoric acid is used as a catalyst. The resulting composite is a homogeneous dispersion of ultrafine iron-containing particles in a silica-like matrix.

The chemical and magnetic states of the iron in these composites can be established in situ by exposure to gaseous reducing or oxidizing environments at temperatures less than 400 °C. Magnetic measurements and Mössbauer spectroscopy on these systems have established that these nanocomposites have magnetic regions with diameters <20 nm. Furthermore, the bulk materials can be controllably engineered to display paramagnetic, superparamagnetic, ferrimagnetic, or ferromagnetic behavior.

EXPERT SYSTEM FOR MATERIAL SELECTION ADVICE FOR THE PETROLEUM INDUSTRY

A knowledge base expert system has been developed in the corrosion data center at NIST in cooperation with the New Zealand Department of Scientific and Industrial Research (DSIR) and the National Association of Corrosion Engineers.

The program operates on personal computers and provides material selection advice for components of pumps used in the downhole environment (sucker rod pumps). Industry standards, together with corrosion advice and information obtained from oil and gas production companies and equipment manufacturers, provide a basis for assessing current industry practice and key environmental factors. The expert system considers a broad range of user-supplied chemical and physical parameters to characterize the anticipated corrosivity of complex downhole environments and the relative suitability of corrosion resistant engineering materials. The system defines the downhole environment by applying rules and inference procedures structured from the domain expertise derived from the information sources. The knowledge base encompasses over 600 rules and provides options of materials selection consultation, review of related domain information, and addition of custom rules to highlight user-specified in-house requirements.

SANDIA TO PARTICIPATE IN COLD NEUTRON FACILITY INSTRUMENT DEVELOPMENT

The Organic and Electronic Materials Department of Sandia National Laboratories (SNL) agreed to participate with NIST in the development and use of two high-resolution instruments at the Cold Neutron Research Facility (CNRF). This is the first such facility in the United States.

The instruments are the high-resolution neutron time-of-flight spectrometer and the back-reflection

spectrometer, both of which are already in the preliminary design phase at NIST. Both instruments are for inelastic neutron scattering studies in which the dynamics and interactions of atoms and molecules are elucidated through the observation of their characteristic energy states and diffusive motions. This type of measurement has already proven highly important in studies of dynamic processes in a wide variety of materials and chemical systems; for example, as a probe of catalysis mechanisms, hydrogen interactions with metals, phase transformations, magnetic materials, and in studies of intermolecular potentials and rotational motions in molecules and macromolecules. The two spectrometers being developed at the CNRF will be equal to or better than similar instruments anywhere in the world.

INDUSTRY SUPPORTS RESEARCH ON THE DEVELOPMENT OF OPTICAL WAVEGUIDE SENSORS

A consortium of biotechnology companies has signed a 3-year cooperative research agreement with NIST to support research in the Organic Analytical Research Division of the Center for Analytical Chemistry. The investigation will entail the design, fabrication, and evaluation of planar and fiber optic waveguide phase-sensitive analytical sensors for real-time monitoring. The device will consist of a Mach Zehnder interferometer onto which analyte-specific antibodies have been immobilized. Analyte quantitation will be achieved by measurement of the enthalpy (heat) of the antigen-antibody binding reaction. The heat generated at the sensing arm of the interferometer will perturb the phase of the guided laser light with respect to the reference arm. Interferences common to both arms will be rejected.

The analyte chosen to evaluate the efficacy of the interferometric immunoassay system is BT toxin, a natural insecticide (entomopathogen) produced biotechnologically from a spore-forming bacteria. This mammalian-harmless toxin is used against larval gypsy moths, as well as mosquitoes and blackflies. To maximize the production of toxin, the sporulation cycle must be terminated before sporulation occurs and this requires a real-time, BT toxin-sensitive sensor. By the appropriate choice of antibody, this approach should be applicable to a broad range of analytes.

FEDERAL INFORMATION PROCESSING STANDARD (FIPS) PROPOSED FOR THE USER INTERFACE COMPONENT OF THE APPLICATIONS PORTABILITY PROFILE (APP)

A Federal Register notice announced and requested comments on a proposed FIPS which would adopt the X Protocol, Xlib Interface, XT Intrinsic, and Bitmap Distribution Format specifications of the X Window System, Version 11, Release 3 (X Window System is a trademark of MIT). The standard covers the data stream encoding, data stream interface, and subroutine foundation layers of the reference model for network-based bit-mapped graphic user interface standards, which is detailed in the appendix to the proposed standard.

The proposed standard is part of a series of specifications required for applications portability, the ability to move or port an application from one operating system environment to another. NCSL has proposed an application portability profile that provides an architectural approach to applications portability and consists of a group of standard elements including database management, data interchange, network services, user interfaces, and programming languages.

OPEN SYSTEMS INTERCONNECTION/ INTEGRATED SERVICES DIGITAL NETWORK (OSI/ISDN) TRIAL HELD

To demonstrate the use of ISDN as a lower layer technology for OSI applications, NCSL organized the OSI/ISDN trial as a necessary first step for including ISDN as a lower layer technology in the Government Open Systems Interconnection Profile (GOSIP) Version 2. Approved as Federal Information Processing Standard (FIPS) 146 in 1988, GOSIP specifies a set of OSI protocols for computer networking for use by government agencies in the procurement of products and services. GOSIP Version 1 supports the message handling systems and file transfer, access, and management applications; GOSIP Version 2 proposes additional functionality including Virtual Terminal Service, Office Document Architecture, and ISDN.

The OSI/ISDN trial was held June 20-21, 1989, at Mather Air Force Base, CA. Trial objectives were to support the inclusion of ISDN transport capabilities in the GOSIP Version 2, to demonstrate the operation of OSI applications using ISDN transport capabilities, and to demonstrate

the interworking of ISDN and existing transport technologies. Among the ISDN functions tested were CLNP over ISDN X.25, X.25 D-Channel, and X.25 Preallocated B-Channel.

The trial successfully demonstrated two ISDN capabilities: ISDN as a transit subnetwork along an end-to-end communication path where neither source nor the destination are directly attached to the ISDN itself and the transit properties of an ISDN as an OSI subnetwork; and the interconnectivity capability of an ISDN subnetwork with other types of subnetworks and end-to-end communication across multiple interconnected subnetworks where one of the subnetworks is an ISDN.

NIST BREAK-JUNCTION MEASUREMENT PROVIDES FIRST DETERMINATION OF SIS TUNNELING GAP OF A THALLIUM-BASED HIGH-TEMPERATURE SUPERCONDUCTOR

A NIST scientist has carried out the first measurements of the superconductor-insulator-superconductor (SIS) tunneling energy gap in thallium-based high-temperature superconductors. Using the break-junction method he pioneered, the scientist measured crystals grown and characterized at Sandia National Laboratories. Energy gap is a fundamental characteristic of a superconductor and in this case is important to the ultimate understanding of the superconducting behavior in thallium-based and other high-transition-temperature materials. The measured gap value of 30 meV is consistent with the Bardeen-Cooper-Schrieffer theory of superconductivity, applied to the configuration of the break junction. The scientist was able to detect a supercurrent when the break junction was operated in a point-contact mode at temperatures as high as 95 K.

NIST TO PARTICIPATE IN CONSORTIUM ORGANIZED TO STUDY S₂F₁₀

NIST is a participant in a new consortium for studying the formation and detection of disulfurdecafluoride (S₂F₁₀) in electrical power systems. A cooperative investigation led by NIST staff recently confirmed for the first time the presence of this extremely toxic gas (threshold limit value of 10 parts per billion) in sulfur hexafluoride (SF₆) exposed to electrical discharge. Because SF₆ is used widely as an insulating gas in high-voltage electric power transmission systems, serious concern exists about the hazards associated with exposure to decomposed SF₆ during maintenance and repair of electric power equipment such as circuit breakers and gas-insulated transmission lines.

NIST MINIATURE BROADBAND ELECTRIC-FIELD PROBE DESIGN COMMERCIALIZED

Two U.S. organizations are offering commercial versions of the 8-mm electric field probe developed by NIST staff that have an isotropic response of better than ± 0.3 dB from 100 kHz to 18 GHz. The NIST probe can measure fields between 1 and 1600 V/m from 1 MHz to 15 GHz, flat to ± 2 dB. Probes are available from the Electro-Mechanics Company of Austin, TX and Denver Research Institute (DRI), affiliated with Denver University; the Italian aerospace manufacturer Aeritalia has also indicated its intention to market the probe. The probe's performance is achieved through the use of thin-film dipole elements having a precisely tailored resistive profile.

Calibration Services

NEW AUTOMATED GAGE BLOCK CALIBRATION SYSTEM AT NIST

A new calibration system has been successfully implemented by the NIST gage block laboratory. The new system allows NIST laboratory personnel to implement routinely a measurement assurance program for all NIST reference standard master gage blocks. With the new measurement design, typical estimates for the uncertainty of the calibrations by mechanical intercomparison have already been substantially reduced from between 2.0 and 4.0 μm (0.05 to 0.10 μm) to between 1.0 and 2.0 μm (0.02 to 0.05 μm) or less for gage blocks under 2 in (50 mm). Although uncertainty estimates for the longer gage block sizes have remained unchanged, improved and frequent surveillance of NIST gage block calibration history are expected to reduce presently reported uncertainty estimates for these sizes in the future. The new system includes a database and analysis software to record and monitor the measurement history of customers' gage blocks and, thereby, reduce risks of reporting inaccurate measurements and improving overall measurement confidence.

Calendar

January 16–18, 1990

HYPertext STANDARDIZATION WORKSHOP

Location: National Institute of
Standards and Technology
Gaithersburg, MD

This workshop will disseminate technical information on Hypertext to users and designers in industry, government, and academia. Workshop goals are to consider Hypertext system definitions, to identify viable approaches for pursuing standards, to seek commonality among alternatives wherever possible, and to make progress towards a coordinated plan for standards development, i.e., a Hypertext reference model. Hypertext technology is an approach to information management in which data are stored in a network of nodes connected by links.

Contact: Jean Baronas, B266 Technology Building, NIST, Gaithersburg, MD 20899, 301/975-3338.

June 11–13, 1990

50th ANNUAL CONFERENCE ON PHYSICAL ELECTRONICS

Location: National Institute of
Standards and Technology
Gaithersburg, MD

The conference will focus on the physics and chemistry of solid surfaces and interfaces. Topics of interest include electronic, chemical and crystallographic properties of surfaces and interfaces as well as kinetic and dynamic mechanisms of physical and chemical reactions, phase transitions, and adsorption. The properties of surfaces that are clean or that incorporate foreign atoms are of interest, as are new methods of surface analysis and

characterization. Emphasis will be placed on the description of surface and interface properties at a fundamental atomic and molecular level. Sponsored by the American Physical Society, NIST, and the University of Maryland.

Contact: Richard R. Cavanagh, B248 Chemistry Building, NIST, Gaithersburg, MD 20899, 301/975-2368.

July 23–26, 1990

CONFERENCE ON ADVANCES IN CEMENTITIOUS MATERIALS

Location: National Institute of
Standards and Technology
Gaithersburg, MD

The purpose of the conference is to advance understanding of cementitious materials so as to provide a rational approach to the design of new cementitious materials and composites. The conference will address the fundamental science underlying the behavior of all cementitious materials, whether mass concrete or chemically bonded ceramics. However, to limit the scope of the conference, degradation processes will not be included. The conference should be of interest to all who are concerned about enhancing the performance of concrete and making it a more predictable material. Holding the conference at the National Institute of Standards and Technology will make it possible for participants to visit the laboratories of the NIST Center for Building Technology. Session topics include characterization of particulate starting materials and of resultant microstructure; physical and chemical phenomena in the flow of cementitious materials prior to hardening; relationships between microstructure and physical and mechanical behavior; interactions of water with the hardened cement paste matrix; the microstructure and micromechanics of cementitious composites, including the

effects of interfaces; and new cements and novel cement matrices.

Contact: Geoffrey Frohnsdorff, B368 Building Research Building, NIST, Gaithersburg, MD 20899, 301/975-6706.

August 16–21, 1990

**INTERNATIONAL CONFERENCE ON THE
CHEMISTRY OF ELECTRONIC
CERAMIC MATERIALS**

Location: Grand Teton
National Park, WY

Materials chemistry has evolved from the more identifiable disciplines of inorganic and solid state chemistry, ceramics, and materials science. It is inherently interdisciplinary, attracting scientists from many different backgrounds, such as materials science, physical, inorganic, and organo-metallic chemistry, physics, ceramics, and mineralogy. This conference will bring together major national and international researchers to bridge the gap between those primarily interested in the pure chemistry of inorganic solids and those interested in the physical and electronic properties of ceramics. One of the primary goals of the conference will be to evaluate our current understanding of the chemistry of electronic ceramic materials and to assess the state of a field that has become one of the most important areas of advanced materials research. Sponsored by NIST, the Office of Naval Research, and other scientific organizations—federal, university, and industry.

Contact: Robert Roth, B126 Materials Building, NIST, Gaithersburg, MD 20899, 301/975-6116 .

September 18–20, 1990

ELECTRONIC PUBLISHING '90

Location: National Institute of
Standards and Technology
Gaithersburg, MD

Electronic Publishing '90 (EP90) will be the third in a series of international conferences established to bring together researchers in all areas of electronic publishing systems. EP86, held in Nottingham, England, was sponsored by the British Computer Society. EP88, held in Nice, France, was sponsored by INRIA. The proceedings of papers presented at the earlier sessions were published by Cambridge University Press and have received wide dissemination. The proceedings of EP90 will also be published in book form and will be available at the conference. EP90 will adopt a broad definition of "electronic publishing." Electronic publishing will be taken to encompass all aspects of computer-assisted preparation, presentation, transmittal, storage, and retrieval of documents. The scope of the conference also includes the design of the related computer systems, the design of their components, and the theory that underlies such systems. Both linear and non-linear documents are appropriate subjects for discussion. Sponsored by NIST.

Contact: Lawrence A. Welsch, B252 Technology Building, NIST, Gaithersburg, MD 20899, 301/975-3345.

Subject Index to Volume 94

Numbers in parenthesis after the page number are the issue numbers

- No. 1 January-February
 No. 2 March-April
 No. 3 May-June
 No. 4 July-August
 No. 5 September-October
 No. 6 November-December

A		conformal mapping	117(2)
absolute ratio	347(6), 357(6)	consensus values	197(3)
analytical chemistry	25(1)	Consultative Committee on Electricity . .	95(2)
assay	347(6)	Consultative Committee on Standards for the Measurement of Ionizing Radiations	363(6)
atomic weight	347(6), 357(6)	convergence proof	197(3)
automation	311(5)	copper oxides	147(3)
B		cotinine	305(5)
becquerel	363(6)	cotinine perchlorate	305(5)
Bergman kernel	117(2)	coupling	117(2)
biological material	215(4)	cryogenic engineering	147(3)
biotechnology	59(1)	crystal structure	147(3)
botanical material	215(4)	crystallographic database	49(1)
C		CRYSDAT	9(1), 49(1)
CAD	281(5)	cubic splines	117(2)
calibration	179(3)	D	
capacitors	179(3)	data banks	85(1)
CBRIS	281(5)	data files	21(1)
CCE	95(2)	database	25(1), 281(5)
¹⁰⁹ Cd	363(6)	database management systems	59(1)
ceramics	37(1), 147(3)	delay	311(5)
characteristic branching ratios of ionic substructures	281(5)	diffusion coefficients	105(2)
chemical thermodynamics data	21(1)	digital systems	311(5)
chemical thermodynamics	21(1)	dimethylglyoxime	347(6)
CIPM	95(2)	dissipation factor	179(3)
coaxial air line	117(2)	E	
collisionally-activated dissociation	281(5)	electric power	179(3)
compact domains	65(1)	electrical standards	179(3)
comparative modeling	79(1)	electron diffraction	15(1)
comparisons of activity measurements . . .	363(6)	electronic structure	147(3)
components of variance (within-and between-groups)	197(3)	electrostatics	79(1)
computer systems	59(1)	energy levels	221(4)
computer communication networks	59(1)	enthalpy	21(1)
computerized database	37(1)	error sources	117(2)
computers	25(1), 311(5)	evaluated data	21(1)
		evaluation	25(1)

F		medical informatics	59(1)
fluids	113(2), 259(4)	modeling	65(1)
frequency	311(5)	molecular biology	59(1), 85(1)
G		molecular graphics	85(1)
GC-MS	305(5)	MS/MS	281(5)
H		N	
heat capacity	21(1)	National Library of Medicine (U.S.)	59(1)
α helix	65(1)	neutron scattering	259(4)
high T_c superconductors	49(1)	nickel	347(6), 357(6)
hydrophobicity	79(1)	NIST services	179(3)
I		NIST-EPA International Round Robin	281(5)
^{125}I	363(6)	nuclear magnetic resonance	25(1)
identification	15(1)	numeric databases	9(1), 15(1), 21(1)
industrial use of numeric databases	9(1)	O	
infrared spectrum	25(1)	ohm	95(2)
International Committee of Weights and Measures	95(2)	on-line searching	9(1)
International Reference System for radionuclides	363(6)	optical molasses	373(6)
International System of Units	95(2)	overview	147(3)
iodine	215(4)	P	
ion-molecule kinetics	281(5)	parameters	221(4)
isotopic abundance	347(6), 357(6)	passive smoking	305(5)
J		periodic surface profile	367(6)
JANAF Thermochemical Tables	21(1)	periodic waveform	367(6)
Josephson effect	95(2)	perovskites	147(3)
Josephson frequency-to-voltage quotient	95(2)	phase characterization	15(1)
L		phase transitions	21(1)
laser cooling	373(6)	piston gage	343(6)
lattice matching	9(1)	platinum	113(2)
M		prediction of ferroelectricity	9(1)
manometer	343(6)	pressure	113(2), 343(6)
mass spectrometry	215(4), 347(6), 357(6)	pressure measurement	343(6)
mass spectrum	25(1)	pressure metrology	343(6)
material properties	37(1)	pressure standards	343(6)
materials science	9(1), 147(3)	principal mode	117(2)
measurement contour	117(2)	propagation delay	311(5)
measurement precision	117(2)	protein structures	65(1), 79(1), 85(1)
measurement protocol	281(5)	Q	
measurement science	147(3)	quantized Hall resistance	95(2)
M		quantum Hall effect	95(2)
manometer	343(6)	R	
mass spectrometry	215(4), 347(6), 357(6)	radioactivity standards	363(6)
mass spectrum	25(1)	random error	367(6)
material properties	37(1)	resistance	113(2)
materials science	9(1), 147(3)		
measurement contour	117(2)		
measurement precision	117(2)		
measurement protocol	281(5)		
measurement science	147(3)		

rheology.....	259(4)		
root-mean-square value.....	367(6)		
S			
SANS.....	259(4)		
scattering parameters.....	117(2)		
⁷⁵ Se.....	363(6)		
sequence alignment.....	79(1)		
sequence profiles.....	65(1)		
shear.....	259(4)		
SI.....	95(2)		
side stream smoke.....	305(5)		
skin effect.....	117(2)		
spectra.....	221(4)		
spectral library.....	281(5)		
SRM 986.....	357(6)		
Standard Reference Materials ...	215(4), 357(6)		
standardization.....	281(5)		
standards.....	305(5)		
Structural Ceramics Database.....	37(1)		
structure prediction.....	65(1), 85(1)		
superconductivity.....	9(1), 147(3)		
supercritical fluid chromatography.....	105(2)		
surface roughness.....	117(2), 367(6)		
synchronization, time.....	311(5)		
T			
tandem mass spectrometers.....	281(5)		
Taylor series.....	197(3)		
telegraphist equations.....	117(2)		
telephone.....	311(5)		
templates.....	65(1)		
terrestrial samples.....	357(6)		
thermal conductivity.....	113(2)		
tobacco.....	305(5)		
trace analysis.....	215(4)		
transient hot-wire.....	113(2)		
tungsten.....	221(4)		
β turn.....	65(1)		
U			
uncertainty.....	367(6)		
user-friendly.....	37(1)		
V			
vapor cell.....	373(6)		
vapor pressure.....	21(1)		
volt.....	95(2)		
voltage transformers.....	179(3)		
W			
wavelengths.....	221(4)		
weighted least squares regression.....	197(3)		
weighted average.....	197(3)		
X			
XQQ instruments (QQQ, BEQQ, etc.) ...	281(5)		

Author Index to Volume 94

Numbers in parenthesis after the volume number are the issue numbers

- No. 1 January-February
- No. 2 March-April
- No. 3 May-June
- No. 4 July-August
- No. 5 September-October
- No. 6 November-December

A

Allan, D. W.

The NIST Automated Computer Time Service. Levine, J., Weiss, M., Davis, D. D., Allan, D. W., and Sullivan, D. B. **94(5)**, 311 (1989).

Anderson, W. E.

Calibration of Voltage Transformers and High-Voltage Capacitors at NIST. Anderson, W. E. **94(3)**, 179 (1989).

B

Barnes, I. L.

Absolute Isotopic Abundance Ratios and Atomic Weight of a Reference Sample of Nickel. Gramlich, J. W., Machlan, L. A. Barnes, I. L., and Paulsen, P. J. **94(6)**, 347 (1989).

The Absolute Isotopic Composition and Atomic Weight of Terrestrial Nickel. Gramlich, J. W., Beary, E. S. Machlan, L. A., and Barnes, I. L. **94(6)**, 357 (1989).

Bean, V. E.

The Reduction of Uncertainties for Absolute Piston Gage Pressure Measurements in the Atmospheric Pressure Range. Welch, B. E., Edsinger, R. E., Bean, V. E., and Ehrlich, C. D. **94(6)**, 343 (1989).

Beary, E. S.

The Absolute Isotopic Composition and Atomic Weight of Terrestrial Nickel. Gramlich, J. W., Beary, E. S. Machlan, L. A., and Barnes, I. L. **94(6)**, 357 (1989).

Bennett, L. H.

A Brief Review of Recent Superconductivity Research at NIST. Lundy, D. R., Swartzendruber, L. J., and Bennett, L. H. **94(3)**, 147 (1989).

Bruno, T. J.

A Supercritical Fluid Chromatograph for Physicochemical Studies. Bruno, T. J. **94(3)**, 105 (1989).

Byrd, G. D.

A Cotinine in Freeze-Dried Urine Reference Material. Sander, L. C., and Byrd, G. D. **94(5)**, 305 (1989).

C

Cabeza, M. I.

The Spectrum of Doubly Ionized Tungsten (W III). Iglesias, L., Cabeza, M. I., Rico, F. R., Garcia-Riquelme, O., and Kaufman, V. **94(4)**, 221 (1989).

Carr, M. J.

NIST/Sandia/ICDD Electron Diffraction Database: A Database for Phase Identification by Electron Diffraction. Carr, M. J., Chambers, W. F., Melgaard, D., Himes, V. L., Stalick, J. K., and Mighell, A. D. **94(1)**, 15 (1989).

Chambers, W. F.

NIST/Sandia/ICDD Electron Diffraction Database: A Database for Phase Identification by Electron Diffraction. Carr, M. J., Chambers, W. F., Melgaard, D., Himes, V. L., Stalick, J. K., and Mighell, A. D. **94(1)**, 15 (1989).

Chase, M. W.

Numeric Databases in Chemical Thermodynamics at the National Institute of Standards and Technology. Chase, M. W. **94(1)**, 21 (1989).

D

Davis, D. D.

The NIST Automated Computer Time Service. Levine, J., Weiss, M., Davis, D. D., Allan, D. W., and Sullivan, D. B. **94(5)**, 311 (1989).

E

Edsinger, R. E.

The Reduction of Uncertainties for Absolute Piston Gage Pressure Measurements in the Atmospheric Pressure Range. Welch, B. E., Edsinger, R. E., Bean, V. E., and Ehrlich, C. D. **94(6)**, 343 (1989).

Ehrlich, C. D.

The Reduction of Uncertainties for Absolute Piston Gage Pressure Measurements in the Atmospheric Pressure Range. Welch, B. E., Edsinger, R. E., Bean, V. E., and Ehrlich, C. D. **94(6)**, 343 (1989).

G

Garcia-Riquelme, O.

The Spectrum of Doubly Ionized Tungsten (W III). Iglesias, L., Cabeza, M. I., Rico, F. R., Garcia-Riquelme, O., and Kaufman, V. **94(4)**, 221 (1989).

Gramlich, J. W.

Determination of Trace Level Iodine in Biological and Botanical Reference Materials by Isotope Dilution Mass Spectrometry. Gramlich, J. W., and Murphy, T. J. **94(4)**, 215 (1989).

Absolute Isotopic Abundance Ratios and Atomic Weight of a Reference Sample of Nickel. Gramlich, J. W., Machlan, L. A., Barnes, I. L., and Paulsen, P. J. **94(4)**, 347 (1989).

The Absolute Isotopic Composition and Atomic Weight of Terrestrial Nickel. Gramlich, J. W., Beary, E. S., Machlan, L. A., and Barnes, I. L. **94(4)**, 357 (1989).

H

Himes, V. L.

NIST/Sandia/ICDD Electron Diffraction Database: A Database for Phase Identification by Electron Diffraction. Carr, M. J., Chambers, W. F., Melgaard, D., Himes, V. L., Stalick, J. K., and Mighell, A. D. **94(1)**, 15 (1989).

Holt, D. R.

Scattering Parameters Representing Imperfections in Precision Coaxial Air Lines. Holt, D. R. **94(2)**, 117 (1989).

Erratum: Scattering Parameters Representing Imperfections in Precision Coaxial Air Lines. Holt, D. R. **94(5)**, 323 (1989).

Hoppes, D. D.

Special Report on Standards for Radioactivity—Report on the 1989 Meeting of the Radionuclide Measurements Section of the Consultative Committee on Standards for the Measurement of Ionizing Radiations. Hoppes, D. D. **94(6)**, 363 (1989).

Hubbard, C. R.

The Structural Ceramics Database: Technical Foundations. Munro, R. G., Hwang, F. Y., and Hubbard, C. R. **94(1)**, 37 (1989).

Hwang, F. Y.

The Structural Ceramics Database: Technical Foundations. Munro, R. G., Hwang, F. Y., and Hubbard, C. R. **94(1)**, 37 (1989).

I

Iglesias, L.

The Spectrum of Doubly Ionized Tungsten (W III). Iglesias, L., Cabeza, M. I., Rico, F. R., Garcia-Riquelme, O., and Kaufman, V. **94(4)**, 221 (1989).

K

Kaufman, V.

The Spectrum of Doubly Ionized Tungsten (W III). Iglesias, L., Cabeza, M. I., Rico, F. R., Garcia-Riquelme, O., and Kaufman, V. **94(4)**, 221 (1989).

L

Lesk, A. M.

The Computational Analysis of Protein Structures: Sources, Methods, Systems, and Results. Lesk, A. M., and Tramontano, A. **94(1)**, 85 (1989).

Levine, J.

The NIST Automated Computer Time Service. Levine, J., Weiss, M., Davis, D. D., Allan, D. W., and Sullivan, D. B. **94(5)**, 311 (1989).

Lias, S. G.

Numeric Databases for Chemical Analysis. Lias, S. G. **94(1)**, 25 (1989).

Lundy, D. R.

A Brief Review of Recent Superconductivity Research at NIST. Lundy, D. R., Swartzendruber, L. J., and Bennett, L. H. **94(3)**, 147 (1989).

M**Machlan, L. A.**

Absolute Isotopic Abundance Ratios and Atomic Weight of a Reference Sample of Nickel. Gramlich, J. W., Machlan, L. A. Barnes, I. L., and Paulsen, P. J. **94(6)**, 347 (1989).

The Absolute Isotopic Composition and Atomic Weight of Terrestrial Nickel. Gramlich, J. W., Beary, E. S. Machlan, L. A., and Barnes, I. L. **94(6)**, 357 (1989).

Mandel, J.

Consensus Values, Regressions, and Weighting Factors. Paule, R. C., and Mandel, J. **94(3)**, 197 (1989).

Martinez, R. I.

Instrument-Independent MS/MS Database for XQQ Instruments: A Kinetics-Based Measurement Protocol. Martinez, R. I. **94(5)**, 281 (1989).

Matula, R. A.

The Importance of Numeric Databases to Materials Science. Matula, R. A. **94(1)**, 9 (1989).

Masys, D. R.

New Directions in Bioinformatics. Masys, D. R. **94(1)**, 59 (1989).

Melgaard, D.

NIST/Sandia/ICDD Electron Diffraction Database: A Database for Phase Identification by Electron Diffraction. Carr, M. J., Chambers, W. F., Melgaard, D., Himes, V. L., Stalick, J. K., and Mighell, A. D. **94(1)**, 15 (1989).

Migdall, A. L.

A Search for Optical Molasses in a Vapor Cell: General Analysis and Experimental Attempt. Migdall, A. L. **94(6)**, 373 (1989).

Mighell, A. D.

NIST/Sandia/ICDD Electron Diffraction Database: A Database for Phase Identification by Electron Diffraction. Carr, M. J., Chambers, W. F., Melgaard, D., Himes, V. L., Stalick, J. K., and Mighell, A. D. **94(1)**, 15 (1989).

Moult, J.

Comparative Modeling of Protein Structure—Progress and Prospects. Moult, J. **94(1)**, 79 (1989).

Munro, R. G.

The Structural Ceramics Database: Technical Foundations. Munro, R. G., Hwang, F. Y., and Hubbard, C. R. **94(1)**, 37 (1989).

Murphy, T. J.

Determination of Trace Level Iodine in Biological and Botanical Reference Materials by Isotope Dilution Mass Spectrometry. Gramlich, J. W., and Murphy, T. J. **94(4)**, 215 (1989).

P**Paule, R. C.**

Consensus Values, Regressions, and Weighting Factors. Paule, R. C., and Mandel, J. **94(3)**, 197 (1989).

Paulsen, P. J.

Absolute Isotopic Abundance Ratios and Atomic Weight of a Reference Sample of Nickel. Gramlich, J. W., Machlan, L. A. Barnes, I. L., and Paulsen, P. J. **94(6)**, 347 (1989).

Perkins, R. A.

Relation Between Wire Resistance and Fluid Pressure in the Transient Hot-Wire Method. Roder, H. M., and Perkins, R. A. **94(2)**, 113 (1989).

R**Reid, L. S.**

The Use of Structural Templates in Protein Backbone Modeling. Reid, L. S. **94(1)**, 65 (1989).

Rico, F. R.

The Spectrum of Doubly Ionized Tungsten (W III). Iglesias, L., Cabeza, M. I., Rico, F. R., Garcia-Riquelme, O., and Kaufman, V. **94(4)**, 221 (1989).

Roder, H. M.

Relation Between Wire Resistance and Fluid Pressure in the Transient Hot-Wire Method. Roder, H. M., and Perkins, R. A. **94(2)**, 113 (1989).

S**Sander, L. C.**

A Cotinine in Freeze-Dried Urine Reference Material. Sander, L. C., and Byrd, G. D. **94(5)**, 305 (1989).

Siegrist, T.

Applications of the Crystallographic Search and Analysis System CRYSTDAT in Materials Science. Siegrist, T. **94(1)**, 49 (1989).

Stalick, J. K.

NIST/Sandia/ICDD Electron Diffraction Database: A Database for Phase Identification by Electron Diffraction. Carr, M. J., Chambers, W. F., Melgaard, D., Himes, V. L., Stalick, J. K., and Mighell, A. D. **94(1)**, 15 (1989).

Straty, G. C.

Apparatus for Neutron Scattering Measurements on Sheared Fluids, Straty, G. C. **94(4)**, 259 (1989).

Sullivan, D. B.

The NIST Automated Computer Time Service. Levine, J., Weiss, M., Davis, D. D., Allan, D. W., and Sullivan, D. B. **94(5)**, 311 (1989).

Swartzendruber, L. J.

A Brief Review of Recent Superconductivity Research at NIST. Lundy, D. R., Swartzendruber, L. J., and Bennett, L. H. **94(3)**, 147 (1989).

T**Taylor, B. N.**

Special Report on Electrical Standards—New Internationally Adopted Reference Standards of Voltage and Resistance. Taylor, B. N. **94(2)**, 95 (1989).

Teague, E. C.

On Measuring the Root-Mean-Square Value of a Finite Record Length Periodic Waveform. Teague, E. C. **94(6)**, 367 (1989).

Tramontano, A.

The Computational Analysis of Protein Structures: Sources, Methods, Systems, and Results. Lesk, A. M., and Tramontano, A. **94(1)**, 85 (1989).

W**Weiss, M.**

The NIST Automated Computer Time Service. Levine, J., Weiss, M., Davis, D. D., Allan, D. W., and Sullivan, D. B. **94(5)**, 311 (1989).

Welch, B. E.

The Reduction of Uncertainties for Absolute Piston Gage Pressure Measurements in the Atmospheric Pressure Range. Welch, B. E., Edsinger, R. E., Bean, V. E., and Ehrlich, C. D. **94(6)**, 343 (1989).